CHALMERS

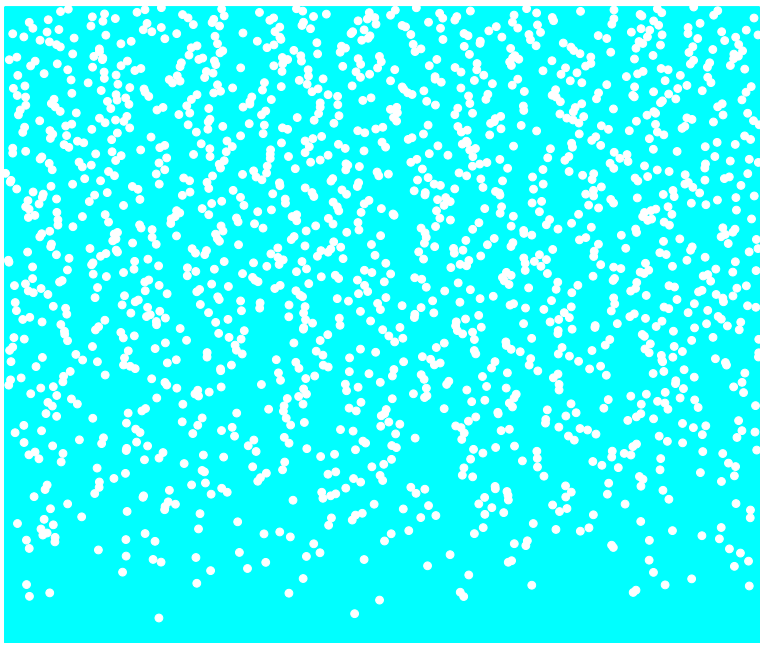

NOISE APPLICATIONS IN LIGHT WATER REACTORS WITH TRAVELING PERTURBATIONS

VICTOR DYKIN

Division of Nuclear Engineering
Department of Applied Physics
CHALMERS UNIVERSITY OF TECHNOLOGY
Göteborg, Sweden 2012

THESIS FOR THE DEGREE OF DOCTOR OF PHILOSOPHY

CTH-NT-263 September 2012

Noise Applications in Light Water Reactors with Traveling Perturbations

VICTOR DYKIN

Division of Nuclear Engineering
Department of Applied Physics
Chalmers University of Technology
SE-412 96 Göteborg, Sweden 2012

Noise Applications in Light Water Reactors with Traveling Perturbations
VICTOR DYKIN
ISBN 978-91-7385-732-1

Doktorsavhandling vid Chalmers tekniska högskola
Ny serie nr 3412
ISSN 0346-718X

Division of Nuclear Engineering
Department of Applied Physics
Chalmers University of Technology
SE-412 96 Göteborg
Sweden
Telephone +46 (0)31 772 1000
Fax +46 (0)31 772 3872

Cover: Illustration of the simulated two-dimensional distribution of bubbles (bubbly flow), propagating axially along the Boiling Water Reactor heated channel (generated from the Monte Carlo model).

Chalmers Reproservice
Göteborg, Sweden 2012

Noise Applications in Light Water Reactors with Traveling Perturbations.

VICTOR DYKIN
Division of Nuclear Engineering
Department of Applied Physics
Chalmers University of Technology

ABSTRACT

Neutron noise induced by perturbations traveling with the coolant of light water reactors (LWRs) is investigated. Different methods to simulate the effect of propagating perturbations are considered. The studies are performed in both open- and closed-loop systems and summarized in three chapters.

In the first chapter, the space-dependence of the neutron noise due to propagating perturbations calculated in one-group theory and one dimension in a pressurized water reactor (PWR) is investigated. A full analytical solution, obtained by the use of Green's function technique, is analyzed for different frequencies and different system sizes. An interesting new interference effect between the point-kinetic and space-dependent components of the induced noise is discovered and interpreted in physical terms. A similar investigation is performed in two-group theory for four reactor systems with different neutron spectra. The goal is to investigate the dependence of the properties of the induced neutron noise on the neutron spectrum. The presence of the fluctuations of several cross sections is also analyzed and resulted in qualitatively and quantitatively new characteristics of the induced noise. Further, a simple numerical Monte Carlo-based model to simulate the boiling process in a boiling water reactor (BWR) heated channel, is constructed. The output of the model is then used to estimate the local component of the neutron noise induced by density fluctuations in the coolant numerically convoluting it with proper transfer functions.

In the second chapter, a four-heated channel reduced order model (ROM), accounting for the first three neutronic modes, is constructed to study both global and regional instabilities. Some additional modifications compared with the earlier-developed models are performed to improve the consistency of the model. It is shown that the ROM is capable to reproduce the main features of core-wide instabilities. Moreover, it is proven that the inclusion of both azimuthal modes brings some importance for the correct identification of stability boundaries. The ROM is also extended to simulate the effect of local instabilities, such as the Forsmark-1 instability event of 1996/1997. A good qualitative agreement with real measurements is found.

In the last chapter, a number of the applications of the noise diagnostics based on the foregoing calculations are discussed. The case when the neutronic response of the reactor is affected by a non-white driving force (propagating perturbation) is studied. It is also investigated how the accuracy of the determination of the so-called decay ratio (DR) of the system, based on the assumption of a white noise driving force, deteriorates with deviations from the white noise character of the driving force. Furthermore, the earlier developed ROM is applied to analyze what stability indicators other than the DR can be used to describe the stability of the system. As a candidate, the coupling reactivity coefficients are chosen and their dependence on the DR is investigated. It is shown that such a dependence deviates form the conventional one, presumably caused by the inherent inertia of the system. Finally, two techniques, one based on the break-frequency of auto power spectral density (APSD) of the neutron noise and another on the transit times

of propagating void fluctuations are discussed for reconstructing the axial void profile from the Monte-Carlo simulated neutron noise. It is shown that both methods provide promising results.

Keywords: propagating density perturbation, Green's function technique, space-dependent neutron noise, reduced order models, global and regional instabilities, density wave oscillations, BWR stability, decay ratio, non-white driving force, Monte Carlo, void fraction, local component, cross-correlation function, transit times.

Appended papers

This thesis consists of an introduction to and a summary of the work published in the following papers:

PAPER I

I. Pázsit and V. Dykin, "Investigation of the space-dependent noise induced by propagating perturbations", *Annals of Nuclear Energy*, **37**, pp. 1329-1340 (2010)

PAPER II

V. Dykin, A. Jonsson and I. Pázsit, "Qualitative and quantitative investigation of the propagation noise in various reactor systems", *Submitted to Progress in Nuclear Energy* (2012)

PAPER III

V. Dykin and I. Pázsit, "Simulation of in-core neutron noise measurements for axial void profile reconstruction in boiling water reactors", *Submitted to Nuclear Technology* (2012)

PAPER IV

V. Dykin, C. Demazière, C. Lange and D. Hennig, "Investigation of global and regional BWR instabilities with a four heated-channel Reduced Order Model", *Submitted to Annals of Nuclear Energy* (2012)

PAPER V

V. Dykin, C. Demazière, C. Lange and D. Hennig, "Investigation of local BWR instabilities with a four heated-channel Reduced Order Model", *Accepted for publication in Annals of Nuclear Energy* (2012)

PAPER VI

V. Dykin and I. Pázsit, "Remark on the role of the driving force in the BWR stability", *Annals of Nuclear Energy*, **36**, pp. 1544-1552 (2009)

PAPER VII

V. Dykin, C. Demazière and P. Vinai, "On the Possible Dependence of the Decay Ratio on the Void Reactivity Feedback", *Accepted for publication in The 2012 ANS Winter Meeting Transactions*, San Diego, California, USA, 11-15 November, 2012

PAPER VIII

V. Dykin and I. Pázsit, "Numerical Simulation of the Two Phase Flow and Investigation of the Induced Neutron Noise ", *Transactions of American Nuclear Society*, Chicago, Illinois, USA, 24-28 June, 2012

Scientific publications not included into the thesis

V. Dykin and I. Pázsit, "Investigation of the space-dependent noise, induced by propagating density perturbation", *Proc. of the International Conference of the Physics of Reactors: Advances in Reactor Physics to Power the Nuclear Renaissance (PHYSOR 2010)*, Pittsburgh, USA, May 9-14, 2010

I. Pázsit, C. Montalvo Martin, V. Dykin and T. Tambouratzis, "Final Report on the Research Project Ringhals Diagnostics and Monitoring", Stage 13, CTH-NT-230/RR-15, Chalmers University of Technology, Göteborg, Sweden, March, 2010

I. Pázsit, V. Dykin and A. Jonsson, "Final Report: Research and Development Programm in Reactor Diagnostics and Monitoring with Neutron Noise Methods ", Stage 16, SSM Report 2010:22, Chalmers University of Technology, Göteborg, Sweden, September, 2010

V. Dykin and C Demazière, "Simulation of local instabilities with the Reduced Order Models", *Proc. of the XV MEETING ON REACTOR PHYSICS CALCULATIONS IN NORDIC COUNTRIES*, Helsinki, Finland, 12-13 April, 2011

V. Dykin and I. Pázsit, "Some curious properties of the reactor noise in simple systems", *Proc. of the XV MEETING ON REACTOR PHYSICS CALCULATIONS IN NORDIC COUNTRIES*, Helsinki, Finland, 12-13 April, 2011

I. Pázsit, C. Montalvo Martin, V. Dykin and H. Nylén, "Final Report on the Research Project Ringhals Diagnostics and Monitoring", Stage 14, CTH-NT-253/RR-16, Chalmers University of Technology, Göteborg, Sweden, March, 2011

I. Pázsit, N. Tran, V. Dykin and A. Jonsson, "Final Report: Research and Development Programm in Reactor Diagnostics and Monitoring with Neutron Noise Methods ", Stage 17, SSM Report 2011:29, Chalmers University of Technology, Göteborg, Sweden, September, 2011

V. Dykin, C. Demazière, C. Lange and D. Hennig, "Simulation of local instabilities with the use of Reduced Order Models", *Proc. of the International Conference on Mathematics and Computational Methods Applied to Nuclear Science and Engineering (MC 2011)*, Rio de Janeiro, Brazil, 8-12 May, 2011

V. Dykin and C. Demazière, "Development of simplified models to understand instabilities in Boiling Water Reactors", Poster Session, *JSPS colloquium: Nuclear Energy and Nuclear Applications*, Gothenburg, Sweden, 13-14 October, 2011

V. Dykin and C. Demazière, "Investigation of instabilities in nuclear reactor systems", Poster Session, *Chalmers Energy Conference: Electricity for Tomorrow*, Gothenburg, Sweden, 28-29 March, 2012

V. Dykin and I. Pázsit, "Simulation of in-core neutron noise measurements for axial void profile reconstruction in boiling water reactors", *Proc. of the International Conference of the Physics of Reactors: Advances in Reactor Physics (PHYSOR 2012)*, Knoxville, Tennessee, USA, April 15-20, 2012

V. Dykin and C. Demazière, "Development of a fully-consistent reduced order model to study instabilities in boiling water reactors", *Proc. of the International Conference of the Physics of Reactors: Advances in Reactor Physics (PHYSOR 2012)*, Knoxville, Tennessee, USA, April 15-20, 2012

C. Lange, D. Hennig, A. Hurtado, V. Dykin and C. Demazière, "Comments on local power oscillation phenomenon at BWRs ", *Progress in Nuclear Energy*, **60**, pp. 73-88 (2012)

A. Jonsson, N. Tram, V. Dykin, and I. Pázsit, "Analytical investigation of the properties of the neutron noise in various reactor systems", *Accepted for publication in Kerntechnik* (2012)

I. Pázsit, N. Tran, V. Dykin and A. Jonsson, "Final Report: Research and Development Programm in Reactor Diagnostics and Monitoring with Neutron Noise Methods ", Stage 18, SSM Report, Chalmers University of Technology, Göteborg, Sweden, September, 2012

Contents

Chapter 1

INTRODUCTION

A clever person solves problem. A wise person avoids it.
— Albert Einstein

Over the past few decades, the analysis of random process signals has become a commonly-used tool to unfold hidden information about the properties of complex systems in various fields of physics. Such a technique is often referred to as "noise analysis" where the term "noise" is usually equivalent to the term "fluctuation". One of the main advantages of the noise analysis technique compared with many other methods is its non-intrusive nature with no need of having a direct access to the system components in order to extract the necessary information. The application of this method is especially interesting for systems such as nuclear reactors, primarily to study the fluctuations of the neutron population inside the reactor core where the access is limited due to the high level of radiation. As a matter of fact, noise analysis is often used to indirectly monitor the state of the core, to detect changes in the state of the system, to identify failures and anomalous reactor behaviour [1]. Moreover, noise diagnostics is also beneficial from an economical point-of-view since it provides a unique opportunity for the online monitoring of the operational parameters of the reactor core, i.e. reactivity coefficients, two-phase properties etc.

The neutron fluctuations in power reactor systems originate from the fluctuations in the system properties, such as temperature, pressure, void, movement (vibrations) of the reactor components etc. These changes manifest themselves in corresponding changes of the nuclear cross-sections that govern the space-time development of the neutron flux. Usually, these fluctuations in the system parameters (i.e. the cross-sections), are represented by small, stationary fluctuations around a mean value. If the feedback effect of the induced neutron fluctuations back to the original physical parameters can be neglected, then the system is called an "open loop system". For small enough fluctuations, higher order quantities can be neglected, and the system will be described by equations that are linear in the searched quantities. In that case the system response, i.e. the neutron fluctuations, can be described as the effect of the noise source (cross-section fluctuations) acting through the system transfer function which corresponds to the unperturbed system. The solution is then given in the frequency domain by a spatial convolution of these two quantities [1]. By measuring the neutron noise with either a given perturbation or a known transfer function, the parameters of the other can be determined by inversion of the convolution integral. In some cases, the perturbation can be measured directly and in others the transfer function can be calculated analytically or numerically. Both cases, i.e. diagnosing either the perturbation or the transfer function, are accounted for in the

reactor noise diagnostics.

An interesting example of noise calculations in open-loop systems is considered in Chapter 2 of this thesis. As for the neutron noise source, the so-called propagating perturbation (i.e. the perturbation traveling with the coolant), defined in a simple analytical form, is chosen. It should be pointed out that most of the previous investigations of the neutron noise given rise by propagating perturbations ("propagating noise") were made only in the point-kinetic approximation which is valid either for very small cores or slowly changing perturbations [2–4]. At that time, the properties of its characteristic sink structure observed in the frequency domain were of the main interest. However, as reported elsewhere [3,4], the sink structure has never been observed in real neutron noise measurements. One possible reason for this, in addition to many others, is the deviation of the shape of the static flux from a pure sine function. Another reason might be the increasing contribution of the space-dependent component of the neutron noise (especially for commercial reactors which are large enough), which due to its smooth spatial behaviour diminishes the sink-structure. Thus, to investigate the latter one as well as the limitations of the point-kinetic model, in the present study, the space-dependence of the propagating noise in one-group theory and in a pressurized water reactor (PWR) together with its frequency dependence were analyzed. It turned out that the propagating noise has a very interesting behaviour in that it shows a remarkable interference between the point kinetic and the pure space-dependent components, which may be either in-phase or out-of-phase, depending on the position in the core, on the frequency and on the reactor size (tightly or loosely coupled system). The space-dependence of the neutron noise induced by propagating perturbations has also become interesting in connection with one of the planned Generation-IV reactors: the molten salt reactor (MSR). In such a reactor the molten salt fuel propagates in the solid moderator core, hence it is envisaged that the fluctuations of the fuel burn-up, poison etc. will represent a strong propagating perturbation. Thus, the calculations of the neutron noise in the traditional commercial light water reactors (LWRs) induced by propagating temperature fluctuations of the coolant might also be helpful to identify the new features of an MSR [5,6].

In a real reactor, the nuclear cross-sections controlling the neutron distribution are strongly energy-dependent and are usually collapsed into two groups, i.e. fast and thermal, respectively [1,7]. Accordingly, all power reactors are classified either as fast or thermal systems, depending on the dominant energy spectra of neutrons. Therefore, it is also interesting to expedite the significance of spectral properties on the propagating neutron noise which is a further topic in Chapter 2. For this reason, the case of noise calculations in two groups with all cross-sections perturbed, for four different reactor designs with different spectra was investigated. The two-group noise calculations are especially important from a diagnostics point-of-view since the so-called local component of the neutron noise can only be observed in such a case [1,8]. The local component of the neutron noise has some significance in determining important boiling water reactor (BWR) characteristics, such as void fraction, flow velocity etc. Moreover, the presence of the local component together with the simultaneous perturbation of several cross-sections results in a very peculiar interference character of the induced noise, qualitatively and quantitatively different from a traditional case with only a single cross-section being perturbed.

The last topic of Chapter 2 is focused on a more phenomenological modeling of the propagating perturbation in a BWR. In the cases studied so far, a simple analytical form of the propagating perturbation has been used. However, as practice shows, it is not

always possible to specify a simple analytical model of the perturbation itself. In such cases, a numerical simulation of the stochastic properties of the underlying physical processes could be used to generate a numerical realization of the perturbation. This method was first used in the localization of vibrating control rods, by generating stochastic two-dimensional mechanical vibrations from the model of two-dimensional random forces [9–11]. In particular, the model proved to be very useful for generating vibrating data in case of impacting when no simple analytical model for the vibrations can be given. Another case when construction of an analytical model for the noise source is not trivial is that of the two-phase flow in a BWR [12, 13]. The corresponding analytical models are sufficient to explain just a few properties of the induced noise but insufficient to elaborate any unfolding methods. As an alternative, a stochastic (Monte Carlo [14]) model of two-phase flow regime is presented in Chapter 2 in order to simulate realistic density fluctuations and, hence, the realistic noise source for the propagating noise. The main advantage of such a numerical representation of the perturbation is the direct access to the properties of the noise source which provides an opportunity to investigate the possibility and accuracy of the different diagnostic methods of unfolding noise source parameters from the induced noise.

In certain cases, especially when the fluctuations of the neutron flux cannot be described as small first order quantities, the feedback of the neutron fluctuations to the original processes, such as temperature, pressure etc., and hence to the nuclear cross-sections, cannot be neglected. For such cases, in particular for a BWR, a more conservative way of modeling the reactor system, namely a "closed loop model", should be applied. Such a system represents a substantially more involved situation as compared to the linear open loop system. That is, there is a conceptual and a practical difficulty involved in the study of coupled (closed-loop) systems. The conceptual difficulty is that it is not possible to factorize the induced neutron noise into the effect of a perturbation, i.e. the deviation of the system parameters from the equilibrium or perturbed values, and the transfer function. This means that the dynamical behaviour of the system is no longer related to a system in equilibrium, rather to the perturbed state in a sophisticated manner. The practical difficulty is that in realistic cases it is impossible to get analytical solutions in closed form, and advanced numerical methods need to be used. As a result, the interpretation of the results, in order to perform the system diagnostics, also becomes more complicated. In particular, this is the case for the so-called system codes where a high number of intertwined parameters and variables are involved. A more pragmatic way is then to simplify the description very significantly regarding both the neutronics and the thermal hydraulics, while preserving the non-linear coupling between them such that the model still reproduces the main features of the BWR dynamics.

Such models are commonly referred to as reduced order models (ROMs) [15–19] and are the main topic of Chapter 3. The basic idea of the ROM modeling is to transform partial differential equations(PDEs) [7, 20], which describe the reactor behaviour, to simplified ordinary differential equations (ODEs). The reduction helps to eliminate drastically the complexity of the system and, hence, allows to simplify the modeling of instabilities and to get deeper understanding of physical phenomena which drive these instabilities in the reactor core.

The simplest prototype of the ROM is a model with a one-dimensional (axially propagating) thermal-hydraulic module and a corresponding homogeneous core treated with point kinetics from the neutronic side [17, 21]. Such models have been in use and stud-

ied for some time. For obvious reasons, such models can only reconstruct the so-called global instability phenomena [1], in which the fundamental mode of the neutron flux oscillates. In addition to global instabilities, so-called regional instabilities [1] can also occur, and in fact co-exist with the global instability. The regional instability is associated with neutron flux fluctuations in the azimuthal modes. Experience shows that it is important to be able to determine the stability properties of these two modes separately, in order to correctly estimate the margins to instability [22, 23]. For these reasons, ROMs have been developed with two thermal-hydraulic channels and corresponding neutronic modes [19, 24–26]. While such a ROM can indeed study two neutronic modes at the same time, in a real BWR two azimuthal modes exist simultaneously and their combined behaviour (frequency and phase delay relative to each other) also carries important information on the system and its stability properties, and also determines whether the simple method of using the linear stability indicator, i.e. the decay ratio (DR), gives at all usable results for non-linear systems. The capability of the ROM to simulate such a behaviour is discussed in Chapter 3. Here, it is important to underline that in most real cases both the global and regional instabilities are primarily triggered by thermal-hydraulic instabilities which occur mainly due to the propagating character of the coolant properties (propagating density/pressure waves). Thus, in Chapter 3, the ROM is applied to simulate yet another case of propagating noise, in a strongly coupled system where the feedback effects are accounted for.

As previous works show [23], when several spatial oscillation modes exist with the same or very similar frequencies, but with different stability properties, the use of the DR as a single global stability indicator fails. One example is an event which took place at the Swedish Forsmark-1 power plant in 96/97 [27–29], where the local power oscillations caused by density wave oscillations (DWOs) [30] were observed. Thus, as a final topic of Chapter 3, the ROM simulation of local instabilities caused by propagating density of the coolant is discussed. One of the reasons to choose this event as an example comes from the interesting phenomena, observed in that event, namely a time-dependent rotation of the symmetry line of the azimuthal modes. In Chapter 3, such a peculiar behaviour is reconstructed and studied with the ROM.

The main goal of this work is not only to demonstrate how the neutron noise induced by propagating perturbations can be modeled under different conditions, but also to explain how this knowledge can be used to study realistic cases. For this reason, a separate chapter (Chapter 4) is devoted to the noise applications based on simulations performed in the previous two chapters. A short overview of this work is summarized below.

In certain cases, one is interested in the slow change of the properties of the core (the transfer function), which obviously cannot be quantified from only the induced noise, without being able to measure the noise source. In such a case one has to make some assumptions about the properties of the noise source, such as assuming it to be a white noise (its auto-power spectral density (APSD) [1] being constant in frequency). Such a case is that of the stability of the BWRs, which is usually monitored by measuring local or averaged (over several detectors) neutron flux values, and calculating the so-called decay ratio from the auto-correlation function (ACF) [1] of the measured neutron noise or, equivalently, from the width of the peak in the APSD of the detector signals. Since, in the frequency domain, the APSD of the neutron noise is given as the product of the frequency dependent core transfer function squared, times the APSD of the driving force (DF), for a white noise driving force the frequency properties (and hence also the properties of the

ACF) of the system are equivalent to that of the measured neutron noise.

Even if the assumption of the white noise character of the driving force is a very plausible one, it is just an assumption which is impossible to prove by measurements. Thus, the first topic taken up in Chapter 4 is an investigation of a case when the driving force is not a white noise. As for the driving force, the propagating two-phase flow perturbation with a characteristic periodic peak-sink structure in the frequency domain, is selected. It is clear intuitively that if the driving force has a peak or a sink at or close to the system resonance, the resulting neutron noise will deviate significantly from that induced by a white driving force, and one will draw erroneous conclusions regarding the stability of the system. Moreover, a change in the properties of the driving force, can be interpreted as a change in the stability of the system.

Further, an application of the four-heated channel ROM for the stability analysis of a BWR is considered. One consequence of the non-linearity of the nuclear systems, such as a BWR, is the fact that the concept of the DR, as a stability parameter, fails in some cases [22,23]. As a matter of fact, it is still not clear what stability indicators could be used for describing the stability of these systems and their evolution in an objective quantitative way. For this purpose, the developed ROM was applied to investigate the correlation between the coupling reactivity coefficients and the decay ratio to study the possibility to use the former one as a new stability indicator. It turned out that the dependence between the coupling coefficients and the DR is different from the conventional one, observed in earlier investigations. Namely, as the coupling becomes more and more negative, the DR increases up to almost unity, (i.e. reaches its saturation point), thus, following the traditional behaviour of the DR for such studies. However, at a certain critical value, the DR starts to decrease for any further change in the coupling coefficients. A possible explanation of this unexpected behaviour as well as a short discussion about the applicability of the coupling coefficients for stability monitoring are given.

Finally, an unfolding technique in neutron noise diagnostics is discussed. Using the Monte Carlo model of two-phase flow developed in Chapter 2, two methods for reconstructing void fraction and void velocity axial profiles from neutron noise measurements are demonstrated. Notably, such MC simulations of bubbly flow in a BWR were already studied in the past, but for a different purpose, namely to check the performance of radiation attenuation based methods for determining local void fraction and local void velocity [13]. The main advantage of such a numerical modeling is the direct access to both the input and the output data. This allows to test different correlations between the first moments of different quantities, i.e. the noise measurements and the mean value of the velocity and void fraction. This is achieved by comparing the input data from the model to the output data taken from the simulation. In real cases, there is always the possibility to measure the neutron noise (the output) whereas the information about the input (the mean void fraction) is missing, i.e. the original (true) void fraction profile is not available. The latter means that even if the reconstruction of the void profile has been performed, there is no chance to validate or estimate the reconstructed void profile. However, as shown in Chapter 4, this is not the case for the MC simulation.

In Chapter 5, a summary of the results together with an outlook for the continuation of the work are given.

A nomenclature of the abbreviations and acronyms used in the thesis is given at the end of the manuscript.

Chapter 2

METHODS FOR MODELING THE EFFECT OF PROPAGATING PERTURBATION IN OPEN LOOP SYSTEMS

A physicist is just an atom's way of looking at itself
— Niels Borh

In this Chapter, the neutron noise induced by propagating perturbations in traditional LWR open-loop systems, i.e. in systems without any feedback, is considered.

First, the axial space-and frequency-dependence of the neutron noise is investigated using a one-group PWR model with one average group of delayed neutrons. The corresponding noise source is represented as an axially propagating temperature perturbation of the coolant, specified in an analytical form as the fluctuation in absorption cross-section. The induced noise is obtained by convoluting the neutron noise source with the analytically calculated Green's function. All calculations are made in first-order perturbation theory. The gradual diminishing of the sink structure with increasing system size and frequency is analyzed. A special attention is paid to the frequency dependence of the calculated neutron noise which is also used to explain the sink structure found in previous calculations for a system of power reactor size [31]. Some interesting interference effect between the point-kinetic and space-dependent components, leading to the spatial oscillation of the amplitudes of the total noise is discovered and explained. More details are given in **Paper I**.

Next, a similar study of the induced neutron noise in two-group theory is performed. What regards the propagating perturbation, an inlet flow temperature fluctuation defined in a similar analytical form as before, is considered. The induced neutron noise is evaluated by analytically solving two-group diffusion equations in the space/frequency domain with an application of standard Green's function technique. In order to study the applicability of noise analysis to systems significantly different from traditional LWRs dominating so far, as well as to study the effect of different spectral properties on the induced noise, four different reactor systems are investigated. In addition, a more advanced modeling of the neutron noise where all cross-sections are affected by the inlet temperature perturbation, is implemented. Some new interesting results due to the presence of the local component, as well as the simultaneous perturbation of several cross-

sections are presented. Further details on this topic can be found in **Paper II**.

Finally, a case with a more fundamental, numerically-simulated model of noise source, i.e. the boiling process representing the propagating perturbation, is investigated. A simple form of the two-phase flow, based on the Monte Carlo technique is chosen, in which the basic process is the random generation and subsequent deterministic transport of the bubbles with the flow. The induced neutron noise is obtained qualitatively in the time domain, by numerically convoluting the simulated neutron noise source with the transfer properties of the system. The main focus is put on the estimation of the local component of the neutron noise. The simulated neutron noise is further processed by standard Fourier transform (FT) techniques to estimate the corresponding APSD. Such a numerical modeling allows to model more advanced and complex noise sources and, hence, provides a more realistic representation of the induced neutron noise, which makes it applicable for testing in real diagnostic applications. A more detailed description is given in **Paper III**.

This Chapter starts with a short description of the noise source for each of the cases mentioned above and proceeds with the calculations of the induced neutron noise and discussion of the results.

2.1 Properties of the noise source

2.1.1 One-group theory

The noise source is specified as an axially propagating perturbation, representing density/temperature fluctuations of the coolant. It is assumed that the fluctuations are generated outside the core and, after entering the core inlet, they propagate through the core in an unaltered form with a constant velocity v [2–4]. With only the absorbtion cross-section perturbed, the perturbation can be written as:

$$\delta\Sigma_a(z,t) = \delta\Sigma_a(0, t - \frac{z}{v})$$

or in the frequency domain after a temporal Fourier transform:

$$\delta\Sigma_a(z,\omega) = \delta\Sigma_a(0,\omega)e^{-\frac{i\omega}{v}z}. \tag{2.1}$$

In the above form $\delta\Sigma_a(0,\omega)$ stands for the fluctuations of the absorption cross-section at the core inlet and is assumed to be a white noise with a constant frequency spectrum. It is worth to point out that in a real reactor the coolant velocity v strongly depends on an axial position, however in the present study, for simplicity of the calculations, v is assumed to be axially-independent. Moreover, the axial dependence of the coolant velocity will apparently destroy the well-pronounced sink structure of the neutron noise (i.e. its reactivity component) which represents the main interest of this study. In the frame of first order perturbation theory with one-energy group involved, for the noise source one obtains:

$$S(z,\omega) = \frac{\phi_0(z)}{D} \cdot \delta\Sigma_a(z,\omega) \tag{2.2}$$

Since for some limiting cases (large frequencies), the space-dependent component of the noise is dominating and follows the source behaviour, it is interesting to consider the source properties: the amplitude and the phase which are given in Fig. 2.1.

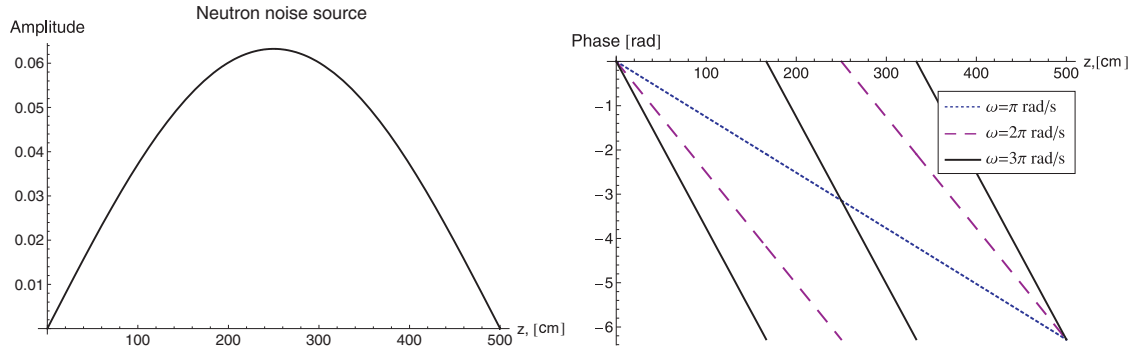

Figure 2.1: Amplitude and phase of the neutron noise source for $H = 500$ cm, $v = 250$ cm/s, $\omega = \pi,\ 2\pi,\ 3\pi$ rad/s

It is demonstrated in the figure that the noise source amplitude resembles the static flux and its phase θ is a linear function in space, as well as in frequency which can be seen from the expression

$$\theta = -\frac{\omega}{v} z \tag{2.3}$$

As is customary in neutron noise diagnostics, for small system sizes and low frequencies, the total noise reconstructs the reactivity behaviour and for the propagating density perturbation in the scope of first order perturbation theory, it reads as:

$$\rho(\omega) = \frac{\omega_T^3}{2\pi\omega(\omega_T^2 - \omega^2)} \left[(1 - \cos\omega T)i - \sin\omega T\right] \tag{2.4}$$

with its corresponding amplitude and phase functions expressed as:

$$APSD_\rho(\omega) = \frac{\omega_T^6}{4\pi^2\omega^2(\omega_T^2 - \omega^2)^2} \left[(1 - \cos\omega T)\right] \tag{2.5}$$

$$\theta = \begin{cases} -\frac{H}{2v}\,\omega = -\frac{T}{2}\,\omega \quad \text{for} \begin{cases} 0 \le \omega \le 2\omega_T \\ \text{and} \\ (2n+1)\omega_T \le \omega \le 2(n+1)\omega_T; \quad n = 1, 2, \ldots \end{cases} \\ \\ -\frac{H}{2v}\,\omega + \frac{\pi}{2} = -\frac{T}{2}\,\omega + \frac{\pi}{2} \quad \text{for} \quad 2n\omega_T \le \omega \le (2n+1)\omega_T; \quad n = 1, 2, \ldots \end{cases} \tag{2.6}$$

where T is the transit time of the perturbation defined as $T = H/v$ and ω_T is defined as $\omega_T = 2\pi/T$. More details are given in **Paper I**. In the present and subsequent calculations, the transit time $T = 2$ s is selected corresponding to the characteristic frequency $f_T = 0.5$ Hz. The corresponding graphical representation of the last two formulae are given below.

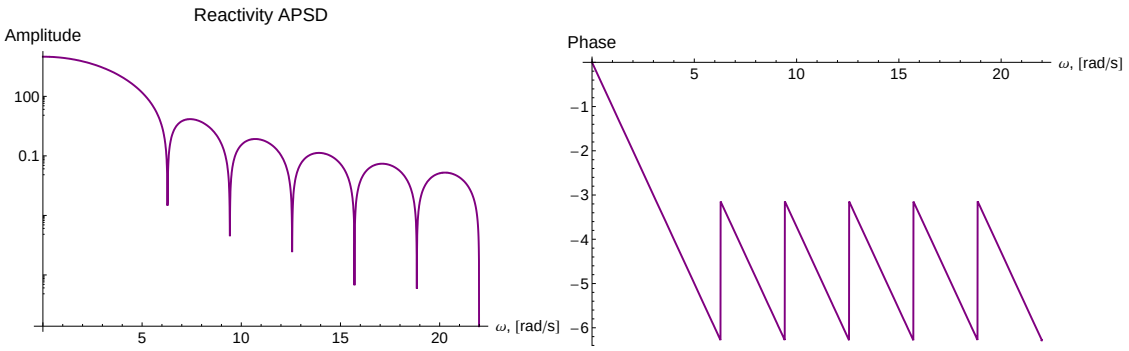

Figure 2.2: APSD and phase of the reactivity $H = 500$ cm, $v = 250$ cm/s

The last two figures show some interesting features of the reactivity, induced by a propagating perturbation. Namely, the amplitude of the reactivity has sinks at $\omega = n\,\omega_T, \quad n = 2, 3\ldots$ and its phase has a discontinuity at the same points.

Below, the analytical expression as well as a graphical representation for the autocorrelation function $ACF(\tau)$, calculated for the corresponding reactivity effect $APSD_\rho(\omega)$ are shown. Utilizing the traditional definition of the ACF as a time convolution, one gets:

$$ACF_\rho(\tau) = \frac{vk^2}{2(\nu\Sigma_f)^2 H^2}\left\{(H - |\tau|v)(2 + \cos\omega_T\tau) + \frac{3H}{2\pi}\sin\omega_T|\tau|\right\}\theta(T - |\tau|). \qquad (2.7)$$

From Eq. (2.7), one can immediately conclude that the correlation of the noise is different from zero only for time differences less or equal to the transit time T of the perturbation, which means that the correlated points should belong to the same entry of the coolant, i.e. to the same perturbation in the coolant. Thus, the maximum width of the ACF corresponds to $\tau = T$. The same result is seen from the corresponding Fig. (2.3) where some examples of this autocorrelation function are shown.

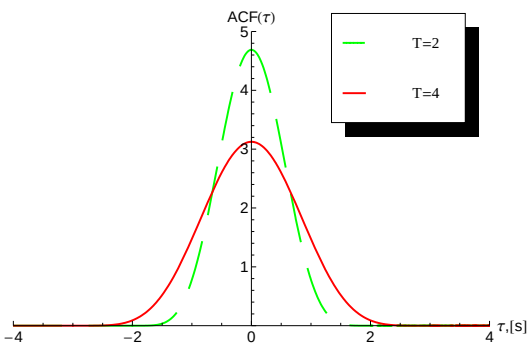

Figure 2.3: The ACF of the reactivity effect of propagating perturbations for two different transit times.

2.1.2 Two-group theory

Eq. (2.2), written for the noise source in one-group theory, can easily be generalized for the case of two-energy groups and reads in a vector form as [1]:

$$\bar{\boldsymbol{S}}(z,\omega) = \begin{pmatrix} S_1(z,\omega) \\ S_2(z,\omega) \end{pmatrix} \tag{2.8}$$

Here the noise sources S_1 and S_2, corresponding to the noise sources in the fast and thermal energy groups, respectively, are defined in terms of the cross-section fluctuations and the static fluxes in the form:

$$\begin{aligned} S_1(z,\omega) = &\left(\delta\Sigma_R(z,\omega) + \delta\Sigma_{a_1}(z,\omega) - \delta\nu\Sigma_{f_1}(z,\omega)\left(1 - \tfrac{i\omega\beta}{i\omega+\lambda}\right)\right)\phi_1(z) - \\ &\delta\nu\Sigma_{f_2}(z,\omega)\left(1 - \tfrac{i\omega\beta}{i\omega+\lambda}\right)\phi_2(z) \end{aligned} \tag{2.9}$$

and

$$S_2(z,\omega) = -\delta\Sigma_R(z,\omega)\phi_1(z) + \delta\Sigma_{a_2}(z,\omega)\phi_2(z) \tag{2.10}$$

where the subscripts a_1, a_2, f_1, f_2, R stand for the absorbtion and fission in the fast and thermal energy groups and removal cross-sections, respectively. Here, for convenience of the calculations, the neutron noise source is defined in a different form compared with the one used in one-group theory (see Section 2.1.1), i.e. the weighting factors D_1 and D_2 (diffusion coefficients) are left out. The corresponding fast and thermal static fluxes are given as:

$$\phi_1(z) = \sin B_0 z \tag{2.11}$$

$$\phi_2(z) = \frac{\Sigma_R}{\Sigma_{a2} + D_2 B_0^2} \sin B_0 z \tag{2.12}$$

with $B_0 = \pi/H$. The normalization of the fluxes is used such that the maximum amplitude value of the fast flux is unity. In the foregoing, the option for any of the cross-sections to be perturbed, as well as a simultaneous perturbation of several cross-sections, is taken into account. For obvious reasons, the frequency-dependence of both the amplitude and phase of the neutron noise source in two-group approach is similar to that in one-group theory and is not repeated here.

2.1.3 Numerical simulation of the neutron noise source

In the examples discussed so far, a simple analytical form for the propagating perturbation has been used. However, as mentioned earlier, this is not always the case and for certain perturbations only a numerical simulation of the perturbation can be constructed. Therefore, in the following, a simple numerical Monte-Carlo based model of the boiling process in a BWR heated channel, representing the more natural example of the propagating perturbation, is discussed. To simplify the simulations, instead of modeling a true 3-D geometry, a two-dimensional model of a real fuel assembly emulating its radial and axial cross-section ((x, z) geometry) with the bubbles simulated as 2-D circles, is chosen. In order to set up a realistic model of the two-phase flow with a proper axial void fraction profile (i.e. similar to the BWR one), a proper distribution for bubble generation should be found. For this reason, the bubble generation rate per unit length, which generates the desired void profile is chosen to be proportional to the gradient of the void fraction.

It should be noted that the latter statement is not true in a real heated channel where the bubble generation rate is proportional to the quality (not to the void fraction) but for reasons of simplicity such an approximation is assumed. Since there are no realistic void fraction profiles available in the form of simple analytical functions, to keep at least the bubble generation model at a simple level, the bubble generation intensity is chosen to be proportional to the static neutron flux, which results in the following cumulative probability function:

$$P(z) = \frac{1}{2} \cdot (1 - \cos(\frac{\pi z}{H})) \tag{2.13}$$

The axial velocity of bubbles can be estimated from the steady-state mass conservation equation and reads as:

$$v(z) \approx \frac{v_0}{1 - \alpha(z)}. \tag{2.14}$$

The diameter of the generated bubbles is set to $d = 0.8$ cm. The coordinates of the bubble centres in the z-direction are generated in such a way to provide a realistic axial BWR void profile, whereas in the x-direction the bubble generation is chosen as a uniform one. The intersection between the bubbles is not permitted. The simulation starts with 100 bubbles generated at $t = 0$ s and proceeds with the random injection of 35 new bubbles at each consecutive time step chosen equal to $\delta t = 0.0008$ s. Both the velocity and the void fraction for each single bubble at each time step are calculated. For realistic applications of the model, the void fraction is kept below 0.5. The bubble absence/presence is recorded at each time step and at each axial elevation using the binary system, i.e. "1" stands for the presence of a vapor bubble (vapor phase) and "0" stands for the absence of a bubble (liquid phase). The corresponding void signals are thereafter used as a numerically-simulated neutron noise source for calculating the induced neutron noise. Some more details are given in **Paper III**.

2.2 Neutron noise calculation procedure

2.2.1 One-energy group approach

Following the standard procedure in noise diagnostics, one starts with the space-/time-dependent one-group diffusion equations, which in one-dimension read as [1]:

$$\frac{1}{v}\frac{\partial \phi(z,t)}{\partial t} = D\triangle\phi(z,t) + [(1-\beta)\nu\Sigma_f - \Sigma_a(z,t)]\phi(z,t) + \lambda C(z,t) \tag{2.15}$$

$$\frac{\partial C(z,t)}{\partial t} = \beta\nu\Sigma_f\phi(z,t) - \lambda C(z,t) \tag{2.16}$$

Approximating both the neutron flux $\phi(z,t)$ and the absorption cross section $\Sigma_a(z,t)$ as small fluctuations $\delta\phi(z,t)$ and $\delta\Sigma_a(z,t)$ oscillating around their mean values, substituting the result into Eqs. (2.15) and (2.16), subtracting the static equations and applying a temporal Fourier transform, one gets:

$$\triangle\delta\phi(z,\omega) + B^2(\omega)\delta\phi(z,\omega) = S(z,\omega) \tag{2.17}$$

with $B^2(\omega) = B_0^2(1 - \frac{1}{\rho_\infty G_0(\omega)})$ being the dynamic buckling, and

$$S(z,\omega) = \frac{\phi_0(z)}{D} \cdot \delta\Sigma_a(z,\omega) \tag{2.18}$$

is the noise source. The rest of the notations is standard. The full solution of Eq. (2.17) is given via the Green's function $G(z, z_0, \omega)$ obtained from Eq. (2.17) with a delta-function source. For a slab reactor between $z = 0$ and $z = H$, the solution for the Green's function is conveniently written as:

$$G(z, z_0, \omega) = \begin{cases} -\frac{\sin(B(\omega)z)\sin(B(\omega)(H-z_0))}{B(\omega)\sin(B(\omega)H)} & \text{if} \quad z < z_0. \\ -\frac{\sin(B(\omega)z_0)\sin(B(\omega)(H-z))}{B(\omega)\sin(B(\omega)H)} & \text{if} \quad z > z_0. \end{cases} \tag{2.19}$$

Finally the total solution for Eq. (2.17) becomes:

$$\delta\phi(z, \omega) = \int G(z, z_0, \omega) S(z_0, \omega) dz_0 \tag{2.20}$$

For the analysis it is useful to re-write the total solution $\delta\phi(z, \omega)$ in such a way that it is split into two terms: point-kinetic and space-dependent term, respectively. Thus, after a standard factorization of the flux $\delta\phi(z, \omega)$ into an amplitude factor $P(t)$ and a shape function $\psi(z, t)$ and approximating each of the two as fluctuations around mean values, in the frequency domain the full solution can be represented as:

$$\delta\phi(z, \omega) = \phi_0(z) G_0(\omega)\rho(\omega) + \delta\psi(z, \omega) \tag{2.21}$$

where $\rho(\omega)$ stands for the reactivity effect of the cross-section perturbation and is defined as:

$$\rho(\omega) = -\frac{1}{\nu\Sigma_f} \int \varphi_0^2(z)\delta\Sigma_a(z, \omega)\, dz \tag{2.22}$$

and $\varphi_0(z)$ is the normalized static flux. The first term in Eq. (2.21) is usually called the point-kinetic or reactivity term and corresponds to the globally excited core response, following the reactivity behaviour of the noise source. The second term is named as the space-dependent term (or sometimes called "pure space-dependent term"), and it describes the locally-distributed space-dependent noise. It is known that for a small system size and/or for small perturbation frequencies, the first term is dominating and follows the reactivity behaviour, whereas for a large system size and/or for the high frequencies the second one is more pronounced and reproduces the noise source profile itself. These general tendencies will be shown to appear also for the noise induced by propagating perturbations, with some interesting consequences, which are specific for just this type of perturbation, as will be seen in Section 2.3.1. For more details one can refer to **Paper I**.

2.2.2 Two-energy group approach

Following the same linearization procedure as described above but rather in two-group diffusion theory this time, after a temporal Fourier transform, the equations for the group noise read as [1]:

$$\begin{pmatrix} D_1\nabla^2 - \Sigma_1(\omega) & \nu\Sigma_{f2}(\omega) \\ \Sigma_R & D_2\nabla^2 - \Sigma_2(\omega) \end{pmatrix} \begin{pmatrix} \delta\phi_1(z, \omega) \\ \delta\phi_2(z, \omega) \end{pmatrix} = \begin{pmatrix} S_1(z, \omega) \\ S_2(z, \omega) \end{pmatrix} \tag{2.23}$$

The corresponding equation for the Green's matrix can be obtained from Eq. (2.23), assuming delta-function shaped sources. Thus, the full solution of Eq. (2.23) is given in a matrix form as:

$$\delta\bar{\boldsymbol{\Phi}}(z, \omega) = \int_0^H \hat{\boldsymbol{G}}(z, z', \omega)\bar{\boldsymbol{S}}(z'\omega) dz' \tag{2.24}$$

The same solution can also be expressed via adjoint Green's function as:

$$\delta\bar{\mathbf{\Phi}}^{\boldsymbol{T}}(z,\omega) = \int_0^H \bar{\boldsymbol{S}}^{\boldsymbol{T}}(z,\omega)\hat{\boldsymbol{G}}^{\dagger}(z',z,\omega)dz' \tag{2.25}$$

where $\hat{\boldsymbol{G}}^{\dagger}(z',z,\omega)$ is called the adjoint Green's function. The full derivation can be found in **Paper II**.

2.2.3 Numerical estimation of the neutron noise

Assuming that the perturbation in the corresponding cross-section (mostly the removal in case of a BWR) is proportional to the fluctuation of the void fraction $\delta\alpha(z,t)$, the induced neutron noise in the space-time domain can be estimated following the same procedure as for the analytical models discussed before, i.e. as [1,8]:

$$\delta\phi(z,t) = \int_0^H G(z,z',t)\phi_0(z')\delta\alpha(z',t)dz' \tag{2.26}$$

where $\delta\alpha(z',t)$ is estimated numerically from the Monte-Carlo model. For the sake of simplicity, it is assumed that the system is one-dimensional and only a one-dimensional cross-section of the fluctuations is taken as the noise source. Since in the present study, only the local component of the neutron noise is of interest, the transfer function $G(z,z',t)$ can be approximated as:

$$G(z,z',t) \sim e^{-\lambda(z)|z-z'|} \tag{2.27}$$

2.3 Quantitative analysis of the space dependence of the noise

This Section shows some results of the neutron noise calculations, performed in the space domain for different system sizes and different frequencies or, equivalently, different propagating velocities in one-group approximation and for four spectrally-different cores with several cross-sections simultaneously perturbed in the two-group case.

2.3.1 One-group calculations

First, the case of very small frequencies $\omega = 0.01$ rad/s both for the small and large system: (*H =50* cm and *500* cm, respectively), is shown:

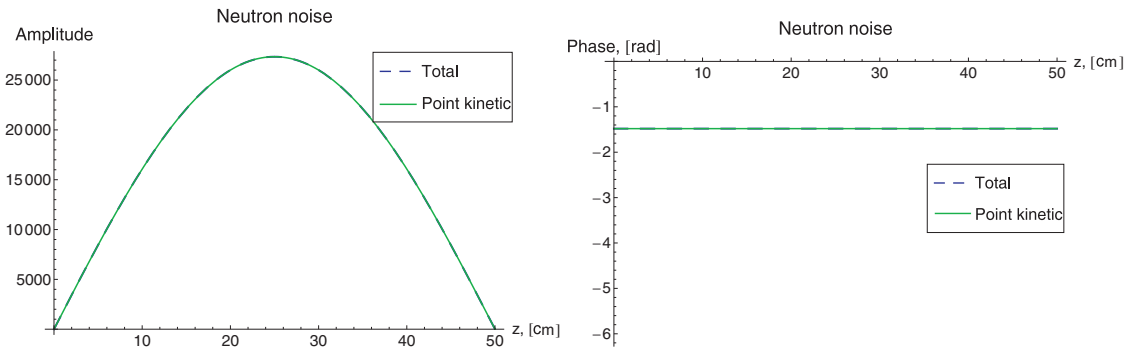

Figure 2.4: Amplitude and phase of the neutron noise for $H = 50$ cm, $v = 25$ cm/s, $\omega = 0.01$ rad/s

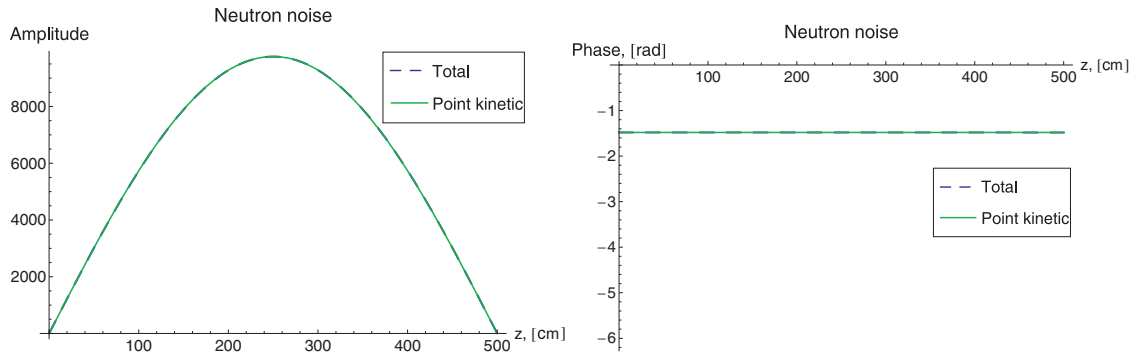

Figure 2.5: Amplitude and phase of the neutron noise for $H = 500$ cm, $v = 250$ cm/s, $\omega = 0.01$ rad/s

As figures (2.4) and (2.5) show, for this specific case (small frequencies) the total noise is fully dominated by the point-kinetic term, whereas the contribution from the space-dependent term is negligible, which agrees with our considerations in Section 2.2.1.

As a next step, another interesting case, that of a large system with an intermediate frequency, namely $\omega = 10\pi$ rad/s, is discussed. This corresponds to a situation when the reactivity effect is very small and, hence, the space-dependent component of the noise fully dominates.

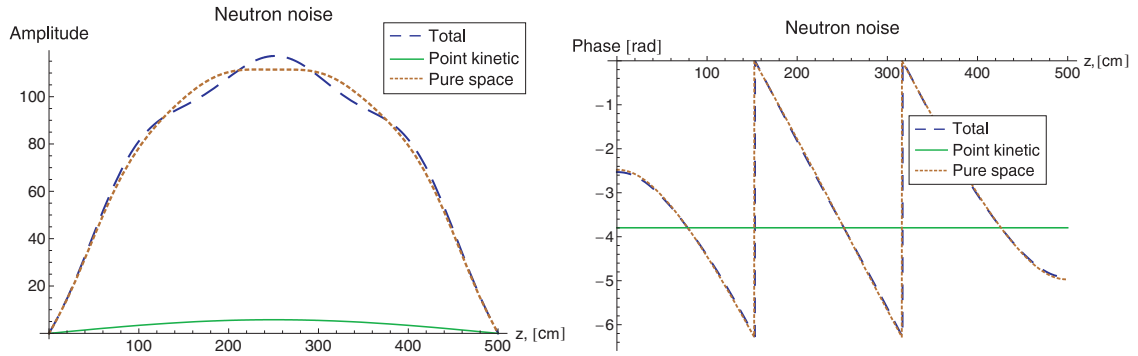

Figure 2.6: Amplitude and phase of the neutron noise for $H = 500$ cm, $v = 250$ cm/s, $\omega = 10$ rad/s

Indeed, as is seen from Fig. 2.6, the amplitude and the phase of the resulting noise follows those of the reactivity (see Fig. 2.1 in Section 2.1.1), as expected. However, it is more interesting to investigate another, less trivial intermediate case, which lies between the two previous ones. Such a case is a frequency lying at the lower end of the so-called plateau region, but not coinciding with a sink frequency of the reactivity, so that both the point kinetic and the space-dependent terms of the noise co-exist. That is what is given in Fig. 2.7 for the case of the small system ($H = 50$ cm) and intermediate frequency ($\omega = 10$ rad/s).

In this case, one can observe that the total noise contains contributions from both the reactivity term and the space-dependent term with comparable amplitudes. One can also notice an interesting behaviour of the full solution, in the sense that both terms are smooth functions in space, but the total solution exhibits some oscillations with a peak-dip structure. The explanation of this phenomenon comes from the phase relations

between the two contributions. Namely, from Fig. 2.7, it is seen that in some of the spatial points both terms are in-phase, which generates a peak in the total noise, whereas in other points they are out-of-phase which results in dips in the full solution. In **Paper I**, some other examples of such interference effects and more detailed discussion are given.

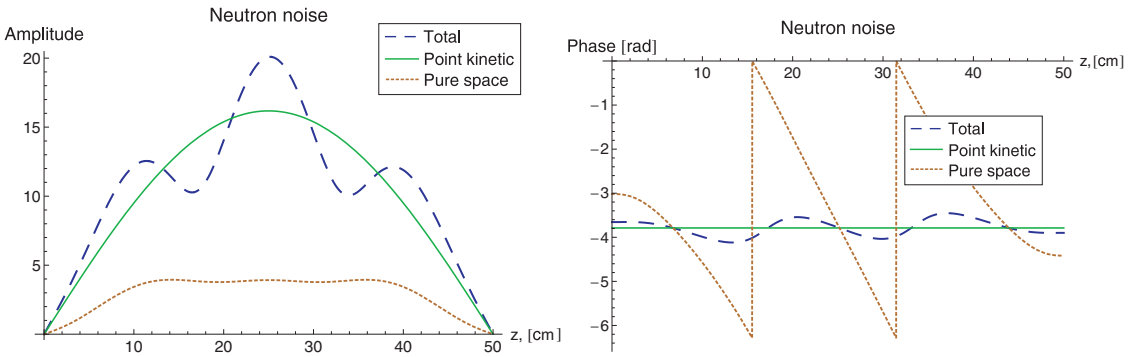

Figure 2.7: Amplitude and phase of the neutron noise for $H = 50$ cm, $v = 25$ cm/s, $\omega = 10$ rad/s

2.3.2 Two-group calculations

The dynamical response of four different cores, having different energy spectra, to various propagating perturbations, is investigated. The selected systems are a MOX fuelled fast reactor, a PWR, a BWR and a heavy water reactor (CANDU). The detailed description of the properties of the cores can be found in **Paper II**. In order to specify the noise source, the static fluxes should be estimated. The corresponding fast and thermal static fluxes together with their static adjoints for all four systems are given in **Paper II**, where, as expected, clear spectral differences resulting in the MOX loaded fast system having the hardest and the heavy water moderated CANDU reactor the softest spectra, can be observed.

Since in most work in the past the space-dependence of the transfer functions was performed by using the dynamic adjoint, it is instructive to analyze the space-dependence of each of the components of the adjoint Green's function. The space-dependence of the amplitude of the components of the fast adjoint function (i.e. $G^{\dagger}_{11}$ and $G^{\dagger}_{21}$) is shown in Fig. 2.8. It should be pointed out that in these Green's function components there is no visible occurrence of the local component.

The space-dependence of the amplitude of the thermal adjoints (i.e. $G^{\dagger}_{12}$ and $G^{\dagger}_{22}$) for the four cores is shown in Fig. 2.9. These results clearly agree with earlier calculations in the literature where a strong local component was observed for the fast and the light water cores. From Fig. 2.9 one can notice that the local component is the largest for the fast spectrum core and it is hardly visible for the CANDU. The latter can possibly be explained due to the large width of the local component which makes the presence of the local component more difficult to see.

Finally, the neutron noise induced by propagating perturbations in the inlet flow temperature is considered. The noise calculations are considered in two steps. First, it is assumed that only the thermal absorption cross-section is perturbed. Such a case is necessary for comparison with earlier obtained results. The space-dependence of the fast and thermal propagating neutron noise induced by fluctuations of the thermal absorbing

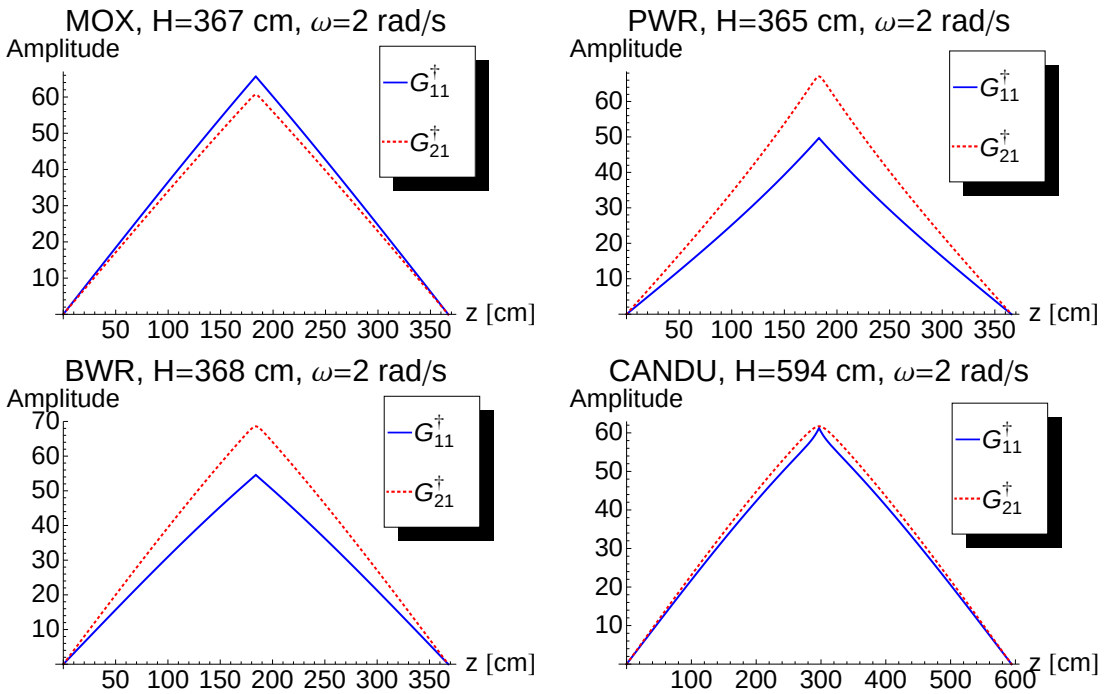

Figure 2.8: Space dependence of the amplitude of the components of the fast adjoint: a MOX reactor (upper left figure) , a PWR (upper right figure), a BWR (lower left figure) and a CANDU reactor (lower right figure) for $\omega = 2$ rad/s and $z' = H/2$.

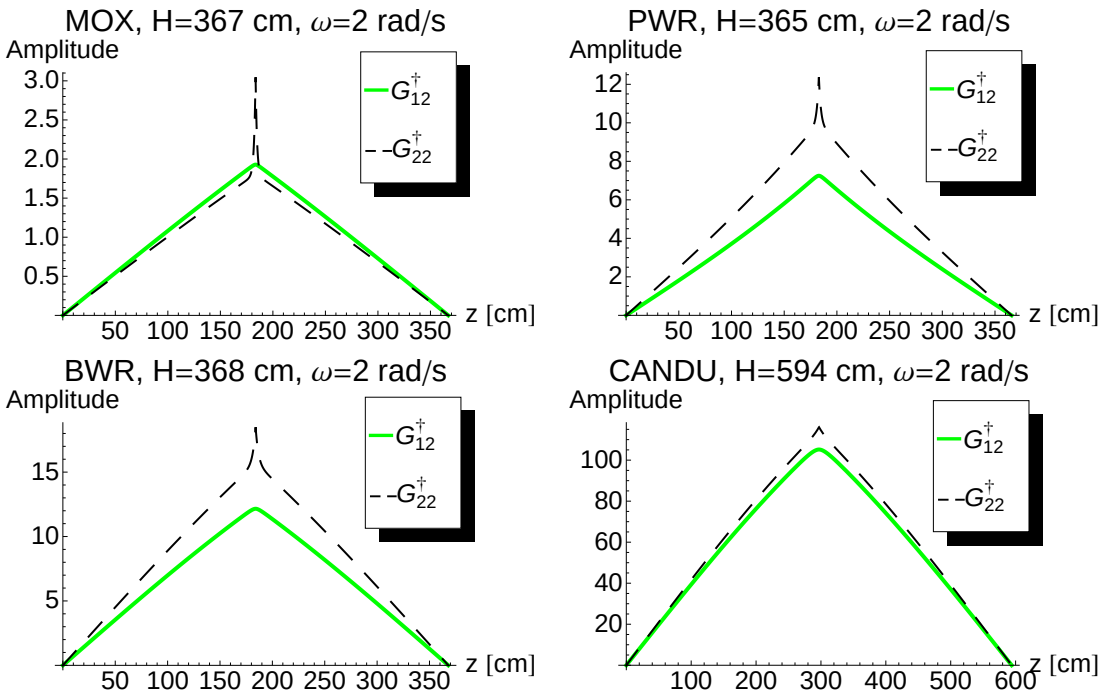

Figure 2.9: Space dependence of the amplitude of the components of the thermal adjoint: a MOX reactor (upper left figure), a PWR (upper right figure), a BWR (lower left figure) and a CANDU reactor (lower right figure) for $\omega = 2$ rad/s and $z' = H/2$.

cross-section is shown in Fig. 2.10 for all four cores investigated. The plots are similar to those of the one-group calculations given in Section 2.3.1 where a similar interference effect between the point-kinetic and space-dependent components leading to the oscillating behaviour of the total noise was observed. The spectral ratio between the fast and thermal neutron noise is similar to that of the static fluxes or of the corresponding Green's function components.

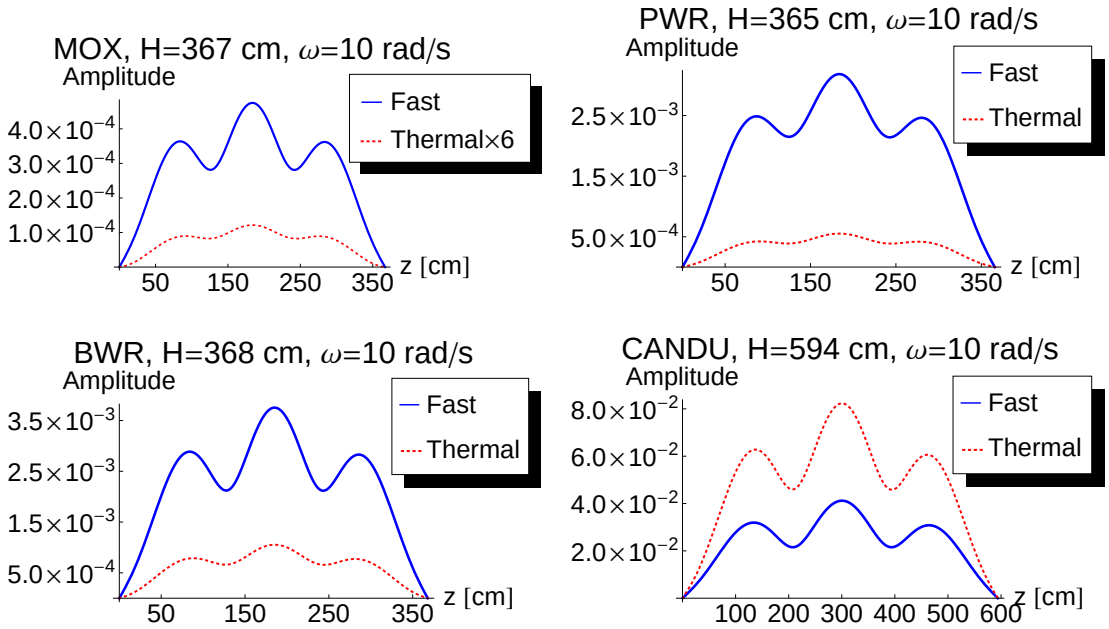

Figure 2.10: Space-dependence of the neutron noise induced by propagating perturbation of the thermal absorption cross-section only: in a MOX reactor (upper left figure), in a PWR (upper right figure), in a BWR (lower left figure) and in a CANDU reactor (lower right figure) for $\omega = 10$ rad/s and $v = H/2$ cm/s. For the MOX core, the thermal noise was multiplied by a factor 6 for better visibility.

Next, the space-dependence of the propagating noise as induced by perturbations of all cross-section is given in Fig. 2.11. As shown in **Paper II**, there are a number of interesting features which can be observed in the characteristics of the propagating noise demonstrated in Fig. 2.11. The fast noise looks similar to that of the previous case, whereas the thermal noise displays several differences. One of these is the case of the MOX where the oscillating structure of the thermal noise is changed, i.e. the maxima and the minima changed place and the spatial oscillations of the fast and the thermal noise are not the same any longer. The explanation is that when fluctuations of several cross-sections take place simultaneously, their effects add up with different signs and different weights in the resulting noise. The sign difference is simply due to the fact that different processes contribute differently to the neutron balance equation, i.e. the generation/destruction of the neutrons in the corresponding groups. The different weighting is related to the fact that the fast and thermal noise sources are contributing to the propagating noise via a weighting by the different components of the Green's function with different amplitudes.

Another interesting difference between Fig. 2.10 and Fig. 2.11 is that the thermal noise is much larger in the BWR than in the case of pure thermal absorption cross-section perturbations. This could be explained by the fact that an increase of the coolant tem-

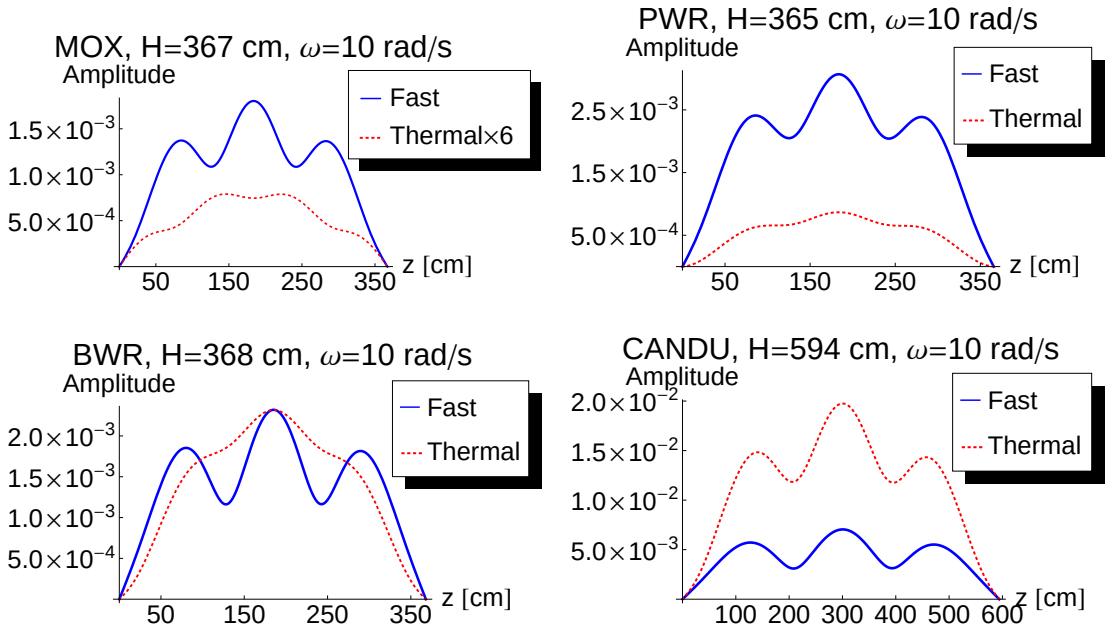

Figure 2.11: Space-dependence of the propagation noise induced by the fluctuations of all cross-sections in the four cores considered, for $\omega = 10$ rad/s and $v = H/2$ cm/s. For the MOX core, the thermal noise was multiplied by a factor 6 for better visibility.

perature leads to an increase of the void fraction, with the result that the change in the removal cross-section becomes larger than that of the thermal absorption cross-section. In its turn, perturbation of the removal cross-section affects the neutron noise much more than the fast noise. This is because in the thermal noise, the component due to the removal cross-section dominates over the noise induced by the other cross-section fluctuations. In the fast noise, the noise induced by the removal cross-section and the noise by the other cross-section fluctuations are of comparable magnitude but have an opposite phase. Thus, there is not any munificent increase of the amplitude observed in the case of the fast noise.

2.4 Qualitative analysis of the frequency dependence of the noise

In this final Section, the results of the investigation, similar to the one in the previous Section, but performed in the frequency domain for several fixed axial positions in the reactor core, as well as the corresponding numerically-simulated neutron noise, are demonstrated.

2.4.1 One-group calculations

In the left plot of Fig. 2.12 the frequency-dependence of the amplitude of the noise, induced by a propagating density perturbation is shown for two different axial core positions. It is clear that in both cases the point-kinetic behaviour dominates, showing a frequency dependence of the noise similar to that of the reactivity.

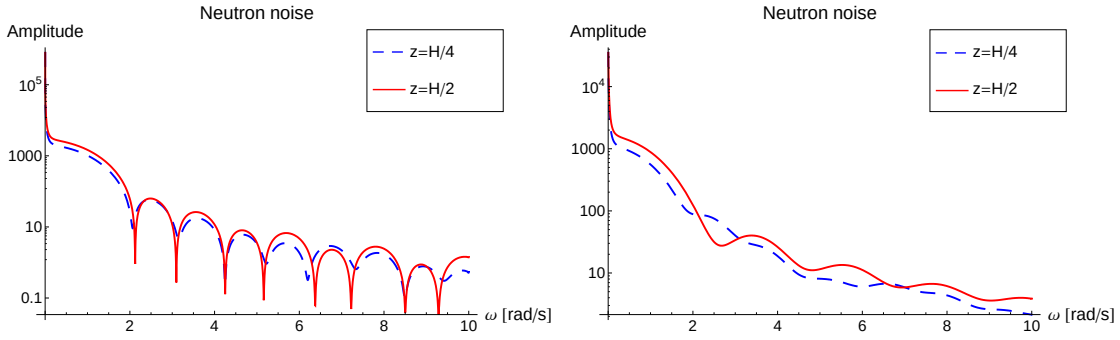

Figure 2.12: Amplitude of the frequency-dependence of the neutron noise for two axial positions in the core $z = 0.25H$ cm and $z = 0.5H$ cm, for $H = 50$ cm, $v = 8.3$ cm/s (left figure) and for $H = 200$ cm, $v = 33.3$ cm/s (right figure), respectively.

A more interesting result is shown in the right plot of Fig. 2.12 where a system with intermediate size was chosen. It is clear from the figure that for this case the total noise still keeps some point-kinetic behaviour, although in a definitely less pronounced way. For instance, for the different axial space points, the solution behaves differently. Namely, at some frequencies, the noise has maximum in both spatial points; at some other frequencies, it has maximum in one spatial point and a minimum in the other position.

This behaviour can be explained using the same approach as the one, applied in the interpretation of the space-dependence of the noise, and is due to the interference between the different noise components. Therefore, the amplitude and phase for both the total neutron noise and for each of its components are analyzed below. The corresponding results are shown in Fig. 2.13 for $z = H/2$.

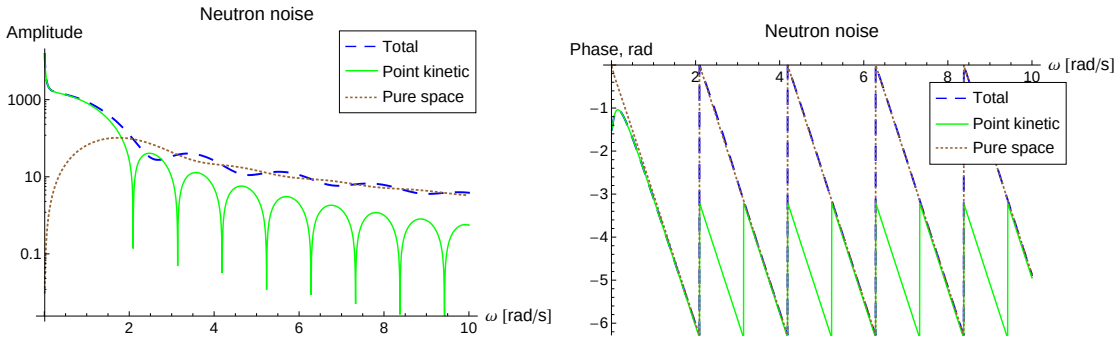

Figure 2.13: Amplitude and phase of the frequency-dependence of the neutron noise for $H = 200$ cm, $v = 33.3$ cm/s, $z = 0.5H$ cm.

From the right part of Fig. 2.13, where the frequency-dependence of the phase for the case $z = 0.5H$ is shown, one can notice that in every second interval between two sink frequencies the phases of the two components are equal, whereas in the alternating every second interval the phases of both terms are out-of-phase. This affects the amplitude of the total noise in such a way that at every second peak of the reactivity term the total noise has a maximum, otherwise it has a minimum. The corresponding study for the case of $z = 0.25H$ can be found in **Paper I**.

2.4.2 Two-group calculations

The same sequence will be followed here as for the space-dependence of the neutron noise in two-group theory discussed in Section 2.3.2, but this time the frequency-dependence of the neutron noise is investigated. First, the frequency-dependence of the amplitude of the propagating noise, induced by the perturbed thermal absorption cross-section is considered. The corresponding results are shown in Fig. 2.14. The frequency-dependence of the amplitude shows a similar structure as in Section 2.4.1, i.e. the periodic sink structure caused by periodic vanishing of the reactivity effect of the propagating perturbation. Several features of these spectra were also observed in similar calculations performed for MSR systems. One is the spectral ratio between the fast and thermal neutron noise. The other two features are the somewhat deeper sinks in the fast than in the thermal noise, and the slower decay of the spectra with increasing frequency in the thermal noise than in the fast. Both these features can be clarified by the fact that the thermal noise is affected by the presence of the strong local component, whereas the weight of the local component is vanishingly small in the transfer functions which are used to calculate the fast noise. Regarding the depth of the sinks, similarly to the pure space-dependent component, the local component does not have any sink structure, hence its presence makes the sinks shallower. The difference in the decay of the spectra of the different components with increasing frequency can be explained as being the consequence of the much slower decay of the local component than that of the global (due to different relaxation lengths between the global and local components) which are integrated with highly oscillating functions.

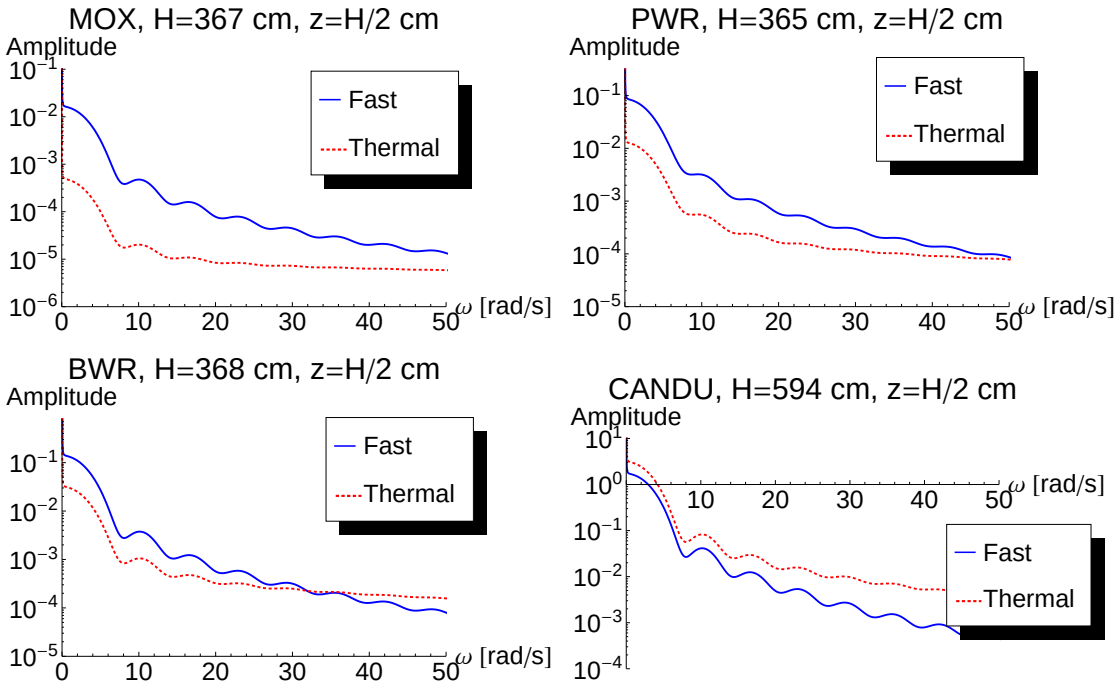

Figure 2.14: Frequency-dependence of the neutron noise induced by propagating temperature perturbation in absorption cross-section only in a MOX reactor (upper left figure), in a PWR (upper right figure), in a BWR (lower left figure) and in a CANDU reactor (lower right figure) for $z = H/2$ cm and $v = H/2$ cm/s.

The next step is the calculation of the propagating noise for the case when several cross-sections are simultaneously perturbed. The results are given in Fig. 2.15. The structure of these spectra is significantly more complicated and irregular than in the previous case, whereas some general properties such as the spectral dependence of the noise, less pronounced sink structures of the thermal noise, etc. are still preserved. However, the sink structure is much diminished and irregular even for the fast flux and there are some peculiar deep dips in either the fast or the thermal noise at a given frequency for all systems. The seemingly irregular sink structure and the single sinks in the spectra can all be explained by the interplay of different components of the noise, i.e. the contribution of various cross-section perturbations together with the presence of local and global components. More details are given in **Paper II**.

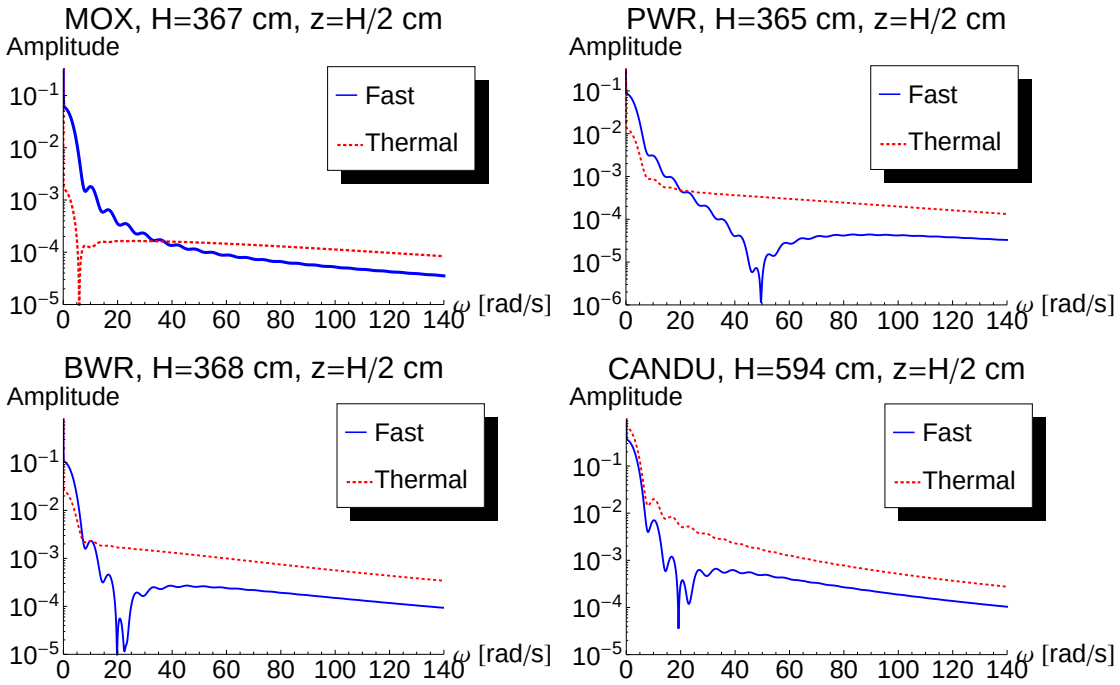

Figure 2.15: Frequency-dependence of the neutron noise induced by propagating temperature perturbation in a MOX (upper left figure), in a PWR (upper right figure), in a BWR (lower left figure) and in a CANDU reactor (lower right figure) for $z = H/2$ cm and $v = H/2$ cm/s.

2.4.3 Numerically simulated neutron noise

As a starting point, 1320 second-long void fraction signals are generated by the Monte-Carlo two-phase flow model described earlier. The measurements of the void fraction are performed at eight different axial levels within the same radial position. The corresponding normalized neutron noise is generated through the spatial convolution between the binary void fraction signals imitating the neutron noise source for the case of the propagating perturbation and the local component of the transfer function. The results of the simulation of the time-dependent behaviour of the neutron noise for the fourth axial level are shown in Fig. 2.16. The synthetic neutron noise looks quite similar to that obtained in real measurements with a clear stochastic character of the induced noise. Then, the

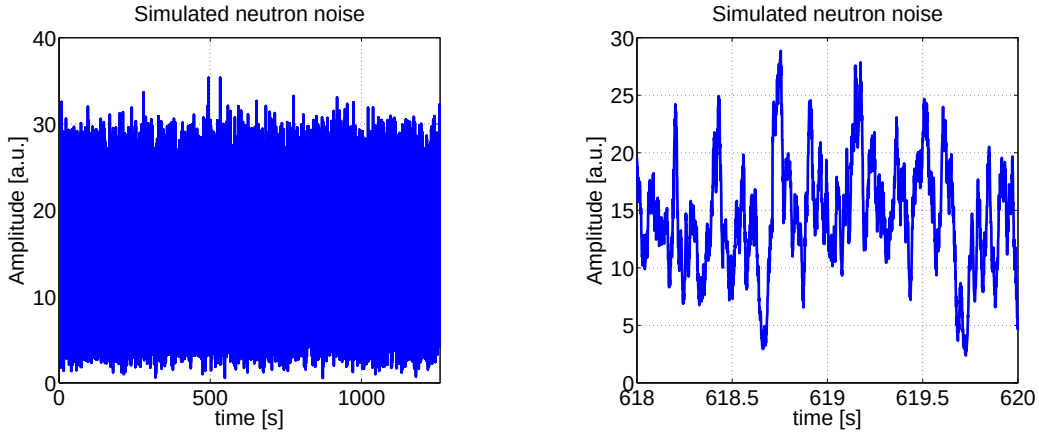

(a) Long time period (b) Short time period

Figure 2.16: Time-dependence of the neutron noise induced by the two-phase flow fluctuations as calculated from the Monte Carlo model for a long and a short time period, respectively.

spectral densities for each of eight detectors are calculated by using standard fast Fourier transform (FFT). The corresponding APSDs of the simulated neutron noise are shown in Fig. 2.17. The interesting feature, observed in all plots shown in Fig. 2.17 and at all axial levels, is the characteristic break of the APSDs, occurring at around 17 Hz which strongly depends on the axial position of the detector and monotonically increases with an increasing axial elevation. This break can be explained due to the finite velocity of the bubbles which acts as a low-pass filter for the neutron noise spectra. Likewise, the amplitude of the APSD for the first four cases also increases with an increasing axial position. One possible reason for such a behaviour of the APSD, is an axially-increasing void fraction as one elevates upwards along the heated channel. However, this is not the case for the last four points $z_d = 180,\ 210,\ 300$ and 380 cm. The results of the neutron noise, generated from this model, will be used in Chapter 4 in the elaboration of unfolding methods to determine the local void fraction.

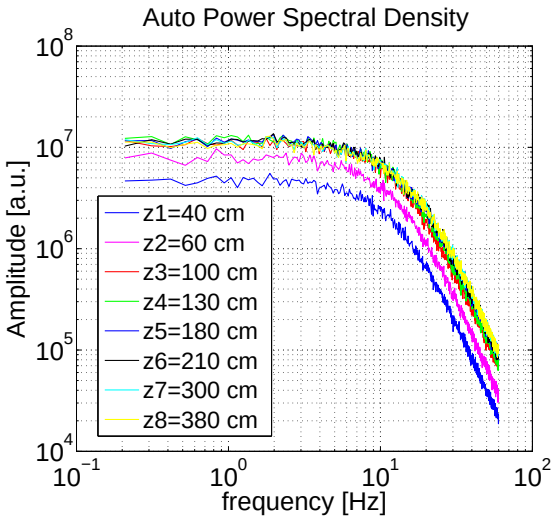

Figure 2.17: Normalized auto power spectral densities of the simulated in-core detector signals calculated for eight axial elevations $z_d = 40,\ 60,\ 100,\ 130,\ 180,\ 210,\ 300,\ 380$ cm, respectively.

Chapter 3

METHODS FOR MODELING THE EFFECT OF PROPAGATING PERTURBATION IN CLOSED-LOOP SYSTEMS

All the waste in a year from a nuclear power plant can be stored under a desk.
— Ronald Reagan

In the present Chapter, which is the summary of **Papers IV and V**, the neutron noise induced by propagating perturbations in closed-loop systems, i.e. in systems with feedback effect included, is analyzed. This Chapter only focuses on BWRs, where two feedback mechanisms, i.e. the Doppler and the void, are usually taken into account, providing the correct coupling between different aspects of physics involved, such as thermal hydraulics, neutron transport, etc. Since different physical phenomena in the reactor core act on different time-scales (i.e. have inherent time delays with respect to each other), such a coupling represents the main origin for instabilities in closed-loop systems, compared with open-loop ones where the properties of the system mainly depend on the properties of the transfer function (i.e. neutron-kinetic properties of the system). As a matter of fact, what regards the instabilities caused by propagating perturbations, the situation in closed-loop systems is much more involved and requires careful investigation. Therefore, to study the stability properties of such complex systems, it is instructive to construct simplified models, commonly named as reduced order models (ROMs). The main idea of a ROM development is to drastically reduce the complexity of the system geometry, but at the same time to preserve all main features of the BWR dynamics, in particular, the ones related to stability. The typical ROM consists of three submodels: the neutron-kinetics, heat transfer and thermal-hydraulics, thus, covering the most important fields of physics that govern BWR behaviour.

Here, the analysis is performed in two steps. First, the modeling of so-called core-wide instabilities including both the global and regional ones with ROMs, is considered [1]. For this purpose, a four heated channel ROM, taking into account the effect of fundamental and first two azimuthal modes, is constructed. It should be pointed out that for the correct representation of both azimuthal modes from the thermal-hydraulic point-of-view, at least four heated channels are necessary. As will be shown later on, the proper modeling of both azimuthal modes is important for reconstructing some in-

teresting features related to the non-linear properties of the system such as an oscillating symmetry line which was observed in several past measurements [32]. The present ROM is developed on the basis of earlier-developed ROMs [21, 25, 26] with some additional modifications implemented. One of them is related to a consistent ROM coupled calculation at steady-state. To achieve this, a special methodology which provides full consistency between the spatial discretization procedures used in the dynamical cases and the ones implemented in static cases is developed. For this purpose, the ROM is coupled to a 3D commercial core simulator in such a way that the balance equations (i.e. neutron flux, heat, mass, momentum and energy balance equations) could be fulfilled for the steady state solution of the coupled problem. In addition, a non-uniform power profile representing the separate heat sources in the single- and two-phase regions is incorporated into the ROM. Special attention is paid to the coupling coefficients for the reactivity effects related to both void fraction and fuel temperature which are explicitly calculated combining the cross-section data from the SIMULATE-3 [33] code and the different neutronic eigenmodes of the heterogeneous core from the CORE SIM tool [34]. A more detailed description is given in **Paper IV**.

Next, a methodology to include the effect of local instabilities into the ROM is investigated and discussed. The modeling of local instabilities with the ROM is a somewhat more challenging task than that of core-wide instabilities, whose modeling is relatively straightforward. The latter can be explained by the fact that any strongly localized phenomenon requires a high-order modal expansion of the neutron flux. As a result, in order to properly simulate any local instability, a very large number of modes should be included which is obviously not feasible for such a simple tool as a ROM. In the present study, another solution, based on the utilization of the spatial distribution of the local instability estimated from the CORE SIM tool is demonstrated. The proposed methodology is tested to model the effect of so-called density wave oscillations originating from the propagating character of the coolant density perturbations traveling along a single heated channel. As an event of interest for the demonstration of the ROM capability, the channel instability event that took place at the Forsmark-1 BWR in 1996/1997 is chosen [23, 28, 29]. This instability was presumably caused by several unseated fuel bundles, creating DWOs [30] and, hence, induced local power oscillations. More details can be found in **Paper V**.

3.1 Modeling of global and regional instabilities

A cursory description of a four heated channel reduced order model, consisting of three separate submodels for the neutron transport, heat transfer and flow transport is given. Some details regarding the development of the ROM are touched upon. Careful attention is payed to the new features implemented, compared to already existing models. Some results of the applications of the ROM to study core-wide instabilities are also discussed.

3.1.1 Neutron kinetic model

This Section gives a brief overview of the neutron-kinetic model, implemented in the ROM. First, the procedure, which is applied to derive the ordinary differential equations from the 3D partial differential reactor-dynamic equations and the assumptions which are needed to be made, are described. One starts with the three-dimensional time-

dependent two-energy group diffusion equations, written in the operator (matrix) form as [7,21]:

$$\bar{\bar{v}}^{*-1}\cdot\frac{\partial\bar{\Psi}^*(\bar{r}^*,t^*)}{\partial t^*}=[(1-\beta^*)\cdot\bar{\bar{F}}^*(\bar{r}^*,t^*)-\bar{\bar{L}}^*(\bar{r}^*,t^*)]\cdot\bar{\Psi}^*(\bar{r}^*,t^*)$$
$$+\sum_{l=1}^{6}\lambda_l^*\cdot C_l^*(\bar{r}^*,t^*)\cdot\bar{X}, \tag{3.1}$$

$$\frac{\partial C_l^*(\bar{r}^*,t^*)}{\partial t^*}\cdot\bar{X}=\beta_l^*\cdot\bar{\bar{F}}^*(\bar{r}^*,t^*)\cdot\bar{\Psi}^*(\bar{r}^*,t^*)-\lambda_l^*\cdot C_l^*(\bar{r}^*,t^*)\cdot\bar{X}, \tag{3.2}$$

where $\bar{\Psi}^*(\bar{r}^*,t^*)$ is the neutron flux vector which consists of the fast $\Psi_1^*(\bar{r}^*,t^*)$ and thermal $\Psi_2^*(\bar{r}^*,t^*)$ neutron fluxes, $\bar{\bar{L}}(\bar{r},t)$ is the net loss matrix operator, which represents the neutron leakage through diffusion, scattering and absorption, $\bar{\bar{F}}(\bar{r},t)$ is the fission production matrix operator, which represents the neutron production through fission reactions, $C_l^*(\bar{r}^*,t^*)$ is the concentration for the lth delayed neutron precursor group and $\bar{X}$ is a unit vector. The rest of the notations are standard. From now on, an asterisk stands for the dimensional quantities, otherwise they are considered to be dimensionless.

Applying first-order perturbation theory, namely assuming small fluctuations of the neutron flux $\bar{\Psi}^*(\bar{r}^*,t^*)$ and $C_l^*(\bar{r}^*,t^*)$ around their steady state values, due to perturbations in both the fission $\bar{\bar{F}}^*(\bar{r}^*,t^*)$ and net loss $\bar{\bar{L}}^*(\bar{r}^*,t^*)$ operators and taking into account static equations, the following equations for the fluctuating parts $\delta\bar{\Psi}^*(\bar{r}^*,t^*)$ and $\delta C_l^*(\bar{r}^*,t^*)$ can be obtained:

$$\bar{\bar{v}}^{*-1}\cdot\frac{\partial\delta\bar{\Psi}^*(\bar{r}^*,t^*)}{\partial t^*}=[(1-\beta^*)\cdot\delta\bar{\bar{F}}^*(\bar{r}^*,t^*)-\delta\bar{\bar{L}}^*(\bar{r}^*,t^*)]\cdot(\bar{\Phi}_0^*(\bar{r}^*)+\delta\bar{\Psi}^*(\bar{r}^*,t^*))$$
$$+\lambda\cdot\delta C_l^*(\bar{r}^*,t^*)\cdot\bar{X}+[(1-\beta^*)\cdot\bar{\bar{F}}_0^*(\bar{r}^*,t^*)-\bar{\bar{L}}_0^*(\bar{r}^*,t^*)]\cdot\delta\bar{\Psi}^*(\bar{r}^*,t^*), \tag{3.3}$$

$$\frac{\partial\delta C_l^*(\bar{r}^*,t^*)}{\partial t^*}\cdot\bar{X}=\beta^*\cdot\delta\bar{\bar{F}}^*(\bar{r}^*,t^*)\cdot(\bar{\Phi}_0^*(\bar{r}^*)+\delta\bar{\Psi}^*(\bar{r}^*,t^*))$$
$$-\lambda\cdot\delta C_l^*(\bar{r}^*,t^*)\cdot\bar{X}+\beta^*\cdot\bar{\bar{F}}_0^*(\bar{r}^*)\cdot\delta\bar{\Psi}^*(\bar{r}^*,t^*). \tag{3.4}$$

Next, one expands both the space-time dependent neutron flux $\delta\bar{\Psi}^*(\bar{r}^*,t^*)$, as well as the space-time dependent concentration of the delayed neutron precursors $\delta C_l^*(\bar{r}^*,t^*)$ in terms of lambda (reactivity) modes as:

$$\delta\bar{\Psi}^*(\bar{r}^*,t^*)=\sum_{n=0}^{\infty}\bar{P}_n^*(t^*)\cdot\bar{\Phi}_n^*(\bar{r}^*), \tag{3.5}$$

$$\delta C_l^*(\bar{r}^*,t^*)\cdot\bar{X}=\sum_{n=0}^{\infty}C_{nl}^*(t^*)\cdot\bar{\bar{F}}_0^*(\bar{r}^*)\cdot\bar{\Phi}_n^*(\bar{r}^*)\cdot\Lambda_n^*, \tag{3.6}$$

where $\bar{\Phi}_n^*(\bar{r}^*)$ is the eigenvector, satisfying the corresponding λ eigenvalue problem.

Substituting Eqs. (3.5) and (3.6) into Eqs. (3.3) and (3.4), multiplying the resulting equation by the adjoint eigenmode $\bar{\Phi}_m^{*\dagger}(\bar{r}^*)$, assuming one group of delayed neutron precursors, after integration and some rearrangements, one gets the following dimensionless point-kinetic equations:

$$\frac{dP_m(t)}{dt}=\frac{1}{\Lambda_m}(\rho_m^s-\beta)P_m(t)+\frac{1}{\Lambda_m}\sum_{n=0}^{2}\rho_{mn}^F(t)P_n(t)+\lambda C_m(t), \tag{3.7}$$

$$\frac{dC_m(t)}{dt} = \frac{\beta}{\Lambda_m} P_m(t) - \lambda C_m(t), \tag{3.8}$$

where $m = 0, 1, 2$ is the mode number, ρ_m^s is the static reactivity, ρ_{mn}^F are the dynamic feedback reactivities and $\Lambda_m = \Lambda_{mm}$ (for $m = 0$ Λ_m gives the prompt neutron generation time). The dynamic feedback reactivities ρ_{mn}^F reflect the feedback mechanism between the neutron kinetics and thermal-hydraulics in terms of void fraction and fuel temperature. In the linear approximation, the feedback reactivities for both void fraction and fuel temperature can be expressed, respectively, as:

$$\rho_{mn}^F(t) = \rho_{mn}^V(t)|_{T_f(t)=const} + \rho_{mn}^D(t)|_{\alpha(t)=const}$$

$$= \sum_{l=1}^{4} C_{mn,l}^V(\alpha_l(t) - \alpha_0) + \sum_{l=1}^{4} C_{mn,l}^D(T_{f,l}(t) - T_{f0}), \tag{3.9}$$

where l stands for the channel number and α_0 and T_{f0} are the steady-state void fraction and fuel temperature, correspondingly. The reactivity coupling coefficients $C_{mn,l}^{*V,T}$ were estimated numerically utilizing the cross-section data from SIMULATE-3 and spatial distribution of the eigenmodes from CORE SIM. A more detailed derivation can be found in **Paper IV**.

3.1.2 Heat transfer model

In the following, the main steps needed to be undertaken to convert the partial differential equations, describing the heat conduction in the fuel rod, into the corresponding ordinary differential equations, are described. The necessary assumptions and mathematical tricks which have to be applied to approach the final goal are also discussed. To begin with, the general three-dimensional time-/space-dependent energy balance equation, written for the single fuel rod reads as [20, 21]:

$$\rho^* c_p^* \frac{\partial}{\partial t^*} T^*(\bar{r}^*, t^*) = q^{*'''}(\bar{r}^*, t^*) - \bar{\nabla}^* \cdot \bar{q}^{*''}(\bar{r}^*, t^*), \tag{3.10}$$

where ρ^* is the density of the rod fuel, c_p^* is the specific heat of the fuel rod under constant pressure, $q^{*'''}(\bar{r}^*, t^*)$ is the volumetric heat production per unit time and per unit fuel rod volume, and $\bar{q}^{*''}(\bar{r}^*, t^*)$ is the heat flux from the fuel rod surface area.

Next, neglecting the axial heat conduction and assuming azimuthal symmetry, the fuel pellet temperature distribution can be approximated through two piece-wise quadratic spatial functions with time-dependent expansion coefficients, written as:

$$\Theta_p(r,t) = \begin{cases} T_1(t) + \eta_1(t) r + \eta_2(t) r^2 & \text{if} \quad 0 < r < r_d, \\ \\ T_2(t) + \sigma_1(t) r + \sigma_2(t) r^2 & \text{if} \quad r_d < r < r_p. \end{cases} \tag{3.11}$$

Here, one notes that the time dependent expansion coefficients $\eta_i(t)$ and $\sigma_i(t)$, $i = \overline{1,2}$ can be expressed through the $T_i(t)$, $i = \overline{1,2}$ and system (design) parameters, utilizing the discontinuity and boundary conditions.

Then, taking into account that there are three radial regions in the fuel rod (i.e. fuel pellet $0 < r < r_p$, fuel gap $r_p < r < r_g$ and fuel cladding $r_g < r < r_p$), after the

application of the variational principle, the following reduced differential equations for $T_i(t)$, describing the fuel rod conduction dynamics, are obtained:

$$\frac{dT_{1,l,j\phi}(t)}{dt} = p_{11,j\phi}T_{1,l,j\phi}(t) + p_{21,j\phi}T_{2,l,j\phi}(t) + p_{31,j\phi}c_q\sum_{i=0}^{2}\xi_i(P_i(t) - \widetilde{P}_i), \tag{3.12}$$

$$\frac{dT_{2,l,j\phi}(t)}{dt} = p_{12,j\phi}T_{1,l,j\phi}(t) + p_{22,j\phi}T_{2,l,j\phi}(t) + p_{32,j\phi}c_q\sum_{i=0}^{2}\xi_i(P_i(t) - \widetilde{P}_i), \tag{3.13}$$

where p_{ij} are complicated coefficients which depend on the design and operational parameters, $j\phi$ stands for the single- (1ϕ) or two-phase (2ϕ) regions, l is the channel number between 1 and 4, and $\widetilde{P}_0$ is the steady state value of the fundamental mode.

3.1.3 Thermo-hydraulic model

In this Section the description of the thermal-hydraulic model for our ROM is given. Since there are two axial coolant regions assumed in the channel, namely single-phase and two-phase regions, with a constant flow cross section, the description is performed in two separate sections, respectively. Within the scope of this Section, the procedure to transform the PDEs, describing thermal-hydraulic processes, into simplified ODEs, applying the variational method, is demonstrated.

Single-phase region

One starts with three local conservation equations written for mass, momentum and energy, respectively, as [20, 21]:

$$\frac{\partial\rho^*(\bar{r}^*,t^*)}{\partial t^*} + \bar{\nabla}^*\cdot(\rho^*\bar{v}^*)(\bar{r}^*,t^*) = 0, \tag{3.14}$$

$$\frac{\partial(\rho^*\bar{v}^*)}{\partial t^*}(\bar{r}^*,t^*) + \bar{\nabla}^*\cdot(\rho^*\bar{v}^*\otimes\bar{v}^*)(\bar{r}^*,t^*) = \bar{\nabla}^*\cdot\bar{\bar{\tau}}^*(\bar{r}^*,t^*) - \bar{\nabla}^*\cdot(P^*(\bar{r}^*,t^*)\bar{\bar{I}}) + \rho^*(\bar{r}^*,t^*)\bar{g}^*, \tag{3.15}$$

$$\frac{\partial(\rho^*e^*)(\bar{r}^*,t^*)}{\partial t^*} + \bar{\nabla}^*\cdot(\rho^*e^*\bar{v}^*)(\bar{r}^*,t^*) = -\bar{\nabla}^*\cdot\bar{q}^{*''}(\bar{r}^*,t^*) + \bar{q}^{*'''}(\bar{r}^*,t^*) + \bar{\nabla}^*\cdot(\bar{\bar{\tau}}^*\cdot\bar{v}^*)(\bar{r}^*,t^*) - \bar{\nabla}^*\cdot(P^*\bar{v}^*)(\bar{r}^*,t^*) + (\rho^*\bar{g}^*\cdot\bar{v}^*)(\bar{r}^*,t^*), \tag{3.16}$$

where $\otimes$ stands for the tensor multiplication and $\bar{\bar{I}}$ is the unit tensor.

Further, assuming the coolant flow mainly in the axial direction (i.e. neglecting the radial flow), the time-dependent single-phase enthalpy $h(z,t)$ can be expressed with a second order polynomial as:

$$h(z,t) \approx h_2(z,t) = h(0,t) + \sum_{i=1}^{2} p_i(t)z^i. \tag{3.17}$$

Then, rewriting the energy balance equation in terms of enthalpy, after cross-section averaging, the following dimensionless ODEs can be derived for the corresponding enthalpy time-dependent expansion coefficients $p_i(t)$ for each of four heated channels:

$$\frac{dp_{1,l}(t)}{dt} = \frac{6}{\mu_l(t)}[N_\rho N_r N_{pch,1\phi,l}(t) - v_{inlet,l}(t)p_{1,n}(t)] - 2v_{inlet,l}(t)p_{2,l}(t), \tag{3.18}$$

$$\frac{dp_{2,l}(t)}{dt} = -\frac{6}{\mu_l^2(t)}[N_\rho N_r N_{pch,1\phi,l}(t) - v_{inlet,l}(t)p_{1,l}(t)], \tag{3.19}$$

where N_r and N_ρ are dimensionless numbers, Fr is the Froude number and $N_{pch,1\phi}(t)$ is the so-called time dependent phase change number in the single-phase region which is proportional to the wall heat flux $q''^*_{1\phi}$ and $\mu(t)$ is the boiling boundary (the axial elevation in the reactor core where boiling starts).

Two-phase region

Following the procedure as in the single-phase region, one starts with the three local conservation equations written for mass, momentum and energy for each coolant phase region, respectively, as [20, 21]:

$$\frac{\partial \rho_k^*(\bar{r}^*, t^*)}{\partial t^*} + \bar{\nabla}^* \cdot (\rho_k^* \bar{v}_k^*)(\bar{r}^*, t^*) = 0, \tag{3.20}$$

$$\begin{aligned} &\frac{\partial(\rho_k^* \bar{v}_k^*)}{\partial t^*}(\bar{r}^*, t^*) + \bar{\nabla}^* \cdot (\rho_k^* \bar{v}_k^* \otimes \bar{v}_k^*)(\bar{r}^*, t^*) = \\ &\bar{\nabla}^* \cdot \bar{\bar{\tau}}^*(\bar{r}^*, t^*) - \bar{\nabla}^* \cdot (P_k^*(\bar{r}^*, t^*)\bar{\bar{I}}) + \rho_k^*(\bar{r}^*, t^*)\bar{g}^*, \end{aligned} \tag{3.21}$$

$$\begin{aligned} &\rho^*(\bar{r}^*, t^*)\frac{\partial h^*(\bar{r}^*, t^*)}{\partial t^*} + (\rho^* \bar{v}^*)(\bar{r}^*, t^*) \cdot \bar{\nabla}^* \cdot h^*(\bar{r}^*, t^*) = \\ &-\bar{\nabla}^* \cdot \bar{q}^{*''}(\bar{r}^*, t^*) + q^{*'''}(\bar{r}^*, t^*) + \bar{\bar{\tau}}^*(\bar{r}^*, t^*) : [\bar{\nabla}^* \otimes \bar{v}^*(\bar{r}^*, t^*)]\frac{\partial P^*(\bar{r}^*, t^*)}{\partial t^*} + \\ &+\bar{v}^*(\bar{r}^*, t^*) \cdot \bar{\nabla}^* P^*(\bar{r}^*, t^*), \end{aligned} \tag{3.22}$$

Here, $k = l, v$ stands for the coolant phase: l for the liquid phase and v for the vapor phase. Further, performing a radial space-averaging on the entire cross-sectional flow area, assuming that both phases are in thermal equilibrium (homogeneous equilibrium model), applying the mixture model and replacing the time-dependent flow quality with the following second order polynomial profile:

$$x(z,t) \approx x_2(z,t) = N_\rho N_r(d_1(t)(z - \mu(t)) + d_2(t)(z - \mu(t))^2). \tag{3.23}$$

and implementing the variational method to the resulting equations, after some rearrangements one gets the following dimensionless ODEs for the corresponding quality time-dependent expansion coefficients $d_i(t)$ for each of the four channels:

$$\frac{dd_{1,l}(t)}{dt} = \frac{1}{f_{2,l}(t)}(f_{3,l}(t)f_{1,l}(t) + f_{4,l}(t)), \tag{3.24}$$

$$\frac{dd_{2,l}(t)}{dt} = \frac{1}{f_{5,l}(t)}(f_{3,l}(t)f_{1,l}(t) + f_{6,l}(t)). \tag{3.25}$$

In the above, $f_i(t)$, $i = 1, ..., 6$ are complicated functions of time, depending on the design and operational parameters, as well as phase variables, i.e. inlet velocity $v_{inlet}(t)$, pellet temperature time-dependent coefficients $T_i(t)$, $i = 1, 2$, phase change number $N_{pch,2\phi}$, mixture density $\rho_m(z,t)$ and boiling boundaries $\mu(t)$.

The remaining two equations (3.15) and (3.21), written for the single- and two-phase pressure drops, are used to derive the ODEs for the inlet velocity, using the pressure drop balance and are not given here.

3.1.4 ROM modifications

In the following, the major modifications of the present ROM, compared to other existing ROMs developed in the past, are pointed out. These modifications were performed in order to improve the consistency of the ROM with the input data used and to better model the physical behaviour of instabilities. The list of the required input parameters for the ROM simulations are given below:

1. the design parameters of the system;
2. the thermal-hydraulic state variables, i.e. saturation temperature, densities, etc.;
3. the operational parameters or conditions, i.e. inlet flow, power, external pressure drop and inlet temperature/enthalpy.

Some of these parameters were extracted from the static core simulator SIMULATE-3 output, providing the detailed description of the BWR core. Others were taken from the technical description of a BWR power plant and water tables.

Adjustment of the homogeneous equilibrium model to a higher order model (drift flux model)

From the ROM analysis, it was found that the models currently used, where the homogeneous equilibrium model (HEM) [20,21] is utilized, significantly overestimate the void faction at the core exit, compared with the one calculated by SIMULATE-3. For comparison, both void fraction profiles are demonstrated in the left plot of Fig. 3.1. From the right plot of Fig. 3.1 where the results of the stability calculations performed with the ROM are shown, one can conclude that the investigated system is very close to an unstable behaviour, whereas a stable behaviour of the system was proven by system codes where the drift flux model (DFM) [20,25,26] is implemented.

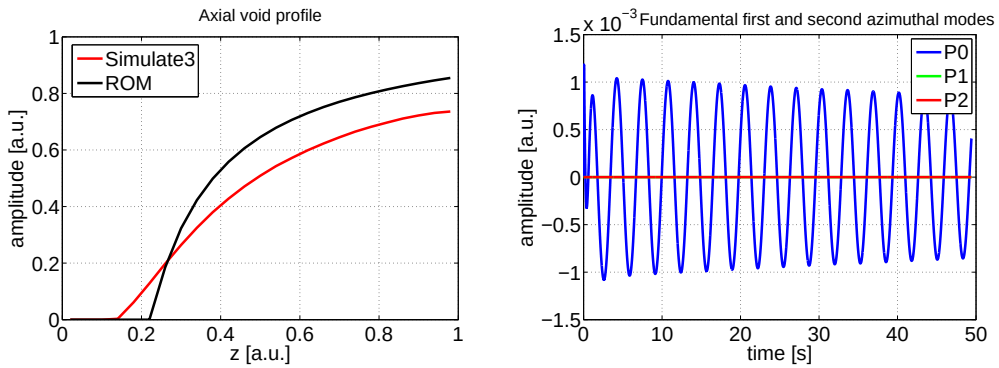

Figure 3.1: Axial void profile calculated by SIMULATE-3 (left figure, red line) and by the ROM (left figure, black line) and the corresponding ROM stability analysis (right figure) with the original value of cross-sectional flow area $A^*_{actual} = 1.3811 \cdot 10^{-4} m^2$.

To overcome this inconsistency between the HEM and the DFM and not to further complicate the ROM system, the cross-section flow area of the heated channel A^*_o was

artificially modified, so that the HEM can reproduce the void profile estimated by higher-order models such as the DFM. The new cross-section flow area was estimated by comparing the exit void fraction calculated from the ROM with HEM and the one from SIMULATE-3 with DFM, i.e. the following relationship between the old and the new cross-section flow areas was obtained:

$$A^*_{o,ROMadj} = \frac{\frac{1}{1+\frac{1-\alpha^*_{exit,ROM}}{\alpha^*_{exit,ROM}}\frac{\rho^*_l}{\rho^*_g}} \cdot (h^*_g - h^*_l) - h^*_{inlet} + h^*_l}{\frac{1}{1+\frac{1-\alpha^*_{exit,SIM}}{\alpha^*_{exit,SIM}}\frac{\rho^*_l}{\rho^*_g}} \cdot (h^*_g - h^*_l) - h^*_{inlet} + h^*_l} \cdot A^*_{o,SIM} \tag{3.26}$$

A more detailed derivation of Eq. (3.26) is given in **Paper IV**. The axial void profile as calculated from the ROM with adjusted cross-section flow area A^*_o is shown in Fig. 3.2 (left figure). Comparing the ROM stability analysis with the actual cross-sectional flow area A^*_{actual} [see Fig. 3.1, right figure] with the one performed with the adjusted flow area A^*_o [see Fig. 3.2, right figure], one can notice that the adjustment of the flow area stabilizes the system due to the reduction of the void fraction at the core outlet.

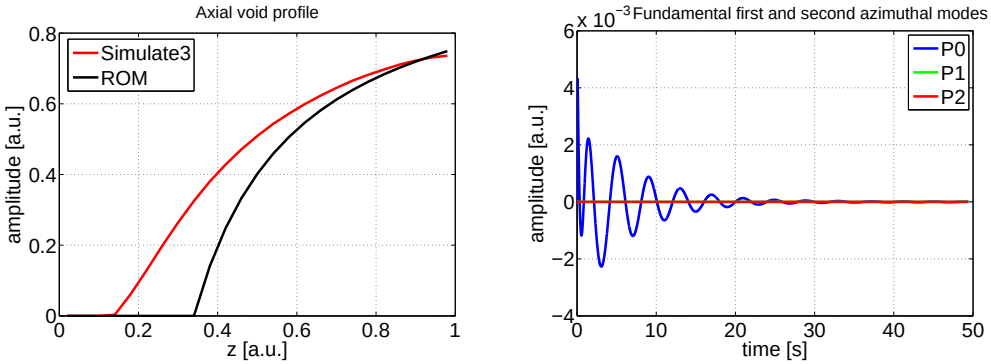

Figure 3.2: Axial void profile calculated by SIMULATE-3 (left figure, red line) and by the ROM with uniform power profile (left figure, black line) and result of the corresponding stability analysis (right figure) with the adjusted value of $A^*_o = 2.049 \cdot 10^{-4} m^2$.

Introduction of non-uniform power profile

Although the cross-section flow area utilized in the ROM was properly adjusted to compensate for the use of the HEM, there is still a big mismatch observed between the void profile as calculated by the ROM with the corrected A^*_o and the one calculated in SIMULATE-3. The reason for this mismatch can be explained by the fact that a uniform axial power profile was assumed when calculating the ROM void profile. However, in real commercial BWRs, the axial power profile is always bottom-peaked due to the better moderation properties of the subcooling region. For this reason, a two-step power density representing the separate power production in the single- and two-phase regions was introduced into the ROM. This was achieved by replacing the uniform power density c^*_q with non-uniform ones $c^*_{q,1}$ and $c^*_{q,2}$ for the single- and two-phase regions, respectively, utilizing the realistic axial power profile from the 3D core simulator CORE SIM. The numerical method for estimating $c^*_{q,1}$ and $c^*_{q,2}$ is presented in **Paper IV**.

Iterative procedure for steady-steady state calculations

It is worth mentioning that the steady-state solution available from a commercial core simulator together with all necessary input data and parameters for the calculations, cannot be directly used in the ROM since such a steady-state solution will not satisfy the corresponding ROM balance equations, i.e. neutron, heat and flow balance equations. The reason lies with the fact that the ROM equations are fundamentally different from the ones used in core simulators, especially what regards the spatial discretization. Consequently, a steady-state solution consistent with models implemented in the ROM has to be found. For this purpose, an iterative procedure was developed to estimate the proper steady-state solution. A short description of this procedure is given below.

From the steady-state solution obtained from a commercial core simulator (i.e. SIMULATE-3), the three-dimensional distributions of the macroscopic cross-sections were obtained together with their relative changes due to either void fraction or fuel temperature perturbations. These cross-section distributions were consequently used in CORE SIM to calculate the static flux. Afterwards, using the boiling boundary estimated from the commercial core simulator SIMULATE-3, the CORE SIM solution was used to estimate the power produced in the single- and two-phase regions. Then, the dimensionless heat transfer equations were correspondingly modified in order to account for a non-uniform power profile.

Next, the fuel temperature and flow properties were estimated using the ROM thermal hydraulic model at the steady-state. Based on the computed thermal-hydraulic solution, a new set of cross-sections as well as a new boiling boundary were calculated. The process is then repeated until convergence. The results of the iterative procedure for estimating the steady-state axial void profile are given in Fig. 3.3. It can be noticed that the recalculated steady-state profile satisfactorily agrees with the SIMULATE-3 solution.

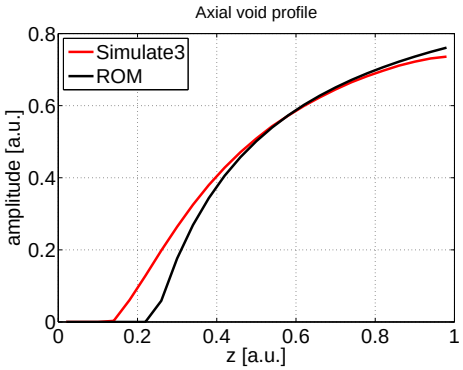

Figure 3.3: Axial void profile calculated by SIMULATE-3 (red line) and by the ROM (black line) for the nonuniform power profile after application of the recalculation procedure (update of the cross-sections).

3.1.5 Analysis of the numerical results

In this Section, some of the results of the numerical integration of the resulting 42 ROM ODEs, describing the dynamical behaviour of a BWR, are demonstrated. A large number of calculations were made from various artificial operational conditions, out of which

only the most interesting ones are shown and discussed below. The term artificial refers to the fact that one of the parameters of the system, namely the cross-sectional flow area A_o^* was adjusted in such a way that it is possible to simulate different oscillating patterns keeping the other parameters as typical ones for a BWR. The present investigation is mainly focused on the qualitative comparison of the ROM results for different operational points, just to demonstrate the capabilities of the ROM to reconstruct different stability behaviour. Emphasis is put on the coupling between different modes.

Depending on the stability properties of the modes, the following three cases were investigated:

1. both the fundamental and azimuthal modes are stable;
2. the fundamental mode is unstable and the azimuthal modes are stable;
3. both the fundamental and azimuthal modes are unstable (combined instability).

The first two cases (1 and 2) are somewhat trivial ones since they have already been studied intensively in the past and can easily be simulated with two heated channel ROM. The detailed investigation of both cases is given in **Paper IV**. Therefore, here, only the case of a combined instability (the 3rd case), when all three modes are unstable, is discussed. The cross-sectional flow area of the channel was chosen equal to $A_o^* = 1.8 \cdot 10^{-4}\ m^2$. In order to excite both azimuthal modes, several additional modifications of the system parameters were made, namely the criticality of the azimuthal modes was set to zero and some of the reactivity coefficients $C_{mn}^{*V,D}$ were properly adjusted. Such modifications were required by the fact that the investigated operating point did not exhibit any azimuthal instabilities and, hence, such instabilities should be introduced artificially.

For illustration, the time evolution of each of the modes is shown in Fig. 3.4. These figures clearly demonstrate the proper excitation of the in-phase and out-of-phase oscillations. The time evolution of the inlet velocities for the corresponding heated channels is also given in Fig. 3.5. From Fig. 3.5 it is clear that two (the first and the third channels) out of four heated channels oscillate out-of-phase compared with the other two (the second and the fourth), thus representing the time-dependent behaviour of the dominant (second) azimuthal mode. Thus, the stability behaviour in this particular case is driven by the second azimuthal mode. However, the effect of the other two modes is also significant. The time evolution of the corresponding inlet velocities for each of the four channels can be found in **Paper IV**. It is interesting to compare the current case with earlier cases reported in the literature. For this purpose, in Fig. 3.6 the time evolution of all three modes for four different cases (A, B, C and D) of mode inclusion is shown. The inclusion of different modes was performed by proper adjustment of the reactivity coefficients $C_{mn}^{*V,D}$. From Fig. 3.6 several interesting features can be observed. In the first case (Case A) where the effect of the first azimuthal mode is excluded (upper left plot of Fig. 3.6), the fundamental mode exhibits monotonically oscillating behaviour with an amplitude 3 times less than the corresponding second azimuthal mode. On the other hand, in the second case (Case B) where the effect of the second mode is excluded (upper right plot of Fig. 3.6), the behaviour of the fundamental mode is not so monotonic, namely it exhibits regular phase jumps of 180° with amplitude 5 times less compared with the first azimuthal mode. Such a peculiar behaviour can be clarified by the different values of the $C_{mn}^{*V,D}$ coefficients corresponding to different modes. From the comparison between these two cases (A and B) and Case C (lower left plot of Fig. 3.6) where both azimuthal

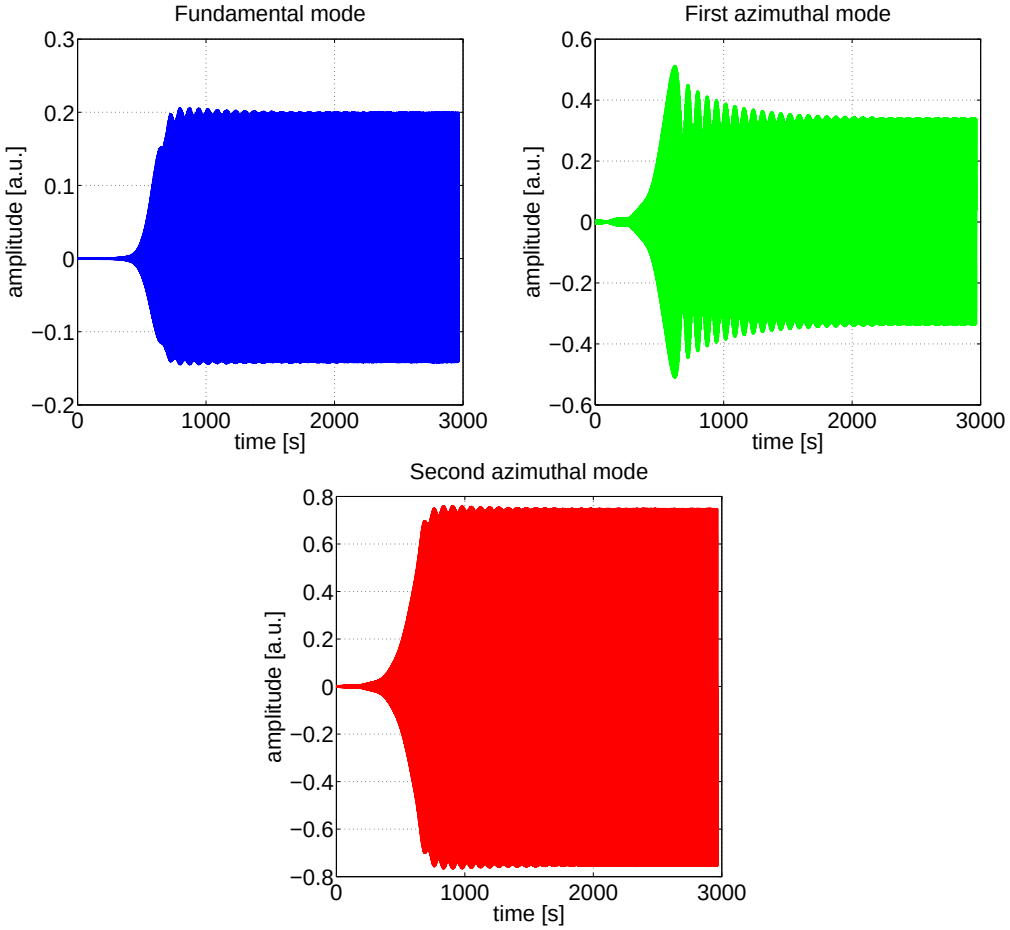

Figure 3.4: Time evolutions of the fundamental (upper left figure), the first (upper right figure) and the second (lower figure) azimuthal modes for the case of combined instability, $\rho_{s1} = \rho_{s2} = 0$, modified reactivity coefficients $C_{mn}^{*V,D}$, $A_o^* = 1.8 \cdot 10^{-4}\ m^2$, $\delta v_{inlet} = 0.1\ [a.u.]$.

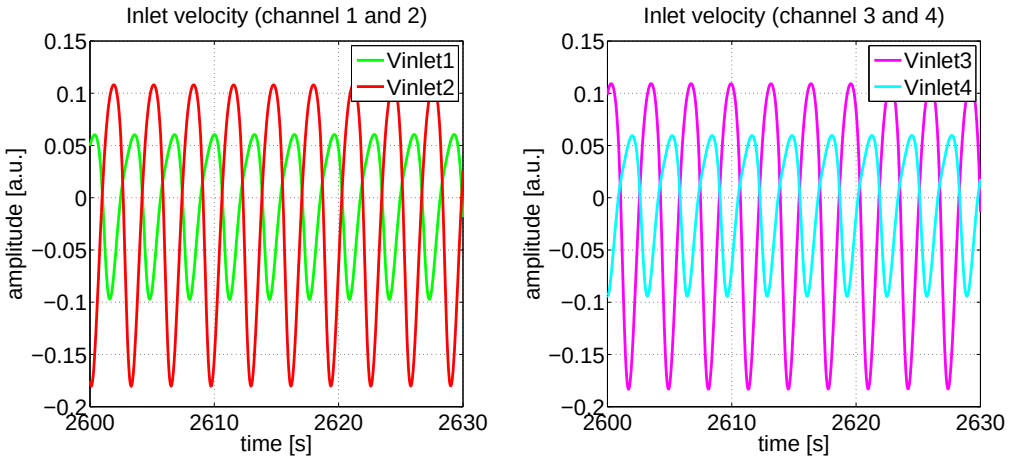

Figure 3.5: Time evolutions of the inlet velocities for the first/second (left figure) and third/fourth (right figure), respectively, heated channels for the case of combined instability, $\rho_{s1} = \rho_{s2} = 0$, modified reactivity coefficients $C_{mn}^{*V,D}$, $A_o^* = 1.8 \cdot 10^{-4}\ m^2$, $\delta v_{inlet} = 0.1\ [a.u.]$.

modes are excluded, it can also be concluded that the inclusion of the azimuthal modes decreases the amplitude of the fundamental mode almost four times. More details can be found in **Paper IV**.

An even more remarkable case is when both azimuthal modes are included simultaneously as shown in the lower right plot of Fig. 3.6 (Case D). Comparing this case with the first two cases discussed above (Cases A and B), one can notice that in the studied case the amplitude of the first azimuthal mode decreases by increasing the amplitude of the other two modes (the fundamental and the second azimuthal modes). Such interference effects between different modes are of particular importance since they affect the stability characteristics of each of the modes and thus, can lead to an incorrect determination of the stability boundaries. Moreover, from this simple analysis one can demonstrate that the inclusion of different azimuthal modes also results in earlier or delayed excitation of the fundamental mode.

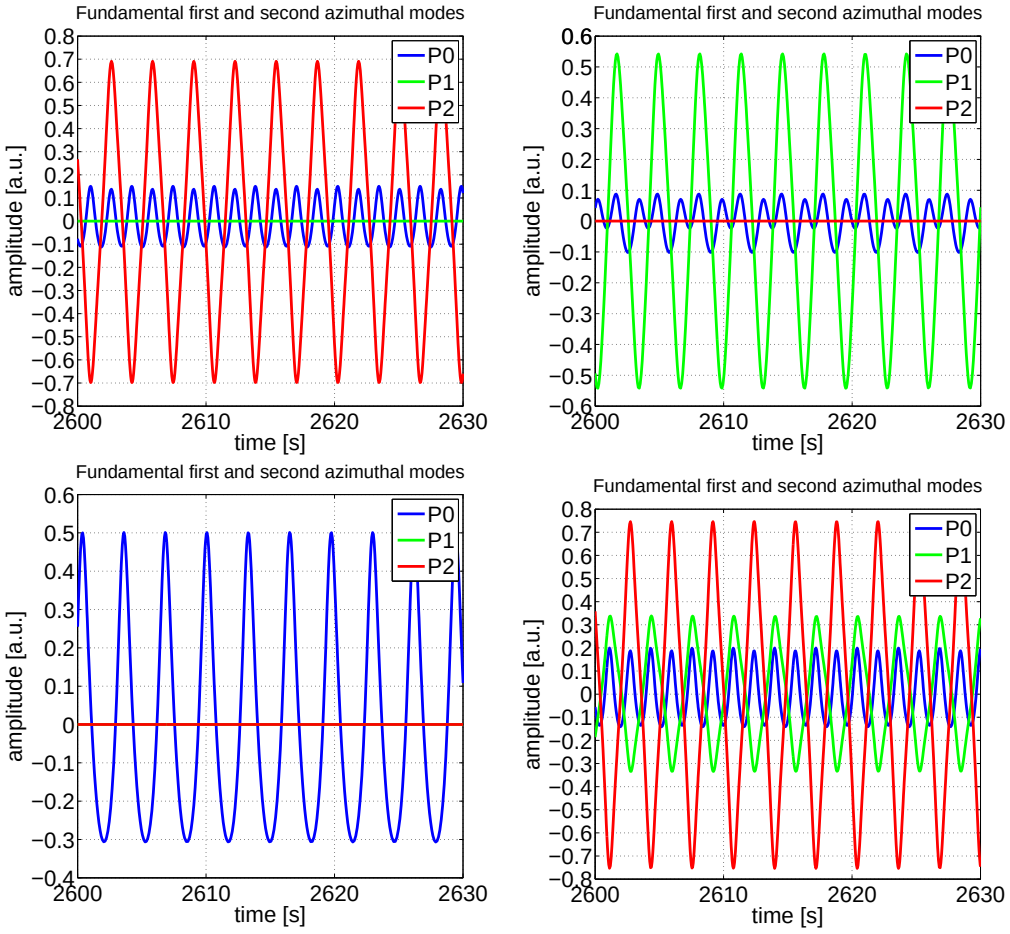

Figure 3.6: Time evolutions of the fundamental, the first and the second azimuthal modes for the case of combined instability, $\rho_{s1} = \rho_{s2} = 0$, modified reactivity coefficients $C^{*V,D}_{mn}$, $A^*_o = 1.8 \cdot 10^{-4}\ m^2$, $\delta v_{inlet} = 0.1\ [a.u.]$; case A - upper left figure, case B - upper right figure, case C - lower left figure and case D - lower right figure (the first azimuthal mode is not visible due to its smallness compared with the other two modes).

To conclude this investigation, another interesting phenomenon, namely the oscillating symmetry line between the first two azimuthal modes, modeled with the present

ROM, is discussed. The oscillating symmetry line has already been observed in some past instability events and several possible explanations of this phenomenon were proposed. Such an oscillating pattern is usually observed when both azimuthal modes are excited and oscillate with close frequencies. This difference in the frequencies thus creates a time-dependent phase shift between the modes resulting in the oscillating symmetry line. Intuitively, it is clear that in order to simulate such a behaviour, the properties of the heated channels should be different. For this reason, in the ROM, the inlet *k*-losses (pressure loss coefficients) were modified resulting in different flow rates in each channel and creating the oscillating pattern. The result of this simulation is given in Fig. 3.7. It should be emphasized that such a time-dependent phase shift between the modes can also lead to an incorrect determination of the stability properties.

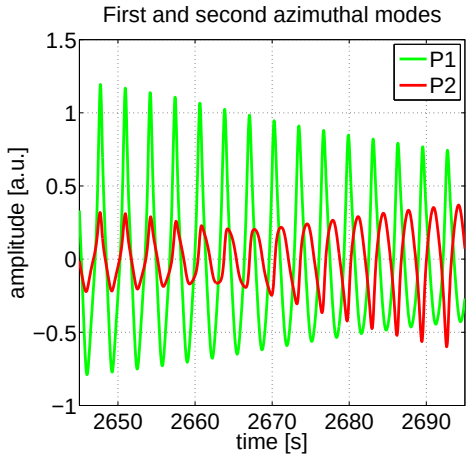

Figure 3.7: Time evolutions of the first and the second azimuthal modes for the case of combined instability, $\rho_{s1} = \rho_{s2} = 0$, modified inlet pressure loss coefficients k_{inlet} and reactivity coefficients $C_{mn}^{*V,D}$, $A_o^* = 1.8 \cdot 10^{-4}\ m^2$, $\delta v_{inlet} = 0.1\ [a.u.]$.

3.2 Modeling of local instabilities

A methodology used to model the effect of local instabilities (in particular, the ones caused by density wave oscillations) in reduced order models is described. The modified ROM is hereafter applied to analyze a realistic local instability event, i.e. the Forsmark-1 instability event of 96/97. A quantitative comparison between the ROM-simulated results and the corresponding power plant stability measurements is performed, out of which some conclusions are drawn.

3.2.1 ROM modifications to account for the effect of local instabilities

Throughout this study, it is assumed that the DWOs are self-sustained and only their effect on the stability properties of the system is investigated. The effect of the core response on the DWOs is thus neglected. Following similar steps as in the case of core-wide instabilities, one starts with the general time- and space-dependent two-group diffusion equations which, after the application of first order perturbation theory (i.e. considering small fluctuations of all quantities around their mean values), can be converted to the

following noise equations (i.e. equations for the fluctuating parts):

$$\bar{\bar{v}}^{*-1}\cdot\frac{\partial\delta\bar{\Psi}^{*}(\bar{r}^{*},t^{*})}{\partial t^{*}}=[(1-\beta^{*})\cdot\delta\bar{\bar{F}}^{*}(\bar{r}^{*},t^{*})-\delta\bar{\bar{L}}^{*}(\bar{r}^{*},t^{*})]\cdot(\bar{\Phi}_{0}^{*}(\bar{r}^{*})+\delta\bar{\Psi}^{*}(\bar{r}^{*},t^{*}))$$

$$+[(1-\beta^{*})\cdot\bar{\bar{F}}_{0}^{*}(\bar{r}^{*},t^{*})-\bar{\bar{L}}_{0}^{*}(\bar{r}^{*},t^{*})]\cdot\delta\bar{\Psi}^{*}(\bar{r}^{*},t^{*})+\lambda\cdot\delta C^{*}(\bar{r}^{*},t^{*})\cdot\bar{X}, \tag{3.27}$$

$$\frac{\partial\delta C^{*}(\bar{r}^{*},t^{*})}{\partial t^{*}}\cdot\bar{X}=\beta^{*}\cdot\delta\bar{\bar{F}}^{*}(\bar{r}^{*},t^{*})\cdot(\bar{\Phi}_{0}^{*}(\bar{r}^{*})+\delta\bar{\Psi}^{*}(\bar{r}^{*},t^{*}))+\beta^{*}\cdot\bar{\bar{F}}_{0}^{*}(\bar{r}^{*})\cdot\delta\bar{\Psi}^{*}(\bar{r}^{*},t^{*})$$

$$-\lambda\cdot\delta C^{*}(\bar{r}^{*},t^{*})\cdot\bar{X}. \tag{3.28}$$

Eqs. (3.27)-(3.28) describe the system response to any type of perturbations including both the ones induced by core-wide and the ones induced by local perturbations. However, one can study the effect of each perturbation separately using a similar approach in each case. That can be achieved by introducing the corresponding noise sources into the cross-section operators $\delta\bar{\bar{F}}^{*}$ and $\delta\bar{\bar{L}}^{*}$, i.e.

$$\delta\bar{X}\bar{\bar{S}}^{*}(\bar{r}^{*},t^{*})=\delta\bar{X}\bar{\bar{S}}^{*h}(\bar{r}^{*},t^{*})+\delta\bar{X}\bar{\bar{S}}^{*i}(\bar{r}^{*},t^{*}), \tag{3.29}$$

which give rise to the corresponding fluctuations in the neutron fluxes written as:

$$\delta\bar{\Psi}^{*}(\bar{r}^{*},t^{*})=\delta\bar{\Psi}^{*h}(\bar{r}^{*},t^{*})+\delta\bar{\Psi}^{*i}(\bar{r}^{*},t^{*}), \tag{3.30}$$

$$\delta C^{*}(\bar{r}^{*},t^{*})=\delta C^{*h}(\bar{r}^{*},t^{*})+\delta C^{*i}(\bar{r}^{*},t^{*}), \tag{3.31}$$

where i stands for inhomogeneous (i.e. local oscillations) and h for homogeneous (core-wide oscillations). The solution of this kind of problem can be found by first determining the response of the core to a pure local oscillations $\delta\bar{\Psi}^{*i}(\bar{r}^{*},t^{*})$, i.e. solving the inhomogeneous problem (derived from Eqs. (3.27)-(3.28)) defined as:

$$\bar{\bar{v}}^{*-1}\cdot\frac{\partial\delta\bar{\Psi}^{*i}(\bar{r}^{*},t^{*})}{\partial t^{*}}=[(1-\beta^{*})\cdot\delta\bar{\bar{F}}^{*i}(\bar{r}^{*},t^{*})-\delta\bar{\bar{L}}^{*i}(\bar{r}^{*},t^{*})]\cdot\bar{\Phi}_{0}^{*}(\bar{r}^{*})$$

$$+[(1-\beta^{*})\cdot\bar{\bar{F}}_{0}^{*}(\bar{r}^{*},t^{*})-\bar{\bar{L}}_{0}^{*}(\bar{r}^{*},t^{*})]\cdot\delta\bar{\Psi}^{*i}(\bar{r}^{*},t^{*})+\lambda^{*}\cdot\delta C^{*i}(\bar{r}^{*},t^{*})\cdot\bar{X}, \tag{3.32}$$

$$\frac{\partial\delta C^{*i}(\bar{r}^{*},t^{*})}{\partial t^{*}}\cdot\bar{X}=\beta^{*}\cdot\delta\bar{\bar{F}}^{*i}(\bar{r}^{*},t^{*})\cdot(\bar{\Phi}_{0}^{*}(\bar{r}^{*})+\delta\bar{\Psi}^{*i}(\bar{r}^{*},t^{*}))+\beta^{*}\cdot\bar{\bar{F}}_{0}^{*}(\bar{r}^{*})\cdot\delta\bar{\Psi}^{*i}(\bar{r}^{*},t^{*})$$

$$-\lambda^{*}\cdot\delta C^{*i}(\bar{r}^{*},t^{*})\cdot\bar{X}, \tag{3.33}$$

where the second order terms were left out. The general solution of Eqs. (3.32)-(3.33) can be found by assuming delta-function (localized) perturbations in the cross-sections and, thus reads as:

$$\delta\bar{\Psi}^{*i}(\bar{r}^{*},t^{*})=\bar{\bar{B}}^{*}\cdot\exp^{i\omega^{*}t^{*}}\cdot\bar{\psi}^{*i}(\bar{r}^{*},\bar{r}_{0}^{*},\omega^{*}), \tag{3.34}$$

$$\delta C^{*i}(\bar{r}^{*},t^{*})\cdot\bar{X}=\bar{\bar{C}}^{*}\cdot\exp^{i\omega^{*}t^{*}}\cdot\bar{\psi}^{*i}(\bar{r}^{*},\bar{r}_{0}^{*},\omega^{*}), \tag{3.35}$$

where $\bar{r}_{0}^{*}$ stands for the location of the local perturbation in the cross-sections, and $\bar{\bar{A}}^{*}$, $\bar{\bar{B}}^{*}$ and $\bar{\bar{C}}^{*}$ are matrix coefficients. Combining Eqs. (3.34)-(3.35) with Eqs. (3.32)-(3.33), one gets the explicit solutions for the neutron flux $\delta\bar{\Psi}^{*i}(\bar{r}^{*},t^{*})$ and the concentration of the delayed neutron precursors $\delta C^{*i}(\bar{r}^{*},t^{*})$ of the inhomogeneous problem (3.32)-(3.33).

Next, subtracting the result, i.e. Eqs. (3.32)-(3.33) with known solutions (3.34)-(3.35) from the generic equations (3.27)-(3.28) and neglecting small terms, one obtains the equation for the homogeneous problem $\delta\bar{\Psi}^{*h}(\bar{r}^*, t^*)$ given as:

$$\bar{\bar{v}}^{*-1} \cdot \frac{\partial \delta\bar{\Psi}^{*h}(\bar{r}^*, t^*)}{\partial t^*} = [(1-\beta^*) \cdot \delta\bar{\bar{F}}^{*h}(\bar{r}^*, t^*) - \delta\bar{\bar{L}}^{*h}(\bar{r}^*, t^*)] \cdot (\bar{\Phi}_0^*(\bar{r}^*) + \delta\bar{\Psi}^{*h}(\bar{r}^*, t^*))$$

$$+[(1-\beta^*) \cdot \bar{\bar{F}}_0^*(\bar{r}^*, t^*) - \bar{\bar{L}}_0^*(\bar{r}^*, t^*)] \cdot \delta\bar{\Psi}^{*h}(\bar{r}^*, t^*) + \lambda^* \cdot \delta C^{*h}(\bar{r}^*, t^*) \cdot \bar{X}, \tag{3.36}$$

$$\frac{\partial \delta C^{*h}(\bar{r}^*, t^*)}{\partial t^*} \cdot \bar{X} = \beta^* \cdot \delta\bar{\bar{F}}^{*h}(\bar{r}^*, t^*) \cdot (\bar{\Phi}_0^*(\bar{r}^*) + \delta\bar{\Phi}^{*h}(\bar{r}^*, t^*))$$

$$+\beta^* \cdot \bar{\bar{F}}_0^*(\bar{r}^*) \cdot \delta\bar{\Psi}^{*h}(\bar{r}^*, t^*) - \lambda^* \cdot \delta C^{*h}(\bar{r}^*, t^*) \cdot \bar{X}, \tag{3.37}$$

where $\delta\bar{\Psi}^{*h}(\bar{r}^*, t^*)$ and $\delta C^{*h}(\bar{r}^*, t^*)$ are defined as:

$$\delta\bar{\Psi}^{*h}(\bar{r}^*, t^*) = (\delta\bar{\Psi}^* - \delta\bar{\Psi}^{*i})(\bar{r}^*, t^*),$$

$$\delta C^{*h}(\bar{r}^*, t^*) = (\delta C^* - \delta C^{*i})(\bar{r}^*, t^*).$$

The solution of Eqs. (3.37)-(3.38) can be found by applying traditional mode expansion, similarly to the one used in earlier calculations. Thus, taking only the first three eigenmodes of the flux expansion into account, the full solution to Eqs. (3.27)-(3.28) is given as:

$$\delta\bar{\Psi}^*(\bar{r}^*, t^*) = \sum_{n=0}^{2} \bar{\bar{P}}_n^*(t^*) \cdot \bar{\Phi}_n^*(\bar{r}^*) + \sum_{k=1}^{N_s} \bar{\bar{B}}_k^* \cdot \exp^{i\omega_k^* t^*} \cdot \bar{\psi}_k^*(\bar{r}^*, \bar{r}_0^*, \omega_k^*), \tag{3.38}$$

where $\bar{\Phi}_n^*(\bar{r}^*)$ is the solution of the corresponding eigenfunction problem, k stands for an index representing a local source and N_s is the total number of local sources in the investigated problem.

It is interesting to point out that, from a mathematical point-of-view, Eqs. (3.36)-(3.37) look exactly the same as the ones solved for the case of pure homogeneous (core-wide) perturbations (see Section 3.1.1) since no explicit presence of local sources can be observed. On the other hand, from a physical point-of-view, the effect of local perturbations is taken into account implicitly via the feedback term $[(1-\beta^*) \cdot \delta\bar{\bar{F}}^{*h}(\bar{r}^*, t^*) - \delta\bar{\bar{L}}^{*h}(\bar{r}^*, t^*)] \cdot \delta\bar{\Psi}^{*h}(\bar{r}^*, t^*)$ where the effect of both the core-wide and local sources is included.

In addition, from Eq. (3.38), one can also conclude that the presence of the local sources simply leads to some extra heating terms in the power oscillations due to the change of the cross-sections resulting from the neutron noise induced by a DWO.

To sum it up, since the power oscillations strongly influence the fuel temperature, one only needs to modify the heat transfer equations to correctly simulate the effect of local perturbations in the ROM compared with the case of core-wide instabilities. The remaining of the ROM can be kept unchanged. The corresponding changes in the fuel temperature and of the resulting void production will induce perturbations in cross-sections, expressed as $\delta\bar{\bar{F}}^{*h}$ and $\delta\bar{\bar{L}}^{*h}$, thus creating an additional thermal-hydraulic feedback effect in the neutron-kinetic model mentioned earlier. Thus, the modified heat transfer equations with the effect of local instabilities included, read as:

$$\frac{dT_{1,l,j\phi}(t)}{dt} = p_{11,j\phi} T_{1,l,j\phi}(t) + p_{21,j\phi} T_{2,l,j\phi}(t)$$

$$+p_{31,j\phi}[c_q(P_{0,j}(t)-\widetilde{P}_{0,j})+c_q\xi_1P_{1,j}(t)+c_q\xi_2P_{2,j}(t)+c_q\sum_{k=1}^{N_s}\gamma_{k,l}\sin(\omega_k t+\varphi_{k,l})], \quad (3.39)$$

$$\frac{dT_{2,l,j\phi}(t)}{dt}=p_{12,j\phi}T_{1,l,j\phi}(t)+p_{22,j\phi}T_{2,l,j\phi}(t)$$

$$+p_{32,j\phi}[c_q(P_{0,j}(t)-\widetilde{P}_{0,j})+c_q\xi_1P_{1,j}(t)+c_q\xi_2P_{2,j}(t)+c_q\sum_{k=1}^{N_s}\gamma_{k,l}\sin(\omega_k t+\varphi_{k,l})], \quad (3.40)$$

where $l=1..4$, $j=1,2$, $P_{0,j}$, $P_{1,j}$, and $P_{2,j}$ take a non-uniform axial power profile into account, and $\gamma_{k,l}$ is defined as:

$$\gamma_{k,l}=\frac{\int_{V_l^*}\bar{\bar{F}}_0^*(\bar{r}^*)\bar{\psi}^{i*}(\bar{r}^*,\bar{r}_0^*,\omega_k^*)d\bar{r}^*}{\int_{V_{core}^*}\bar{\bar{F}}_0^*(\bar{r}^*)\bar{\Phi}_0^*(\bar{r}^*)d\bar{r}^*}. \quad (3.41)$$

3.2.2 Analysis of the measurements

In this Section, the neutron flux measurements performed during the stability tests to study the Forsmark-1 local instability event of 1996/1997, are investigated [23, 27, 28]. First, a brief introduction into the instability event itself is given.

The event took place in 1996 when start-up tests were carried out at the Swedish BWR Forsmark-1 for the fuel cycle 16. During these tests, some unstable operational conditions at reduced power and reduced flow, were detected. Later on, in January 1997, new stability measurements were performed, in order to investigate the instability event. In one of them, when the reactor was operated at 63.3 % of power and at a core flow of 4298 kg/s, the same instability pattern was again observed with an oscillation frequency around 0.5 Hz. The appearance of this instability was somewhat surprising since all earlier stability calculations indicated a completely stable core [23,27,28].

During these stability measurements, the lower axial plane of the core was well equipped with LPRMs, placed at 36 different radial positions and in 2 axial levels. The signals from only 27 were recorded at a sampling frequency of 12.5 Hz. As an illustration of these measurement tests, one of the signals, filtered between 0.4-0.6 Hz and corresponding to the strongest detector response is shown in Fig. 3.8.

After a spectral analysis of the measurements, several even more interesting features were discovered. The first one is related to the space-dependence of the decay ratio, namely one half of the core oscillated with DR=0.6 whereas the other half with DR=0.9 [23, 27, 28]. However, in all previous studies, the DR was always assumed to be a global stability indicator and, hence, space-independent. Another interesting feature is the rotating symmetry line between the first two azimuthal modes which was observed as a result of the modal decomposition of the corresponding measurements. The time evolution of the first three modes after the decomposition, namely the fundamental, the first and the second azimuthal modes, is given in Fig. 3.9. For the purpose of comparison, both azimuthal modes are shown in the same plot. As one can see from these figures, both global and regional instabilities corresponding to the fundamental and the first two azimuthal modes, respectively, are present. An even more remarkable feature which can be clearly seen from the right Fig. 3.9, is the changing phase shift between the azimuthal modes, resulting in a rotating symmetry line of the regional oscillations.

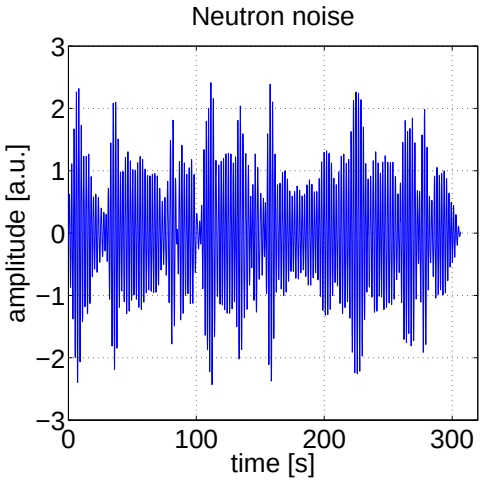

Figure 3.8: Time evolution of the filtered neutron noise, measured by LPRM7.

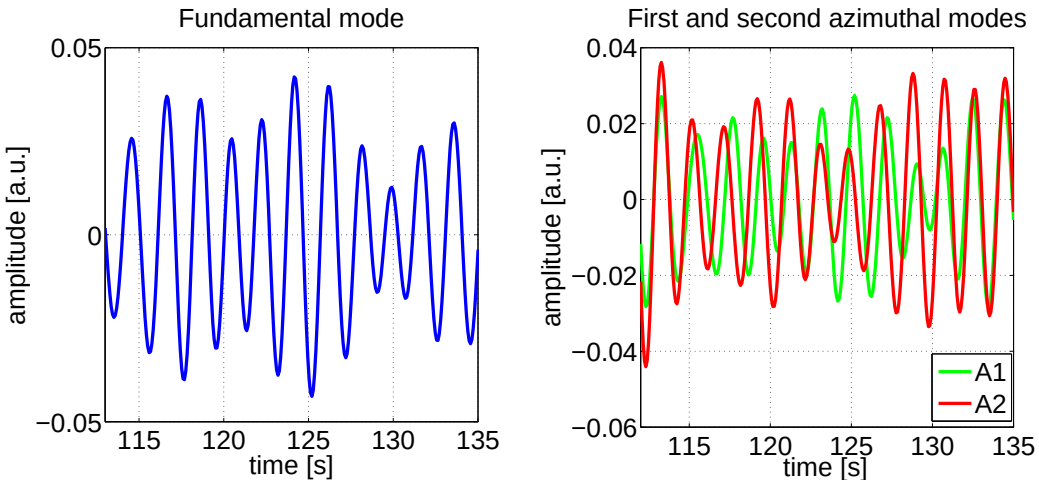

Figure 3.9: Time evolution of the fundamental, fist and second azimuthal modes after modal decomposition of the measurement data.

Further studies of the measurements indicated that the instability was driven by most likely two or even more local noise sources. Later on, it was suggested that these local noise sources are presumably caused by unseated fuel assemblies leading to density wave oscillations and, hence, to local power oscillations.

3.2.3 ROM simulation of the local instabilities

In the following, the results of the simulation of the Forsmark-1 channel instability event using the extended ROM are presented. The time-dependent amplitude factors for each of the three modes were calculated by numerical integration of 42 ROM ODEs.

First, the case without the introduction of any DWO, i.e. the case when only core-wide instabilities can occur, is considered. The corresponding results are given in Fig. 3.10. As Fig. 3.10 shows, for this specific case, the ROM predicts a stable core, both with

the respect to in-phase and out-of-phase oscillations, and no oscillating symmetry line is observed. This simulation perfectly agrees with earlier stability calculations performed by the utility according to which the core was proven to be stable.

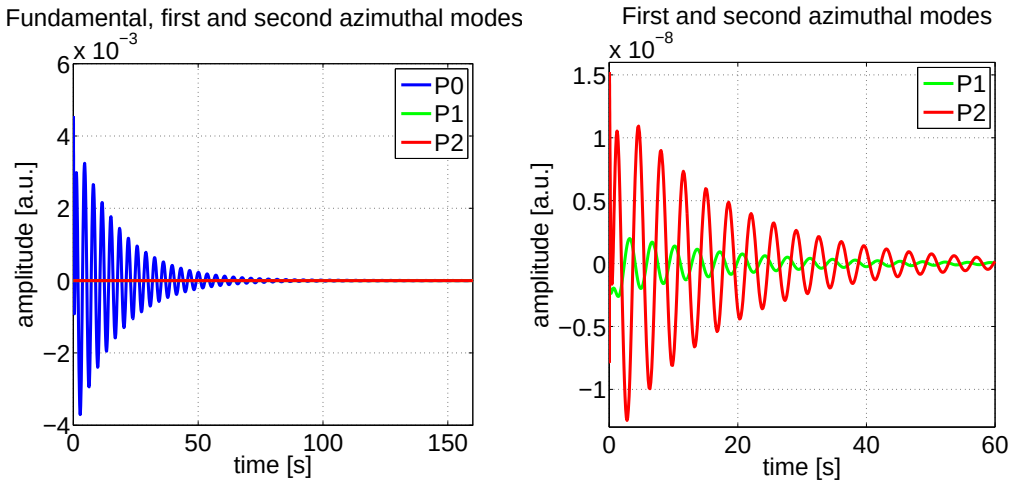

Figure 3.10: Time evolutions of the fundamental, the first, and the second azimuthal modes, as computed by the ROM, $\delta V_{inlet} = 0.1[a.u.]$.

Next, the case when three local sources were introduced into the ROM is discussed. Some results of this simulation are shown in Fig. 3.11. The dynamical characteristics of the corresponding sources together with their spatial distributions and locations in the core are given in **Paper V**.

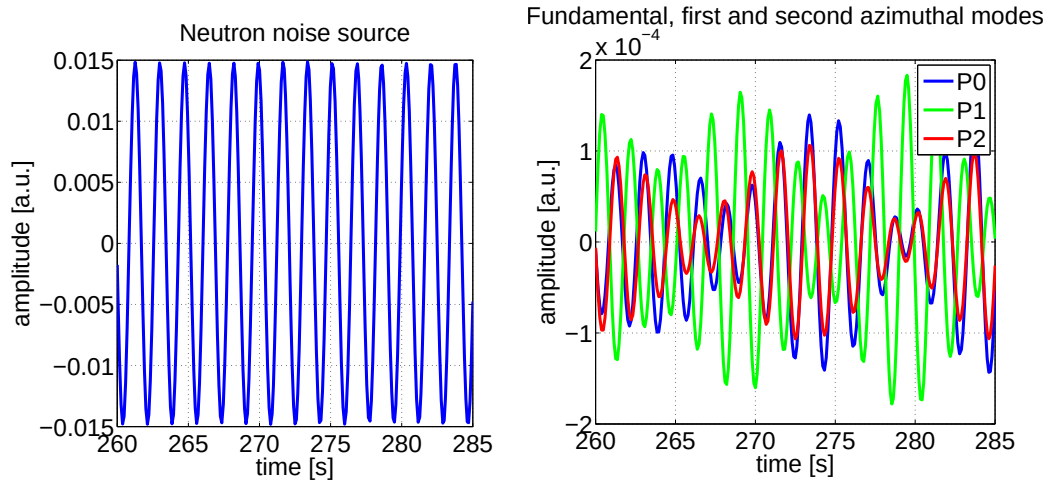

Figure 3.11: Time evolution of the neutron noise source (left figure) and the induced neutron noise decomposed into the fundamental, the first, and the second azimuthal modes (right figure), as computed by the ROM.

In Fig. 3.11, the time-dependence of the strongest local noise source is given, as well as

the decomposition of the corresponding induced neutron noise into the fundamental, the first and the second azimuthal modes. It is worth to point out that all three modes are oscillating with a DR of unity. This is explained by the fact that all modes are driven by the external local sources.

For the purpose of comparison, in Fig. 3.12 the time evolution of the first three modes, obtained as a result of the modal decomposition of the real measurements, together with the strongest neutron noise, is given. From Figs. 3.11-3.12, it can be clearly seen that

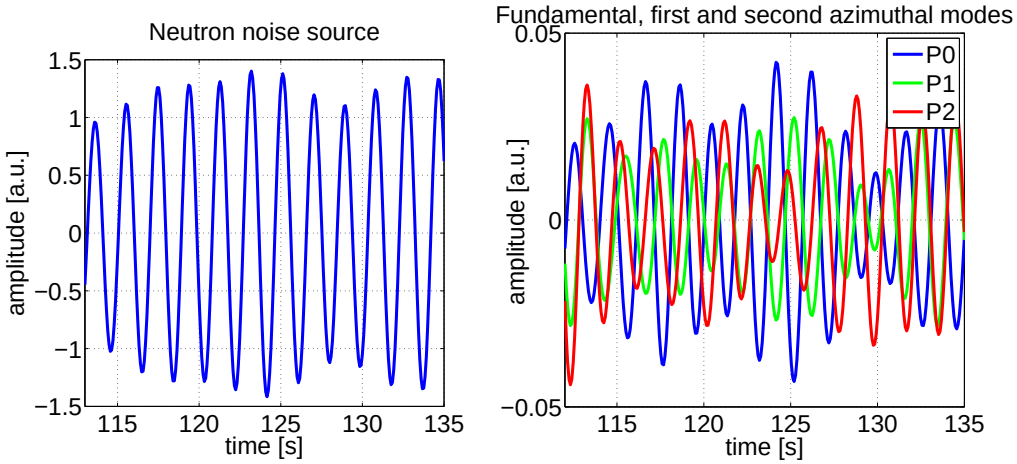

Figure 3.12: Time evolution of the neutron noise source (left figure) and the induced neutron noise decomposed into the fundamental, the first, and the second azimuthal modes (right figure), as determined from the measurements.

both cases exhibit qualitatively a similar behaviour. Namely, all modes are properly excited and oscillate with comparable amplitudes. Furthermore, the mode amplitudes have approximately the same ratio, compared with the respective strongest source. Another interesting feature which can be seen in both the ROM simulation and the measurements is the oscillating symmetry line. For better visibility, both azimuthal modes as calculated from the ROM are shown separately in Fig. 3.13.

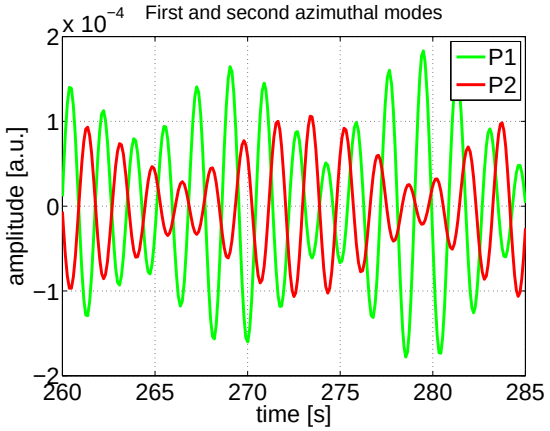

Figure 3.13: Time evolution of the first and the second azimuthal modes, as computed by the ROM.

In order to better understand the studied stability event, it is also instructive to perform two other ROM simulations, i.e. the one when the system response is calculated separately from the DWOs and another one when the neutron noise, induced by only the local sources (the system response being excluded), is considered. As shown in **Paper V**, from the comparison between these two cases (in terms of decomposed results), one can clearly show that the effect of the system dynamics on the total noise is quite negligible (due to the stable behaviour of the system) and, thus, the full core (measured) response is mainly driven by the local power oscillations induced by the DWO.

Chapter 4

APPLICATIONS

Try everything. Do everything. Nuclear. Biomass. Coal. Solar. You name it. I support them all.

— Boone Pickens

In this Chapter, some applications of the neutron noise investigations, performed in the previous two chapters are shown. In general, depending on the area of applicability, the neutron noise diagnostics can be classified into several different categories. The first of these, named as "stability" applications, is aimed at monitoring the core stability, determining the margins to the instability, as well as providing information about the stability properties of the system by analyzing the neutron noise measurements (whether locally with local power range monitor (LPRM) or globally with averaged power range monitor (APRM) detectors). In order to quantify the instability, a reliable stability indicator is required. The most commonly used stability indicator, especially in real power plant measurements is the so-called decay ratio [1]. In order to utilize the DR as a stability indicator, it should be assumed that the system dynamics can be modeled as a second order damped linear oscillator driven by a white driving force. In such a case, the DR gives a measurement of the damping of the system and is defined as the ratio between two consecutive maxima of the solution to the second order oscillator. In practice, it is not the signal itself, but the auto-correlation function of the normalized neutron density that is used. The DR is then defined as the ratio of two consecutive maxima of the ACF, such as A_2/A_1 or A_3/A_2, as illustrated in Fig. 4.1.

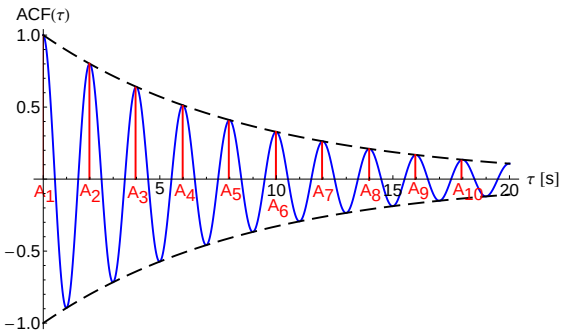

Figure 4.1: An analytical ACF is shown where the decay ratio is defined as DR= $\frac{A_2}{A_1}$

Since in a linear system the APSD of the noise is given as a product of the transfer

function squared, multiplied by the APSD of the driving force, with the assumption of white character of the driving force, the APSD of the induced neutron noise is related only to the system transfer function. Therefore, in real practical applications (in particular, in BWR stability measurements where the driving force cannot be measured), the ACF is usually estimated from the corresponding APSD of the measured noise after an inverse Fourier transform [1].

However, for a driving force which deviates from a white noise, i.e. a driving force that has its own frequency dependence, the frequency characteristics of the neutron noise (APSD) will deviate from that of the system transfer function. Investigation of such a case is the subject of **Paper VI**, which will be briefly summarized below. The frequency dependence of the perturbation is determined as the reactivity effect of the void propagating fluctuations, and the APSD of the resulting neutron noise (after multiplication with the system transfer function) is Fourier-inverted analytically, to reconstruct the ACF of the detector signal for the case of such a non-white driving force. Then the decay ratio is determined by the traditional method, assuming white noise driving force. Since the system properties are known in advance, the possible error in the estimation of the stability properties of the system (DR) between two cases, i.e. the white and non-white DF, is investigated with a curve fitting procedure.

As mentioned earlier, in order to utilize the DR as a stability indicator, the assumption about the linearity of the system is one of the most crucial ones. However, a real reactor system is non-linear, due to many feedback effects between neutronics, heat transfer and fluid flow. As several instability events showed, for such cases, the concept of the DR as a stability indicator might give erroneous results (see e.g. the space-dependent DR in the Forsmark-1 instability event [23]). It is therefore instructive to investigate what stability parameters, other than the DR can be used for describing the stability properties of non-linear systems. As a tool for such an investigation, the reduced order model of a BWR (with major non-linear characteristics preserved, i.e. the ones due to the feedback), developed in the previous Chapter is used. In this study, the so-called reactivity coefficients C_{mn} characterizing the change of the cross-sections with respect to the void fraction and fuel temperature fluctuations are chosen as a possible candidate for the new stability indicator. For this purpose, the dependence between the reactivity coefficients and the decay ratio is qualitatively investigated. The C_{mn}-coefficients are gradually changed and the decay ratio for the most important quantities is estimated by a proper curve fitting. As observed in the past, an increase of the amplitude of the C_{mn}-coefficients should lead to an increase of the DR (due to the more negative coupling) until it reaches its saturation value of DR=1 and becomes constant for any further change in the C_{mn}- coefficients. However, as will be shown later in this Chapter, this is not the case for the present ROM, i.e. the DR starts to decrease after reaching some critical value. Possible explanations for this unexpected behaviour of the DR together with the technique used for its investigation are summarized below. More details can be found in **Paper VII**.

Another type of noise diagnostics applications can be specified as "unfolding techniques" where the main objective is to extract hidden information about system parameters from neutron noise measurements. Shortly, the basis of this unfolding technique can be expressed through the following relation [1]:

$$\delta\phi(\bar{\boldsymbol{r}},\omega) = \int G(\bar{\boldsymbol{r}},\bar{\boldsymbol{r}}',\omega)\cdot S(\bar{\boldsymbol{r}}',\omega)d\bar{\boldsymbol{r}}' \tag{4.1}$$

Eq. (4.1) shows that the effect of the perturbation $\delta\phi(\bar{\boldsymbol{r}},\omega)$ can be factorized into the noise

source $S(\bar{\boldsymbol{r}}', \omega)$ and the system transfer $G(\bar{\boldsymbol{r}}, \bar{\boldsymbol{r}}', \omega)$. In the diagnostic task, $G(\bar{\boldsymbol{r}}, \bar{\boldsymbol{r}}', \omega)$ is usually assumed to be known since it depends only on the parameters of the unperturbed system and, hence, can be calculated analytically. Thus, the task is to quantify the noise source $S(\bar{\boldsymbol{r}}', \omega)$ from the measured neutron noise $\delta\phi(\bar{\boldsymbol{r}}, \omega)$. In practice, $\delta\phi(\bar{\boldsymbol{r}}, \omega)$ is only known in a few spatial points and, thus, the direct inversion of Eq. (4.1) is not of much practical use. Instead, some simple analytical model for the neutron noise (which qualitatively reproduces the behaviour of the perturbation) with just a few unknown parameters, is constructed. Using this model together with the measured neutron noise combined with spectral analysis provides the opportunity to quantify unknown parameters.

Such unfolding procedures were proven to work fairly well in many cases, e.g. in the case of vibrating control rods that need to be identified, the averaged flow velocity of the coolant in the heated channel that should be estimated, etc. One example of the application of such a technique, but with numerically simulated neutron noise (see Chapter 2) will be given below where the possibility to extract axial void fraction and velocity profiles from the measured neutron noise is investigated. In such a case the noise source is specified as the fluctuations in the coolant density which are obviously difficult to simulate analytically and the application of the numerical simulation is thus justified. Two methods for the reconstruction will be tested. One is based on the dependence of the break frequency of the APSD of the simulated neutron noise on the void content [8] and another one utilizes the transit times of the void fluctuations [1]. Comparing the results of the reconstruction with input data of the model, the accuracy of both methods can be estimated. Further details are given in **Papers III** and **VIII**.

4.1 Stability

This Section shows some examples of stability applications of neutron noise analysis. Two cases are considered. The first case is related to open-loop systems where the driving force is assumed to have a non-white character, i.e. some frequency-dependence. The second case refers to closed-loop systems, where the correlation between the DR and the coupling reactivity coefficients as well as the possibility to use the latter one as a new stability indicator are analyzed. Some main features of the calculation procedure are summarized below and some conclusions from this study are also drawn.

4.1.1 BWR stability in open-loop system (non-white driving force)

ACF calculation procedure for the white noise driving force

Following the same methodology as in **Paper VI**, one begins with the second order equation, describing a linear damped oscillator, written as:

$$\delta\ddot{\phi}(t) \; + \; 2\xi\omega_0\delta\dot{\phi}(t) \; + \; \omega_0^2\delta\phi(t) \; = \; f(t), \tag{4.2}$$

where $\delta\phi(t)$ stands for the induced neutron noise, ξ is the damping factor, ω_0 is the system resonance frequency and $f(t)$ is the driving force. Performing a temporal Fourier transform of (4.2) and taking into account that the system is linear, one obtains:

$$\delta\phi(\omega) \; = \; \frac{f(\omega)}{(\omega_0^2 \; - \; \omega^2) \; + \; 2\xi\omega_0\omega i} \; \equiv \; H(\omega)f(\omega), \tag{4.3}$$

where $H(\omega)$ is the system transfer function. Assuming a white-noise behaviour of the driving force and applying the Wiener-Khinchin theorem, the APSD of $\delta\phi(t)$ can be written as

$$APSD_{\delta\phi}(\omega) \;=\; APSD_f(\omega)|H(\omega)|^2 = C\,|H(\omega)|^2, \tag{4.4}$$

where C denotes the white noise character of $f(t)$. The auto-correlation function of the neutron noise $\delta\phi(t)$ is calculated by applying an inverse FT to the noise $APSD_{\delta\phi}$. The corresponding integration in the inverse FT is performed by using the theorem of residues which requires the poles of $H(\omega)$ to be known. From **Paper VI**, the corresponding poles can be written as:

$$\omega_{1,2,3,4} \;=\; \pm\,\omega_0(1 \,\pm\, i\xi).$$

It should be pointed out that the expression above is valid under the assumption that the decay ratio $\beta = e^{-\xi 2\pi} \;\geq\; 0.5$, which allows neglecting second order terms in ξ. More detailed calculations are given in **Paper VI**. Thus, for the numerical values of ξ which are commonly used, the ACF for the neutron noise is given as:

$$ACF(\tau) \;=\; \frac{C\,e^{-\xi|\tau|\omega_0}}{4\xi\omega_0^3}\,\cos(\tau\omega_0). \tag{4.5}$$

ACF calculation procedure for the non-white noise driving force

In this Section one repeats the same calculations which were performed in the previous Section, but this time one assumes a non-white noise character of the driving force, which in the frequency domain has the same functional form as the reactivity effect of the propagating density perturbation. Some of the properties of the propagating perturbation as a source for the neutron noise, such as its APSD, ACF, phase and the corresponding reactivity effect, have earlier been discussed in Chapter 2 and, hence, are not repeated here. Thus, omitting some constant factors for simplicity, one has:

$$APSD_f(\omega) \;=\; \frac{1-\cos\omega T}{\omega^2(\omega^2-\omega_T^2)^2}. \tag{4.6}$$

Using this result and again assuming a linear system, the total APSD for the neutron noise is given as

$$APSD_{\delta\phi} \;=\; \frac{(1-\cos(\omega T))}{\left[(\omega_0^2 \;-\; \omega^2)^2 \;+\; 4\xi^2\omega^2\omega_0^2\right]\omega^2(\omega^2-\omega_T^2)^2}, \tag{4.7}$$

where $APSD_f$ is defined by Eq. (4.6) and the rest of the notations has the same meaning as earlier. Following the same steps as in the previous Section and performing an inverse FT, one obtains an analytical expression for the auto-correlation function. However, as is shown in **Paper VI**, this task is more challenging than the white noise driving force case, since this time there are two contributions to the poles. One of them comes from the transfer function $|H(\omega)|^2$ and another one from the driving force $APSD_f$. The last contribution complicates the calculations and creates some peculiarities in the total ACF. Namely, as will be demonstrated below, the result in the ACF consists of two parts. The first is related to a case when $|\tau| > T$, and is called the asymptotic part. The second one is defined for $|\tau| < T$ and is named as the transient part. As will be seen in the next Section, the asymptotic part of the ACF has exactly the same oscillating character as the ACF for

the white driving force and hence, has the same decay ratio which will be designated as the true one, since it is related to the system properties. In contrast, the transient part does not exhibit the same behaviour and deviates from that observed in the case of the white driving force. The explanation of this unusual behaviour comes from the fact that the driving force, namely $APSD_f$, contributes to the poles only for $|\tau| < T$ but not for $|\tau| > T$ (see Chapter 2 for the properties of the ACF_f). This results in the fact that the ACF of the noise induced by a non-white driving force deviates from the one induced by a white driving force. Thus, for a finite correlation time, the transient part of the total ACF is affected by both the driving force and the system itself over the corresponding finite time region, which is not the case for the asymptotic one which follows a white noise behaviour.

Finally, applying an inverse Fourier transform to $APSD_{\delta\phi}$ and assuming small ξ values, one obtains the following expression for the ACF of the oscillations, induced by a non-white driving force:

$$\begin{aligned} ACF(\tau) = {} & e^{-\xi\omega_0|\tau|} A \cos\left[\sqrt{1-\xi^2}\omega_0|\tau| - \alpha\right] \Theta[|\tau|] \\ & -0.5e^{-\xi\omega_0|T-\tau|} A \cos\left[\sqrt{1-\xi^2}\omega_0|T-\tau| - \alpha\right] \Theta[|\tau - T|] \\ & -0.5e^{-\xi\omega_0|T+\tau|} A \cos\left[\sqrt{1-\xi^2}\omega_0|T+\tau| - \alpha\right] \Theta[|\tau + T|] \\ & + \frac{T^4}{128\pi^5}\left((T-|\tau|)(\frac{4\pi}{\omega_0^4} + F\cos[\omega_T\tau]) + Y\sin[\omega_T|\tau|]\right)\Theta[T-|\tau|]. \end{aligned} \tag{4.8}$$

Here A, B, F and Y are complicated functions of the system parameters. The correctness of the above solution was checked by Fourier transforming it back to the frequency domain and comparing it with Eq. (4.7), as well as calculating the inverse transform of Eq. (4.7) numerically by MATLAB and comparing it with the analytical result quantitatively.

Qualitative and quantitative analysis of the results

This Section summarizes all calculation results for both a white and a non-white driving force and supplies their qualitative and quantitative analyses. In the qualitative analysis the focus is put on the behaviour of the ACF as well as that of the APSD, performing a parallel investigation of both functions. One starts with a case when $f_0 = f_T = 0.5$ Hz, which in terms of the transit time corresponds to $T = 2$ s. The corresponding APSD and ACF are shown in Fig. 4.2.

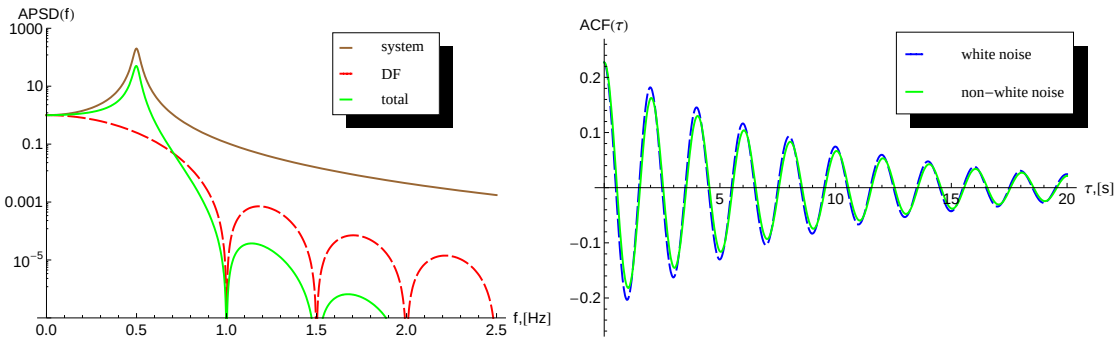

Figure 4.2: APSD and ACF of the system transfer and the total resulting noise for $f_T = f_0 = 0.5$ Hz for the case of DR = 0.8; in the legend DF stands for the "driving force"

In order to simplify the discussion, the following notations are defined: the ACF for the non-white driving force will be designated as virtual or measured ACF; the ACF for the white-noise driving force will be denoted as the true one. Thus, analyzing the APSD profile, one can end up with two interesting cases which are quite important from a stability point of view. If both the driving force and the system transfer function have a narrow peak around the same frequency, the total or virtual APSD will be even narrower than that of the true one, indicating a less stable system as determined from measurements, than the true system stability. That can be a drawback from the operational point-of-view since the operators might try to change the operational point, to avoid the instability.

Another important case is when the APSD of the driving force has a minimum around the system resonance frequency. Due to the joint effect of the APSDs of the driving force and the system transfer, the total APSD becomes broader than that of the system, hence indicating better stability from the measurement than the true one (smaller DR compared with the true one). This means that the driving force decreases the power oscillation and the situation becomes especially dangerous in the case of quite unstable system behaviour, since in that case it will be hidden under the driving force.

However none of these situations are accounted in our model, which is clearly seen from Fig. 4.2 where the virtual and true DR are both equal to 0.8. In the case shown in the figure, the APSD of the driving force has a first sink at $\omega = 2\omega_T$ and exhibits a quite smooth, almost constant frequency behaviour around the system resonance frequency ω_T, which keeps the shape of total (measured) APSD similar to that of the system. Thus, both curves, namely the system and the measured APSDs are quite narrow and result in DR=0.8.

Some further cases, keeping the system resonance frequency constant, but changing the resonance frequency of the driving force, have been also studied. As is shown in **Paper VI**, the increase of f_T does not give any new information, since the driving force APSD keeps the same constant behaviour over the system resonance, and hence it does not affect the system stability. It is much more interesting to investigate cases when one decreases f_T so much that one of the dips of the driving force APSD approaches the system resonance peak. One such case is shown in Fig. 4.3 (left figure) where $f_T = 0.51 f_0$. This will lead to a coincidence between the resonance peak of the system APSD and the first dip of the driving force APSD, and hence to a dip for the total APSD. As a result the total ACF demonstrates quite a stable system, since there are almost no oscillations in its profile, shown in Fig. 4.3 (right figure). It is interesting to note that ACFs with such a character were observed in real measurements. For the analysis of a real measurement, such situations can lead to serious problems. That is, despite the fact that the asymptotic DR is similar to the true one, it will not be possible to determine it correctly, since in practice this part of the ACF will be masked due to the scatter of measurement data and presence of background noise, hence the oscillations will not even be visible. Thus, the only DR ratio which will be accessible is the virtual one, related to the transient part of the ACF which does not reflect the real stability property of the system and makes instabilities undetectable. The real problem appears when some of the thermal hydraulic parameters suddenly change their values and consequently move f_T away from the system resonance frequency. As a result the instabilities would appear in a very unexpected and sudden way. Some other interesting cases of the similar study can be found in **Paper VI**.

From the operational point-of-view, it is always good to know the DR of the asymp-

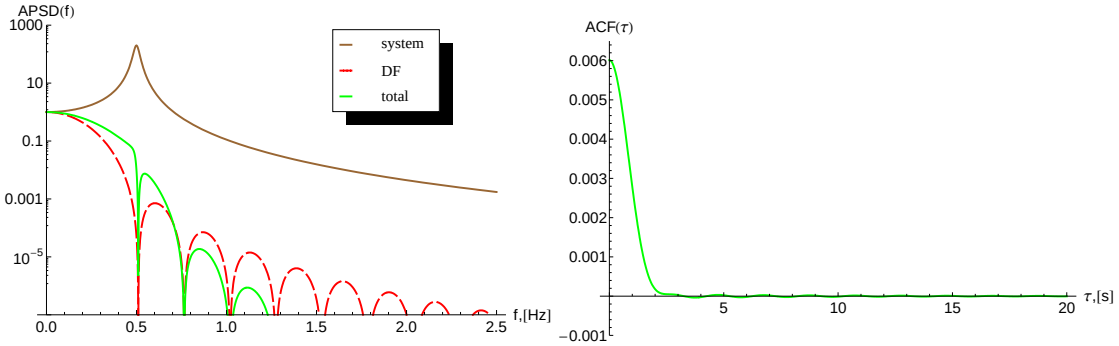

Figure 4.3: APSD and ACF of the system transfer and the total resulting noise for $f_T = 0.51 f_0$ for the case of DR = 0.8

totic part of the ACF, since it gives true information about the reactor stability. But as previously said, it is not always possible to evaluate the DR sufficiently accurately from the asymptotic part which is usually not even known. Instead, one can only estimate the DR for the total ACF. In this context it might be useful to estimate the error in DRs between two cases: for the measured or total ACF and the asymptotic or true ACF.

In **Table 4.1**, some results of a series of such calculations, performed for different transit times T_f(and ω_T) of the driving force, are given. The estimations of the DR were

Table 4.1: Results of curve fitting with the ACF of white driving force, Eq. (4.5), to the ACFs with non-white driving force spectra

	Decay Ratio			Frequency,Hz		
	DR	DR_{tr}	DR_{asy}	f_0	f_f	f_p
$Case\,1.\ DR = 0.6$						
$f_T = f_0 = 0.5Hz$	0.6	0.57	0.6	0.5	0.5	0.5
$f_T = \frac{2}{3} f_0 = 0.33Hz$	0.6	0.38	0.6	0.5	0.49	0.5
$f_T = 0.55 f_0 = 0.29Hz$	0.6	0.11	0.6	0.5	0.5	0.5
$f_T = 0.51 f_0 = 0.26Hz$	0.6	0.085	0.6	0.5	0.49	0.5
$f_T = 0.5 f_0 = 0.25Hz$	0.6	0.059	0.6	0.5	0.5	0.5
$f_T = 2.5 f_0 = 0.2Hz$	0.6	0.15	0.6	0.5	0.49	0.5
$Case\,2.\ DR = 0.8$						
$f_T = f_0 = 0.5Hz$	0.8	0.8	0.8	0.5	0.5	0.5
$f_T = \frac{2}{3} f_0 = 0.33Hz$	0.8	0.65	0.8	0.5	0.51	0.50
$f_T = 0.55 f_0 = 0.29Hz$	0.8	0.21	0.8	0.5	0.5	0.5
$f_T = 0.51 f_0 = 0.26Hz$	0.8	0.14	0.8	0.5	0.5	0.5
$f_T = 0.5 f_0 = 0.25Hz$	0.8	0.1	0.8	0.5	0.5	0.5
$f_T = 2.5 f_0 = 0.2Hz$	0.8	0.31	0.8	0.5	0.5	0.5
$Case\,3.\ DR = 0.98$						
$f_T = f_0 = 0.5Hz$	0.98	0.98	0.98	0.5	0.5	0.5
$f_T = \frac{2}{3} f_0 = 0.33Hz$	0.98	0.97	0.98	0.5	0.5	0.5
$f_T = 0.55 f_0 = 0.29Hz$	0.98	0.53	0.98	0.5	0.5	0.5
$f_T = 0.51 f_0 = 0.26Hz$	0.98	0.23	0.98	0.5	0.52	0.5
$f_T = 0.5 f_0 = 0.25Hz$	0.98	0.11	0.98	0.5	0.5	0.5
$f_T = 2.5 f_0 = 0.2Hz$	0.98	0.61	0.98	0.5	0.51	0.5

made in several ways or for several parts of the total ACF using curve-fitting procedure: namely the DR for the separate asymptotic part of ACF, denoted as DR_{asy}, and the DR for the total ACF together with its transient part, denoted as DR_{tr}. The results given in **Table 4.1** confirm the expectations and predictions mentioned above. Namely, if one has access to the ACF without any effect from measurement uncertainties and background noise, the asymptotic DR is always equal to the true one. On the other hand, the curve fitting to the whole curve gives completely different results, resulting in an overestimated DR. Thus, one can conclude that the presence of the colored noise source leads to an error in DR estimations. But as also pointed out, the coloured noise source as represented by propagating void perturbations in a BWR does not lead to such problems in practical cases.

4.1.2 BWR stability in closed-loop systems

Dependence of the decay ratio on the reactivity coefficients (C_{mn}- coefficients)

The ROM, developed and described earlier in Chapter 3, is applied to expedite the dependence between the DR and the coupling reactivity coefficients C_{mn}. A number of different cases where the C_{mn}-coefficients were manually modified are analyzed. For each case studied, the DR corresponding to the fundamental mode is numerically estimated. The corresponding dependence of the DR on the C_{mn}-coefficients is shown in Fig. 4.4

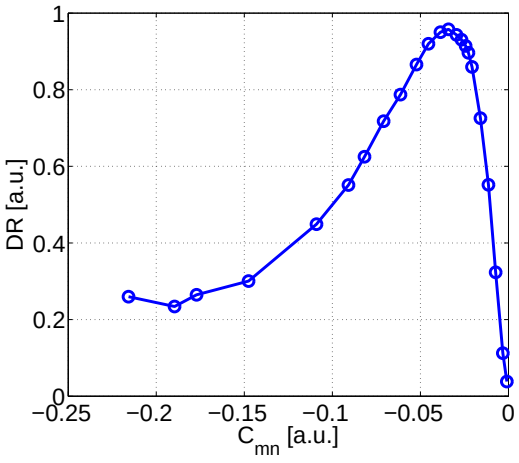

Figure 4.4: Dependence of the Decay Ratio on the reactivity C_{mn}-coefficients

As Fig. 4.4 demonstrates, the dependence between the DR and the C_{mn}-coefficients is not monotonic over the whole range of the C_{mn}-coefficients. First the DR increases with increasing amplitude of the C_{mn}- coefficient (following the conventional behaviour of the DR), whereas at approximately $C_{mn} = -0.0361$ a.u., the DR suddenly starts to decrease approaching a low-value region at around $C_{mn} = -0.2$ a.u.

Estimation of the dynamical properties of the system (amplitude, phase, frequency and decay ratio)

To provide some insight into the origins of the sudden drop in the DR curve, a curve-fitting procedure is applied to all physical quantities available from the ROM, where it is assumed that the behaviour of a BWR can be described as a second-order decaying oscillator, i.e. fitted to the following decaying sine-function:

$$\phi(t) = A\exp(-\gamma t)\sin(\omega t + \varphi) \tag{4.9}$$

Such a curve-fitting procedure is applied to four given C_{mn} values, thus providing information about the amplitude A, frequency ω, decay constant γ and phase φ of some key parameters, i.e . void fraction α, averaged surface fuel temperature T_{fs}, power P and inlet pressure drop δP_{inlet}. The corresponding results (except for the phase) are shown in Figs. 4.5, respectively.

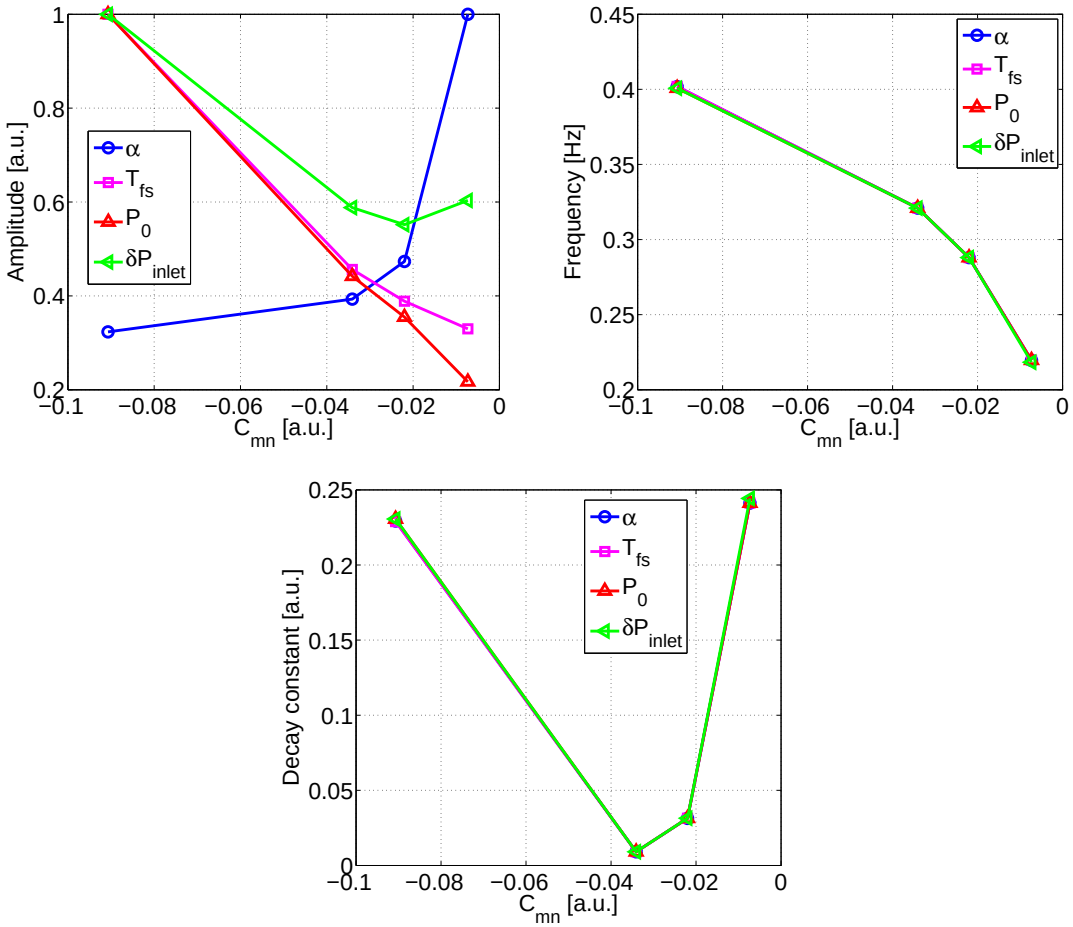

Figure 4.5: Dependence of the amplitudes A, frequency ω and decay constant γ of the void fraction α, averaged surface fuel temperature T_{fs}, power P and inlet pressure drop δP_{inlet} on the C_{mn} coefficients; for the amplitude all the quantities were weighted to their corresponding maximum values.

A careful analysis of the upper left part of Fig. 4.5 shows that, as the C_{mn} coefficients

decrease down to -0.0341 a.u., the amplitude change in both the void oscillations and the power oscillations is significantly larger compared with the ones in the surface fuel temperature and the inlet pressure drop oscillations. This leads to the conclusion that most of the produced fuel heat is transferred into the change of the void fraction. However, for C_{mn} values between -0.034 a.u. and -0.0907 a.u., the situation is reversed, namely the amplitudes of the surface fuel temperature as well as the inlet pressure drop oscillations experience a drastic jump whereas the amplitude of the oscillations in the void fraction do not change so much.

Such a peculiar behaviour of the quantities can be interpreted as if all the heat from the fuel is converted into an increase of the amplitudes of the surface fuel temperature and the inlet pressure drop oscillations, leaving the void change mostly unaffected. The increase in the amplitude of the inlet pressure drop oscillations apparently stabilizes the system (due to the phase delay between the power change and the feedback which becomes closer to -180°) and thus contributes to the decrease in the DR. Such an unexpected transition of the energy transfer from the void change into the surface fuel temperature/inlet pressure drop change can be explained by the inertia of the heat transferred between the fuel and the coolant (i.e. it takes some time for the heat to be transferred from the fuel to the coolant) leading to some time-delay between the change in the power and the corresponding change in the feedback.

One can also show that for the last two cases, i.e. $C_{mn} = -0.034$ a.u. and $C_{mn} = -0.0907$ a.u., the characteristic time of the power oscillations is less than the time it takes for the system to transfer heat from the fuel to the coolant. As a result, for a certain critical value (in our case $C_{mn} = -0.036$ a.u.), the changes in the power (which frequency is a function of C_{mn}) become too fast for the system to be able to transfer all the heat into the coolant, but instead the energy oscillations are mostly transferred into changes in the surface fuel temperature and the inlet pressure drop. Such a phenomenon might then lead to an additional stabilization of the system and thus a decrease of the DR.

Thus, one can conclude that the dependence between the DR and the reactivity coefficients (C_{mn}-coefficients) is not a trivial one, i.e. the DR experiences some peculiar drop at a certain critical value of the C_{mn}-coefficient. Although the C_{mn}-coefficients might provide some information about the stability properties of the system, additional more detailed investigations on this topic are necessary.

4.2 Unfolding technique

Some preliminary results of the reconstruction of the void fraction and velocity profile from the simulated neutron noise using two different methods are presented and discussed. The description of the Monte Carlo technique applied to simulate synthetic neutron noise signals induced by fluctuations in the coolant density, as well as the description of the model involved have already been given earlier in Chapter 2 and, therefore, will not be repeated here.

4.2.1 Methods for void content estimation

Two possibilities of estimating the averaged void fraction from the neutron noise measurements are analyzed in this Section. The first method (for convenience called "break frequency" method), suggested in the late 70s, is based on the correlation between the

so-called break frequency of the APSD of the measured neutron noise and the corresponding axial positions of the detectors [8]. As will be shown later on, this method requires the knowledge of the velocity of the fluctuations which, for reasons of simplicity, will be expressed with the void fraction by Eq. (2.14), thereby eliminating it as an unknown quantity. The second method also utilizes Eq. (2.14) combined with the information about the transit times of the void fluctuations which can be estimated from the cross-correlation of two axially distant neutron detector signals.

Break frequency method

The principles of the break frequency method can be summarized as follows. Assuming the following simple form for the propagating character of the void fluctuations [8]:

$$\delta\alpha(z',\omega) \propto e^{-i\omega\frac{z'}{v(z')}} \tag{4.10}$$

letting the velocity $v(z')$ and the static flux $\phi_0(z')$ be constant within the range $\lambda^{-1}(z)$ of the local component at any given axial elevation z and combining Eq. (2.26) with Eq. (2.27) (see Chapter 2), after FT one obtains the following simplified relation between the normalized auto-power spectral density of the density fluctuations and the one corresponding to the induced neutron noise:

$$NAPSD_z^{\delta\phi_\lambda} = C \cdot NAPSD_z^{\delta\alpha}(\omega) \cdot \frac{1}{(1+\omega^2\tau_\lambda^2)^2}, \tag{4.11}$$

where

$$\tau_\lambda(z) = \frac{1}{v(z)\cdot\lambda(z)}.$$

is the time it takes for the perturbation to pass the range of the local component.

From Eq. (4.11) it can be clearly seen that the fluctuations in the neutron flux $\delta\phi_\lambda$ at a certain axial position z are proportional to the corresponding fluctuations in the void fraction $\delta\alpha$ at the same location z, times a frequency-dependent term (Lorentzian term) with a break frequency [8]

$$f_b(z) = \frac{1}{2\pi}\cdot v(z)\cdot\lambda(z) = \frac{1}{2\pi}\cdot v(\alpha(z))\cdot\lambda(\alpha(z)). \tag{4.12}$$

Eq. (4.12) shows that the break frequency is dependent on the void fraction through the local void velocity and the local range (often called "field of view") of the local component. This dependence is rather implicit, but in principle it lends a possibility to determine the local void fraction.

The dependence of the local root λ on the local average void fraction can be approximated as:

$$\lambda(\alpha(z)) = \lambda_0 - k\cdot\alpha(z) \tag{4.13}$$

where λ_0 is the value of the local root with zero void fraction. The linear term k together with λ_0 can easily be extracted from the lattice physics code calculations, such as CASMO-4 [35]. A more detailed derivation of Eq. (4.13) is given in **Paper III**.

Then, combining (4.12) and (4.13) yields

$$\alpha(z) = \frac{1}{k}\left[\frac{2\pi f_b(z)}{v(\alpha(z))} - \lambda_0\right] \tag{4.14}$$

Further, assuming the simplified relationship (2.14) between the local average void fraction and the local two-phase flow velocity yields for the axial void fraction the expression

$$\alpha(z) = \frac{u-1}{u-k}. \tag{4.15}$$

Here u is defined as

$$u = \frac{v_0 \cdot \lambda_0}{2 \cdot \pi \cdot f_b(z)}$$

where v_0 is the (known) inlet velocity of the coolant and $f_b(z)$ can be estimated numerically for the corresponding APSDs.

Transit time

Another possibility to determine the void fraction is to use some simple explicit relationship between the local void velocity and local void fraction such as (2.14) and combine it with the measurements of the local velocity itself (e.g. from transit times using the CCF of the neutron noise measurements [1]). Although the relationship (2.14) is an approximate one since it assumes the same velocity for the vapour and liquid phases, it is advantageous for practical application since the knowledge of extra parameters is not required.

As has long been known, the transit times of two-phase flow fluctuations between pairs of detectors axially away from each other (i.e. the time it takes for the fluctuation to propagate between two axial points, e.g. z_1 and z_2) can be determined from noise measurements. This can be performed both from the cross-correlation function (CCF) or from the phase of the cross-power spectral density (CPSD). In the present work, for the sake of simplicity, the transit times are estimated from the CCF by using the maximum of this function.

However, the transit time does not give any direct information of the velocity $v(z_1)$ or $v(z_2)$ because it is related to the integral of the inverse velocity as

$$\tau_{12} = \int_{z_1}^{z_2} \frac{dz}{v(z)}, \tag{4.16}$$

Then, assuming the following 3rd order polynomial approximation for the velocity profile:

$$v(z) = a \cdot z^3 + b \cdot z^2 + c \cdot z + d, \tag{4.17}$$

and taking into account Eq. (4.16), the following system of equations can be used for identifying the unknown coefficients a, b, c and d :

$$\int_{z_i}^{z_{i+1}} \frac{dz'}{a \cdot z^3 + b \cdot z^2 + c \cdot z + d} = \tau_{i,i+1}, \tag{4.18}$$

for four pairs of detectors $i = 1, 2, 3, 4$. In the above, it is assumed that the transit times $\tau_{i,i+1}$ can be estimated from the CCF between the neutron noise measurements performed in five different axial levels. From this non-linear system of equations, the coefficients $a...d$ can be determined. Once the unknown coefficients are evaluated, the axial velocity profile can be reconstructed and hence the void profile can be calculated from Eq. (2.14).

This method is more straightforward from a practical point-of-view since it does not require any additional data other than noise measurements. However, it is important to emphasize that since the whole procedure is based on one single physical quantity, the transit times should be estimated in a quite precise way or an increased number of detectors should be used.

4.2.2 Analysis of numerical results

In this Section, the corresponding parameters for both methods are determined from the simulated neutron noise measurements, provided by the Monte Carlo model.

The results of the Monte Carlo simulation including simulated neutron noise signals together with their calculated APSDs, have already been demonstrated and discussed earlier in Chapter 2. Therefore, here, only the results of the quantitative processing of these data are shown and analyzed.

Table 4.2: Results of the curve fitting procedure of the APSD of the Monte Carlo simulated neutron noise to the Lorentzian coefficient (Eq. (4.11)).

Det. pos., z_d [cm]	Amp., A [a.u.]	τ_λ [s]	Break freq., f_b [Hz]
$z_1 = 40$ cm	$4.82 \cdot 10^6$	0.0650	15.38
$z_2 = 60$ cm	$8.08 \cdot 10^6$	0.0649	15.51
$z_3 = 100$ cm	$1.14 \cdot 10^7$	0.0602	16.61
$z_4 = 130$ cm	$1.21 \cdot 10^7$	0.0593	16.87
$z_5 = 180$ cm	$1.19 \cdot 10^7$	0.0565	17.69
$z_6 = 240$ cm	$1.17 \cdot 10^7$	0.0557	17.94
$z_7 = 300$ cm	$1.13 \cdot 10^7$	0.0540	18.51
$z_8 = 380$ cm	$1.10 \cdot 10^7$	0.0534	18.72

The break frequencies for each of the eight APSDs as well as their amplitudes were numerically estimated by fitting the corresponding curves to the Lorentzian coefficient defined in Eq. (4.11) (see **Table 4.2**). As can be seen from the table, both the amplitude of the APSD (except for the last four cases) and the break frequency rise axially in the core. As a further step, the estimated break frequencies are substituted into Eq. (4.15) to recalculate the void fraction in eight detector locations. The result is plotted in Fig. 4.6 (blue line). For comparison, the "true" void profile (the output from Monte Carlo simulations calculated by time averaging over the corresponding set of void fraction signals) is also given in Fig. 4.6 (red line). From the two figures, one can conclude that the void fraction calculated from the simulation qualitatively reproduces the behaviour of the true one. However, the break frequency method overestimates the void fraction, primarily in the lower part of the channel. From a practical point-of-view, this region is less interesting since it usually corresponds to the subcooling area where the bubbles are primarily generated rather than propagate.

Next, the results for the second method are discussed. The CCF function between different detector pairs is estimated using the detector signals generated by the Monte Carlo model. Then, the corresponding transit times τ_{exp} and averaged velocities v_{exp} are calculated and the results are given in **Table 4.3**. For comparison, the true transit times τ_{tr} calculated from the true velocity profile are also given in the last column of **Table 4.3**. As one can see, the results from both methods are in a good agreement with each other. Once

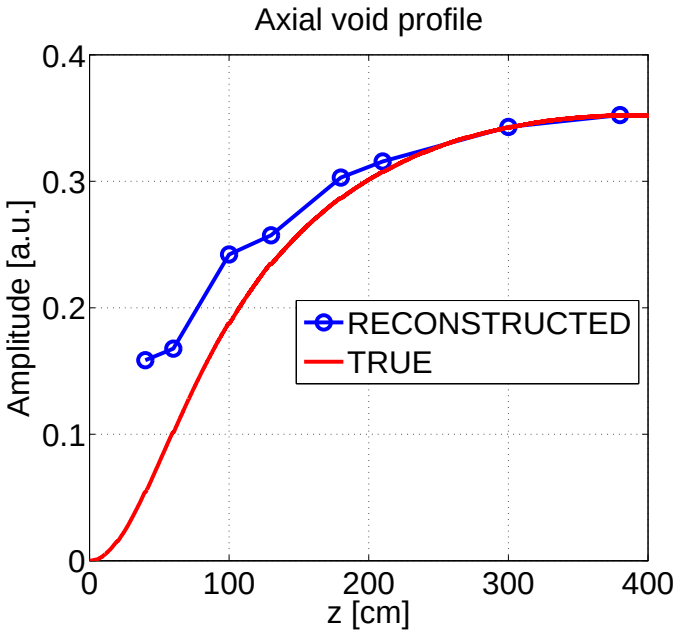

Figure 4.6: True axial void profile (the output from Monte Carlo model, red) and "reconstructed" ("experimental", blue) axial void profile, as calculated by the break frequency method (Eq. 4.15).

Table 4.3: Results of the transit time calculations from the Monte Carlo simulation (both the true and reconstructed ones).

Det. dist. d_{ij} [cm]	τ_{tr} [s]	τ_{exp} [s]
$z_{13} = 60$ cm	0.263	0.262
$z_{35} = 80$ cm	0.302	0.302
$z_{57} = 120$ cm	0.408	0.410
$z_{78} = 80$ cm	0.261	0.262

the transit times are found, one can estimate the unknown coefficients for the velocity profile (see Eqs. (4.17)-(4.18)), as mentioned in the previous Section.

Chapter 5

CONCLUDING REMARKS

Success is not the key to happiness. Happiness is the key to success.
If you love what you are doing, you will be successful.
— Albert Einstein

Some of the dynamical properties of the neutron noise in light water reactors concerning the inter-related areas of traveling perturbations and BWR instability problems have been investigated, using different techniques for modeling the neutron noise. The analysis was made in both open-loop systems, where the system properties are mainly defined by those of the transfer function (calculated for the unperturbed core) and all feedback effects are neglected, as well as in closed-loop systems, where the strong coupling between neutron-kinetic and thermo-hydraulic models are accounted for. As for the noise source, the main perturbation type which dominates in BWRs, i.e. the propagating type of perturbation traveling axially with a coolant, was chosen.

First, for the case of open-loop systems, the space-/frequency-dependence of the propagating neutron noise in one group theory was analyzed. Some interesting interference effects between the point-kinetic and pure space-dependent terms for the medium size systems/medium frequencies were discovered and explained. As a consequence, in practical cases, the presence of both components will apparently complicate the utilization of the induced noise for diagnostic purposes. Next, a similar study was performed in two-group theory to expedite the interpretation of the effect of different spectral properties on the induced neutron noise. As a result, it was suggested that it might be beneficial to include fast neutron detection methods in the noise diagnostic systems for fast reactors. In addition, it was demonstrated that for the correct description of the induced noise, it is important to model the noise source by accounting for its effect on all cross-sections. Such results have a significance both to BWRs and PWRs, as well as for some planned future reactor types, in particular Generation IV MSRs, where the propagating perturbations could have a stronger effect due to the circulating properties of the fuel.

In the case of closed-loop systems, a simple reduced order model (ROM) with four heated channels was applied to study both global and regional instabilities in BWRs. It was found that the inclusion of the fundamental and both azimuthal modes is crucial for the characterisation of BWR stability, and their interference can lead to an incorrect determination of the corresponding stability boundaries. Apart from this, it was demonstrated that the developed ROM is capable to handle not only core-wide instabilities, but also the effect of local ones (induced e.g. by DWOs) in a simplified manner. Moreover, the ROM is able to provide a deeper insight and understanding into the origins of studied instability events. As a continuation, a more realistic model for the propagating DWOs,

based on the data from system codes and taking into account the axial phase shift between different core elevations, is planned to be introduced into the ROM to investigate its effect on the stability properties of the system.

Finally, some applications of the neutron noise diagnostics, based on the foregoing studies, were discussed. As a first step, the effect of the non-white character of the driving force on the stability properties in a BWR was investigated. From this analysis, it was concluded that for the practical cases, the non-white character of the driving force does not induce any significant change on the determination of the stability properties of the system, as compared with the case of a white driving force. However, as shown in the thesis, in some pathological cases, the unstable state of the system might not be detected until the properties of the driving force change.

Then, using the newly-developed ROM the possibility to utilize the coupling reactivity coefficients as a new stability parameter, instead of the traditional DR, was investigated. It was found that in the frame of the present ROM, the behaviour of the DR as a function of C_{mn} is not monotonic which makes the alternative to use the reactivity coefficients as a new stability indicator questionable. To clarify this problem, further investigation is necessary.

Next, the unfolding technique of the neutron noise was considered. Two methods (the break frequency and transit time) for the reconstruction of the axial void profile from the MC simulated neutron noise were tested. Both methods show promising results and can be considered as good candidates for testing them on actual neutron noise measurements. However, further developments of the model are necessary in order to improve the consistency of the estimations. It should also be mentioned that the investigation was limited to bubbly flows only, whereby a more sophisticated model may be required for other flow regimes. As a future work, a more fundamental application of the break frequency method, i.e. combining both methods together to increase the accuracy of the void reconstruction, will be considered. Furthermore, the transit time method is also planned to be tested on real neutron noise measurements performed in the Swedish Ringhals-1 power plant, as a continuation of the present work.

To summarize, the problems of traveling perturbations discussed in this thesis, as well as the methods elaborated for their solution, bring some significance for both the safety and economy of reactor operation. What regards the first item, using simple models for the neutron noise, some intuition into the characteristic properties of the reactor system and the methods to quantify them was obtained. Such knowledge will obviously help to detect and identify abnormal (unstable) reactor behaviour long before it leads to serious consequences and, thus, to operate the reactor in a much safer manner. In terms of economical benefits, the implemented diagnostic methods proved to be a powerful tool for the online monitoring and unfolding of reactor parameters, important for both core management and surveillance. In addition, compared to other methodologies, such techniques do not require any installation of additional equipment and can be performed on already existing instrumentation. However, to improve the quality of the obtained results as well as the efficiency of the employed algorithms, a more sophisticated modeling of the governing physical processes providing a better representation of realistic cases are necessary and will be undertaken in the future.

ACKNOWLEDGEMENTS

I would like to take the opportunity to thank those people who spent their time and shared their knowledge for helping me to complete my work with the best possible result.

First and foremost, I am very grateful to my supervisor professor Christophe Demazière for his important support, for his detailed and constructive comments throughout this work. I thank him very much for the untiring help during my difficult moments. His extensive discussions around my work have been very helpful for this study.

My deep and sincere gratitude to my co-supervisor, professor Imre Pázsit[1] who gave me the opportunity to work with his team. His immense knowledge, logical way of thinking, guidance and support enabled me to develop better understanding of the subject. Throughout my research work and study, he provided encouragement, sound advice, good teaching, good company, and lots of good ideas. I will never forget his sincerity, tolerance and inspiration.

During this work I have collaborated with many colleagues of the department for whom I have great regard, especially Paolo Vinai and my former room mate Andreas Enqvist for interesting suggestions and solutions.

Thanks to my present room mate Cheuk for the exciting chess matches, trying to beat me each time. You finally did it- well done! (Klas, you are quite close to it).

Great thanks to my dance partner, Irina, for her inspiration and endless support not only during the dancing courses.

I warmly thank Eva Streijffert, former secretary of the Division of Nuclear Engineering at Chalmers University for her sympathetic help in my everyday routine. Her positive and loving feedback has supported me greatly.

Special thanks to our IT group, Lennart and Lasse for helping me with computer issues.

I wish to extend my warmest thanks to all other past and present colleagues: Albert, Alexander, Anders J., Anders N., "football dude" Augusto, Berit, Britta, Dina, "nightclub partner" Florian, Geri, Henrik, Istvan, Jan, Johan, Joska, Kateřina, Klara, Klas, Larisa, Lembit, Monika, Nam, Nils-Göran, Ondřej, Petty, Shuya, Sara, Tünde, Viktor, Yevgen. Thanks you all!

The financial support of SKC, SSM, Ringhals and NORTHNET are gratefully ac-

[1] Although professor Imre Pázsit was officially my co-supervisor, both professor Christophe Demazière and and professor Imre Pázsit contributed equally to my supervision. In addition, professor Imre Pázsit provided the main supervision up to the Licentiate stage.

knowledged.

Many thanks to the Technical University of Dresden, namely Dr. Carsten Lange and professor Dieter Hennig, for endless help and good ideas which they provided me within this work. I would like to thank Vattenfall Nuclear Fuel, in particular, Dr. Hongwu Cheng for providing the necessary data for this work.

I owe my loving thanks to my parents. Without their encouragement and understanding it would have been impossible for me to finish this work. My special gratitude is due to my elder sister for believing in me and motivating me to higher achievements.

NOMENCLATURE

ACF	Auto Correlation Function
APRM	Averaged Power Range Monitor
APSD	Auto Power Spectral Density
BWR	Boiling Water Reactor
CANDU	CANada Deuterium Uranium
CCF	Cross Correlation Function
CPSD	Cross Power Spectral Density
DF	Driving Force
DFM	Drift Flux Model
DR	Decay Ratio
DWO	Density Wave Oscillation
(F)FT	(Fast) Fourier Transform
HEM	Homogeneous Equilibrium Model
LPRM	Local Power Range Monitor
LWR	Light Water Reactor
MOX	Mixed Oxide
MSR	Molten Salt Reactor
ODE	Ordinary Differential Equation
PDE	Partial Differential Equation
PWR	Pressurized Water Reactor
ROM	Reduced Order Model

References

[1] Pázsit I. and Demazière C., "Noise Techniques in Nuclear Systems", Chapter in Handbook of Nuclear Engineering-Reactors of Generation II, Ed. D. G. Cacuci, **Vol. 3**, **Chapter 2**, *Springer Verlag*, New York, USA, 2010.

[2] Kosály G. and Williams M. M. R., "Point theory of the neutron noise induced by inlet temperature fluctuations and random mechanical vibrations", *Atomkernenergie*, **18**, 203-208, 1971.

[3] Kosály G. and Meskó L., "Remarks on the transfer function relating inlet temperature fluctuations to neutron noise", *Atomkernenergie*, **18**, pp. 33-36, 1972.

[4] Pázsit I., "Neutron noise theory in the P_1 approximation", *Progress in Nuclear Energy*, **40**, pp. 217-236, 2002.

[5] Pázsit I. and Jonsson A., "Reactor kinetics, dynamic response and neutron noise in Molten Salt Reactors (MSR)", *Nuclear Science and Engineering*, **167**, pp. 61-76, 2010.

[6] Jonsson A. and Pázsit I., "Two-group theory of neutron noise in Molten Salt Reactors", *Annals of Nuclear Energy*, **38**, pp. 1219-1246, 2011.

[7] Bell G. I. and Glasstone S., "Nuclear Reactor Theory", *Van Nostrand-Reinhold Company*, New York, USA, 1970.

[8] Kosály G., "Noise investigations in boiling-water and pressurized-water reactors", *Progress in Nuclear Energy*, **5**, pp. 145-199, 1980.

[9] Pázsit I., Antonopoulos-Domis M., Glöckler O. "Stochastic aspects of two-dimensional vibration diagnostics", *Progress in Nuclear Energy*, **14**, pp. 165-196, 1984.

[10] Pázsit I. and Glöckler O., "On the neutron noise diagnostics of PWR control rod vibrations II. Stochastic vibrations", *Nuclear Science and Engineering*, **Vol. 88**, pp. 77-87, 1984.

[11] Pázsit and Glöckler O., "BWR Instrument Tube Vibrations: Interpretation of Measurements and Simulation", *Annals of Nuclear Energy*, **21**, pp. 759-786, 1994.

[12] Pázsit I. and Glöckler O., "Cross sectional identification of two-phase flow by correlation technique", *Progress in Nuclear Energy*, **Vol. 15**, pp. 661-669, 1985.

[13] Pázsit I., "Two-phase flow identification by correlation technique", *Annals of Nuclear Energy*, **Vol. 13**, pp. 37-41, 1986.

[14] Brown F. B. and Sutton T. M., "Monte Carlo fundamentals", *The 1996 Frederic Joliot summer school in reactor physics. Modern reactor physics and the modeling of complex systems proceedings*, Cadarache & France, August 19-28, pp. 348-352, 1996.

[15] March-Leuba J., "Dynamic behaviour of Boiling Water Reactors", *Ph.D. Dissertation*, University of Tennessee, USA, 1984.

[16] Muñoz-Cobo J. L., Perez R. B., Ginestar D., Escriva A. and Verdú G., "Nonlinear Analysis of Out-of-Phase Oscillations in BWRs", *Annals of Nuclear Energy*, **23**, pp. 1301-1335, 1996.

[17] Karve A. A., Rizwan-uddin and Dorning J. J., "Stability Analysis of BWR Nuclear Coupled Thermal-Hydraulics Using a Simple Model", *Nuclear Engineering and Design*, **177**, pp. 155-177, 1997.

[18] Muñoz-Cobo J. L., Chiva S., and Sekhri A., "A reduced order model of BWR dynamics with subcooled boiling and modal kinetics: application to out-of-phase", *Annals of Nuclear Energy*, **31**, pp. 1135-1165, 2004.

[19] Dokhane A., Hennig D., Rizwan-uddin and Chawla R., "Nonlinear Stability Analysis with a Novel BWR Reduced Order Model", *Proceedings of International Conference on the New Frontiers of Nuclear Technology: Reactor Physics, Safety and High Performance Computing*, PHYSOR 2002, Seul, Korea, October 7-10, 2002.

[20] Todreas N. E. and Kazimi M. S., "Nuclear System I. Thermal-Hydraulic Fundamentals", *Hemisphere*, New York, 1990.

[21] Karve A. A., "Nuclear-Coupled Thermal-hydraulic Stability Analysis of Boiling Water Reactors", *Ph.D. Dissertation*, Virginia University, USA, 1998.

[22] Pázsit I., "Determination of reactor stability in case of dual oscillations", *Annals of Nuclear Energy*, **22**, pp. 378-387, 1995.

[23] Demazière C. and Pázsit I., "On the possibility of the space-dependence of the stability indicator (decay ratio) of a BWR", *Annals of Nuclear Energy*, **32**, pp. 1305-1322, 2005.

[24] Zhou Q. and Rizwan-uddin, "Bifurcation Analyses of In-phase and Out-of-phase Oscillations in BWRs", *Proceedings of International Conference on the New Frontiers of Nuclear Technology, Reactor Physics, Safety and High Performance Computing*, PHYSOR 2002, Seoul, Korea, October 7-10, 2002.

[25] Dokhane A., "BWR Stability and Biffurcation Analysis using a Novel Reduced Order Model and the System Code RAMONA", *Ph.D. Dissertation*, EPFL, Switzeland, 2004.

[26] Lange C. A., "Advanced Nonlinear Stability Analysis of Boiling Water Nuclear Reactors", *Ph.D. Dissertation*, Dresden Technical University, Germany, 2009.

[27] Oguma R., "Application of Noise Analysis for the Study of Core Local Instability at Forsmark-1", *SKI Report 97:42*, Statens Kärnkraftinspektion (Swedish Nuclear Power Inspectorate), Stockholm, Sweden, 1997.

[28] Analytis G. Th., Hennig D., and Karlsson J. K.-H.. "The general mechanism of core-wide and local instabilities at the Forsmark-1 BWR", *Nuclear engineering and design*, Vol. **205**, pp. 91-105, 2001.

[29] Verdú G., Ginestar D., Muñoz-Cobo J. L., Navarro J., Palomo M. J., Lansaker P., Conde J. M. and Sartori E., "Forsmark-1 & 2 Boiling Water Reactor Stability Benchmark. Time Series Analysis Methods for Oscillation during BWR Operation", *Final Report* NEA/NSC/DOC, 2001.

[30] Lahey T. R., "Boiling Heat Transfer. Modern Developments and Advances", *Elsevier Science Publishers*, Amsterdam, London, New York, 1992.

[31] Behringer K., Kosály G., Pázsit I., "Linear response of the neutron field to a propagating perturbation of moderator density (two-group theory of BWR noise)", *Nuclear Science and Engineering*, **72**, pp. 304, 1979.

[32] Zinzani F., Demazière C. and Sunde C., "Calculation of the eigenfunctions of the two-group neutron diffusion equation and application to modal decomposition of BWR instabilities", *Annals of Nucl. Energy*, **35**, pp. 2109-2125, 2008.

[33] "SIMULATE-3: Andvanced Three-Dimensional Two-Group Reactor Analysis Code", SIMULATE-3 User's Manual, *Studsvik Scandpower Inc.*, Massachusetts, USA, *Studsvik Scandpower AB*, Nyköping, Sweden, 2001.

[34] Demazière C., "CORE SIM: A multi-purpose neutronic tool for research and education", *Annals of Nuclear Energy*, **38**, pp. 2698-2718, 2011.

[35] "CASMO-4: A Fuel Assembly Burnup Program", Casmo-4 User's Manual, *Studsvik of America Inc.*, Massachusetts, USA, *Studsvik Core Analysis AB*, Nyköping, Sweden, 1995.

Papers I-VIII